

Reviewer #1

We thank the reviewer for the thoughtful and constructive comments. In the following we address the comments and suggestions.

General comments

Overall, I found the manuscript scientifically interesting, well written and structured. The topic is of interest for the geomorphological community, however its acceptance could be strengthened after minor corrections (see details below).

We are pleased that the reviewer appreciates our work and sees it as a contribution to the community. In the following, we address his specific comments.

1. *I would suggest that the authors use a different misfit function for calculating the fit of the model to the data (see details in technical corrections).*

We think it is an interesting suggestion to calculate a model performance metric which considers the analytical uncertainty on the observed data (E_{CRN}). However, errors on CRN data are heteroscedastic: they systematically increase with increasing erosion rates. Although the ME thus provides a good metric to evaluate overall model performance, the metric is not well suited to optimize model parameters in an optimization procedure: during the optimization of the model, too much weight will be given on the lower regime of the erosion spectrum where the analytical errors on E_{CRN} are low whereas the higher E_{CRN} data will not be approximated well because of their large associated errors. To compensate for the effect of heteroscedasticity we rescale values of O_i , M_i and E_i using a logarithm with base 10 when calculating ME . In the revised version of the paper, the ME will be reported as a metric to evaluate model performance, but not to optimize model parameters. Model optimization is done using the Nash Sutcliffe model efficiency, and we will explain this in the revised version of the manuscript.

2. *It is not clear if the gained conclusions are applicable or transferable to other settings and therefore how much impact the manuscript will have in the community. The scientific relevance could be significantly strengthened if other available datasets are compared to the presented study (e.g. from DiBiase or Carritier in the the San Gabriel Mountains and the Andes). I hope you find my comments and suggestions helpful.*

We propose a methodology for studying the spatial variability of river incision rates which can be used as a framework to study the coupling between river incision, lithological heterogeneity and climate at larger continental to global scales. However, developing a regional erodibility index and compiling hydrological datasets for regions others than the one studied here would be a project on its own and is therefore beyond the scope of this paper. In the revised version of the

paper, we do stress that our findings are based on a study case and that the significance of our results should be tested by applying a similar methodology to continental or global scales.

Technical corrections

Line 16-27: Since there is not word limit on the Abstract you should give some more details here. For instance, what are the erosion rates and how they differ in different lithologies/rainfall? Would be nice to have some absolute or relative values on erosion/incision depending on lithology/rainfall.

We will follow the suggestion of the reviewer to extend the abstract. However, since reviewer 2 requested more clarification on the main objectives and conclusions of our paper, we will elaborate the abstract along those lines rather than giving specific values.

Line 38: I would not give a fixed minimum catchment area since this is site-to-site depending, e.g. Koberet al. (2012) or West et al. (2014) found that nuclide concentrations of larger catchments are perturbed by single mass-wasting events.

We will remove the minimum catchment area as suggested

Line 42: Change to '... have been found to correlate with a...'

Noted, we will revise.

Line 55: Delete 'external'.

Noted, we will revise.

Line 58-62: Please rewrite/reorder this sentence.

Noted, we will revise.

*Line 144: I would suggest to use a different misfit function, since the result is depending on the distribution of measured erosion rates and does not take into account the analytical uncertainties. Use a simple misfit function such as: $Misfit = \sum_{i=1}^{nb} \sqrt{\frac{(O_i - M_i)^2}{E_i}}$ A misfit of nb or smaller would indicate that you predict the observations within the e.g. 1 standard deviations of all observations (if E is the standard deviation) and a value of 2*nb would mean you are within 2 standard deviations. . .*

$$\sum_{i=1}^{nb} \sqrt{\frac{(O_i - M_i)^2}{E_i}}$$

See reply general comment 1.

Equation (10): Not sure, but have you explained what K_{st} is?

Thanks for pointing this out, should be K . We will revise.

Equation (11): I guess it should be k_{sn} and not k_s .

Thanks for pointing this out, should be k_{sn} . We will revise.

Line 182: Please refer to the corresponding equations (4).

Noted, we will revise.

Line 184: Please make sure that all local names of locations, mountain ranges, basins. . . are shown in a figure for those reader that are not familiar with the geological/geographic setting.

Noted, we will adjust Figure 1.

Line 216: A recent paper (DiBiase et al. 2018) showed that TCN do not need to be corrected for topographic shielding because of deep non-vertical attenuation paths.

Thanks for pointing us to this paper. Since our paper uses the data as processed in Vanacker et al. 2015 (where a correction was applied), we will keep this section as it is.

Line 378: Would be nice to show that the fits to your data are statistically different for your different complex models. Visually they are look very similar and if I take the confidence intervals shown that overlap.

We agree: the fits for the different scenarios are similar. We feel that our sample size does not warrant a thorough statistical analysis. However, we will add the following sentences to the revised version of the paper:

“Note that differences in model performance between R-SPM scenario 2 and ST-SPM scenarios 5-8 are existent but not very pronounced. To evaluate the significance of these differences, our analysis should be repeated on larger datasets capturing a wider variability in erosion rates and hydrology”

Line 384: I would not use a chapter heading without text.

Given the different topics covered in the discussion section, we feel the use of subsections is warranted here to structure the flow of the paper and to keep the overview.

Line 391: In addition to the supplementary figure please add the position of knickpoints in one of your maps.

Good suggestions, we will adjust the figure.

Line393: Is the baselevel lowering or the uplift increasing, please clarify!

Here we refer to the effect of propagating pulses of river incision. We will clarify: "Facing a sudden lowering of their base level after river rejuvenation, ..."

Line 430: Why do you assume that hydrological/climate changes occurred more likely on Myr-time scale compared to timescales erosion rates are averaging over? Please explain this.

We do not know for sure, but given that k_{sn} values integrate over several thousands to millions of years, and CRN data only over 100-100k years, it is *more* likely that the climate has changed over the integration time captured in river steepness than over the time represented by CRN data. We will clarify as such in the text.

Line432: Add '...timespan of ECRN and ksn measurements.'

Noted, we will revise.

Table 1: Change to 'Flow resistance. . .'

Noted, we will revise.

Figure 1: The faults and labelling of faults is difficult to see. Larger line width and fonts, maybe even colour would help. Please show the main streams as lines.

Good suggestions, we will adjust the figure.

Figure 5: Add coordinates.

Figure will be moved to the SI in the new version of the paper.

Reviewer #2

We thank the reviewer for the thoughtful and constructive comments.

General comments

Given the focus on rainfall variability in the introduction text, I expected a paper that would advance our knowledge on the impact of rainfall variability on long term incision rates. Essentially what I read was a paper that concludes that lithological strength variability is very important in correctly predicting erosion rates and that accounting for rainfall variability also helps some (results in table 5, especially).

The reviewer her/his main concern is on the role of lithology versus rainfall variability in controlling erosion rates. The reviewer concludes that lithology dominantly controls erosion and that rainfall helps some in explaining spatial patterns of erosion. In fact, that is indeed one way of looking at the problem: The Area-Based Stream Power Model (A-SPM) does a good job in predicting spatial pattern of erosion rates after correcting for lithological heterogeneity. However, the goal of this paper is not only to come up with just a model that describes the spatial variation in erosion rates. What we aim to do, is to explain the spatial pattern of erosion rates and to identify the factors controlling it. Therefore, we do not propose to use the R-SPM and ST-SPM erosion models as tools to 'better' predict incision, rather we use them as tools to get additional insights in the existence of a non-linear relationship between CRN-derived erosion rates and river steepness (k_{sn}). That said, we agree with the reviewer that we were not entirely clear in passing on that message to the reader, which is why we will rewrite those parts of the manuscript where we justify the use of the different incision models. In the abstract, for example, we will add the following lines to clarify this:

" ... First, we use an area-based stream power model to scrutinize the role of lithological heterogeneity on river incision rates. We show that lithological heterogeneity is key to predicting spatial patterns of incision rates. Accounting for lithological heterogeneity reveals a non-linear relationship between river steepness, a proxy for river incision, and cosmogenic radio nuclide (CRN) derived denudation rates. Second, we explore this nonlinearity using runoff-based and stochastic-threshold stream power models, combined with a state-of-the-art hydrological dataset to calculate spatial and temporal runoff variability. Statistical modelling suggests that the non-linear relationship between river steepness and denudation rates can be attributed to a spatial runoff gradient and incision thresholds. Our findings have two main implications for the overall interpretation of CRN-derived denudation rates and the use of river incision models : (i) applying sophisticated stream power models to explain denudation rates at the landscape scale is only relevant when accounting for the confounding role of environmental factors such as lithology and (ii) spatial patterns in runoff due to orographic precipitation in combination with incision thresholds explain part of the non-linearity between river steepness and CRN-derived denudation

rates. The methodology that we present can be used as a framework to study the coupling between river incision, lithological heterogeneity and climate at regional to continental scales. “

We will also add the following paragraph to clarify the objectives of the paper:

“Based on current limitations, we formulate two main objectives for this paper: we want (i) to assess the impact of lithological heterogeneity on river incision and (ii) to unravel the role of allogenic (spatial and/or temporal runoff variability) versus autogenic (incision thresholds) controls on river incision. We develop and evaluate our approach in the southern Ecuadorian Andes where detailed lithological information is available as well as a database of CRN-derived denudation rates (Vanacker et al., 2007, 2015)..

...

In the following sections, we first describe the study area, characterize the lithological configuration by developing a lithological erodibility index and compile a database to represent runoff variability. Second, we present the methods and assumptions used for calibrating and simulating river incision. In a third section, the modelling results are presented: we start by evaluating the impact of lithological heterogeneity on river incision rates using an area-based river incision model (A-SPM). We then evaluate to what extent the variability in denudation rates can be explained by spatial and/or temporal runoff variability and the existence of incision thresholds using the R-SPM and ST-SPM. Note that the goal of using R-SPM and ST-SPM models is not to improve the statistical explanatory power of the A-SPM but rather to get insights in the potential drivers of incision variability which are otherwise lumped in the parameters of the A-SPM. In a final section, we discuss our findings, highlight the implications of our work and discuss further perspectives. “

In the discussion, we added:

“Model performance of the ST-SPM equals the performance of an empirical A-SPM with a slope exponent $\gg 1$ (Figure 9). Our interpretation is that (i) spatial variations in runoff and (ii) the incision thresholds are the causes of an observed non-linear relation between k_{sn} and ECRN. With a seemingly equal model performance, one could wonder what the benefit of the more complex ST-SPM model is over a simple, non-linear A-SPM. The aim of using a ST-SPM is however beyond fitting observed denudation rates: we want to identify to what extent the system is forced by internal allogenic dynamics such as the presence of incision thresholds or external autogenic forces such as runoff variability. Use of the ST-SPM illustrated that both processes can be accounted for in a quantitative way so that future studies can explicitly consider their role when reconstructing past landscape response to external perturbations (e.g. climate change).”

To Further clarify and stress this, we also adjusted the tile:

“Parameterization of river incision models requires accounting for environmental heterogeneity: insights from the tropical Andes”

I think the introduction needs to be revised somewhat to better reflect the results presented in the paper. The abstract does a better job of communicating the essence of the paper. Generally, the manuscript is very heavy on the methodology and too light on the discussion of the results and why these results matter.

We agree with the reviewer that we can organize our introduction somewhat better. As suggested in the line specific comments, we will also add some additional sentences throughout the manuscript to guide the reader better through the paper and to maintain a good flow in general. Our updated paper will be reorganised using the following section headers: 1.

1. Introduction
 - 1.1. Background
 - 1.2. River incision models
 - 1.2.1. Area-based Stream Power Model
 - 1.2.2. Stochastic-Threshold Stream Power Model
 - 1.2.3. Runoff-based Stream Power Model
 2. Study area
 - 2.1. Geology
 - 2.1.1. Tectonics and geomorphic setting
 - 2.1.1.1. Lithological strength
 - 2.2. CRN-derived denudation rates
 - 2.3. River morphology
 - 2.4. Runoff variability
 - 2.4.1. Spatial runoff patterns
 - 2.4.2. Frequency magnitude distribution of orographic discharges
 3. Methods
 - 3.1. CRN-derived denudation rates to calibrate river incision
 - 3.2. River incision models
 - 3.3. Optimization of model parameters
 4. Comparing model results with CRN-derived denudation rates
 - 4.1. Area-based stream power model
 - 4.2. Runoff-based and Stochastic-Threshold Stream Power Models
 - 4.2.1. Runoff-based SPM (R-SPM)
 - 4.2.2. Stochastic-Threshold SPM (ST-SPM)
 5. Discussion
 - 5.1. Are CRN-derived denudation rates representative for long term river incision processes?
 - 5.1.1. Equilibrium between river incision and hillslope denudation
 - 5.1.2. Integration timescales of ECRN and ksn
 - 5.2. Environmental control on long term river incision rates
 - 5.2.1. Geology
 - 5.2.2. Rainfall
 6. Conclusions
 7. References

We will also expand the result section and remove some of the methodology sections where possible. We will keep the section on the lithology since we think this part is necessary for the paper.

I also think the authors sometimes overreach on the significance of some results.

In the context of the clarified focus of the paper, discussed before, we will frame the results more clearly and mention the limitations explicitly.

It seemed like a long slog through the methodology section with many figures that did not seem terribly relevant OR were uninterpretable (Figures 3,5,7,8,9,11,13). Not all of these need to be relegated to Supplementary Material, but it would be helpful if some of them were and the important figures referenced more prominently in the text.

We will reduce the number of figures to 9, by merging some and moving others to the SI. We will remove the figure on PGA as suggested by the reviewer. In the updated version of the manuscript, we will also provide more details in the subtitles of the figures to make them understandable and readable as stand-alone objects.

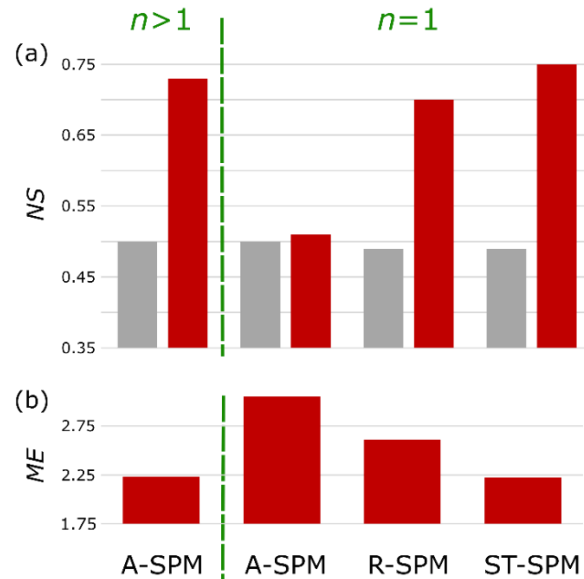
I often felt like I had to hunt down the authors motivation for a methodology or intuit the reasons why results were significant. The authors need to be clearer throughout the manuscript on both of these points.

Noted, we will revise.

With some substantial improvements to this manuscript, particularly in cutting down the methodology section and refining and expanding the results section, I think it can be published as a valuable contribution to the geomorphology community.

We appreciate that the reviewer sees our work as a valuable contribution to the community. As mentioned before, we will try to cut down the methodology section where possible. Two essential parts of this paper – the high-resolution hydrological product and the lithological erodibility index will be kept in the main part of the manuscript, although we will cut down the text and move non-essential methodological aspects to the supplementary materials.

We will streamline the results section by consistently documenting all model parameters in one table (Table 4 rather than table 4 and 5) and will consistently refer to the scenarios as documented in the table. For the sake of clarity, we will present the model fits of all the scenarios in the supplementary information. Moreover, we realized that the discussion section could benefit from an additional graph reporting the overall model performance of the different models and will include this new figure (see below) in the revised document.



Additional figure: Comparison of model performance of four selected river incision models. (a) Nash Sutcliffe model efficiency (NS) for different model scenarios, without (grey bars) or with (red bars) considering lithological heterogeneity. (b) shows the corresponding Model Error (ME). The A-SPM model scenario corresponds to the Area-Based Stream Power Model (cf. Figure 7). It performs well when lithological heterogeneity is considered and all parameters are freely calibrated, resulting in a slope-steepness exponent (n ; cf. Eq. 1) of 1.62 (for a full overview of model parameters, see Table 4). However, for an A-SPM scenario where n is fixed to the theoretically derived value of 1, the model performance strongly deteriorates (see main text). R-SPM represents a model scenario that explicitly incorporating runoff variability (cf. Figure 8a). The ST-SPM scenario also includes an incision threshold (cf. Figure 8b). Both scenarios perform well when n is fixed to 1 and when considering lithological heterogeneity. Overall, the best model performance (highest NS and smallest ME) is obtained under the ST-SPM scenario where lithological and runoff variability, as well as river incision thresholds are considered. *I have many specific comments on science issues and several technical corrections that are included in an annotated PDF that I will attach.*

We will address all the specific comments in the revised version of the manuscript.

Line specific comments

Line 16: 'enable to assess': typo

Where is the typo? Sentence rephrased.

Line 18 'variability of rock strength and its resistance to incision': wc

Isolating the role of rainfall variability remains difficult in natural environments, in part because environmental controls on river incision such as lithological heterogeneity are poorly constrained

Line 22 'Using ^{10}Be catchment-wide erosion rates, meteorological and hydrological data, as well as data on bedrock erodibility, we provide quantitative constraints on the importance of rainfall variability and lithological variations': main point of the paper

That is right...

Line 29 wc (word choice, reconsider)

Research on how rainfall variability and tectonic forcing interact to make a landscape evolve over time has long been limited by the lack of techniques that measure erosion rates over sufficiently long timespans

Line 64 several small grammar mistakes: subject verb agreement

Noted, we will revise.

Line 88: spelling

We will write a new 'objectives' paragraph (see above)

Line 124 this needs to be broken up into completely separate equations or at least labeled 4a, 4b, 4c. Ψ is not defined in words and needs to be, as the threshold parameter.

Noted, we will revise.

Line 127 a little confusing here as I was looking for the second component in equation 4. starting new paragraph should solve the problem

Noted, we will revise.

Line 142. this is a big assumption. What needs to happen to make this true? some additional info from discussion can be moved up here.

Good suggestion, we will add a paragraph with assumptions and revisit them in the discussion.

Line 152 model set 1: trad stream power

That's right. We will name this one A-SPM consistently

Line 156 second set of model runs with R-SPM. Above, should describe sets of model runs in the same order as incision models

In the theoretical section we first describe the ST-SPM because the R-SPM is a simplification of the ST-SPM. In the result section however, we believe it makes more sense to first present the R-SPM because it assumes constant k values and no thresholds. By presenting R-SPM first and then moving on to ST-SPM we gradually add layers of complexity which we find easier to navigate the reader through the result section.

Line 179: I see values of k (little k , no subscript) in table 2, but I don't see where it comes into the incision models. This needs to be explained and clarified. There are many parameters that are some version of big or little k with subscripts, superscripts, exponents, etc.

Noted, we will revise.

Line 184: I think the paper would flow better if the organization was like this:

1. Introduction
2. all study area section
3. Explanation of River Incision models
- 4.1 Model runs using river incision models
- 4.2 Optimization of model parameters.

Good suggestion, see structure of updated manuscript as a response to general remark before.

Line 191 It doesn't seem like all of this information is necessary to arrive at the critical information in the final sentence of the paragraph.

We removed part of this section.

Line 206 possible to include a MAP map of the study area? That would be useful given the focus on characterizing the impacts of rainfall variability. If not feasible, at least give a value for MAP on the western slopes as well.

MAP is represented in Figure 6 of the updated manuscript, we will clarify.

Line 212 At some point in the paper (and maybe it's coming later), I would like to see a summary of the catchment erosion rates from these 30 sub-basins.

The erosion rates are given in Table 2. We will increase the size of the labels in Figure 1 to enhance clarity.

Line 227 Are these important for supporting the results/interpretations of this paper? Seems out of place to mention them here.

We suggest keeping the reference to these plots as they are key to understand the discussion on transient incision pulses (in the discussion section of the paper). We will however, move these lines to the new section 'River morphology' where they will be better in place.

Line 239 it would be helpful to readers to explain at the beginning of section 4.4 that the reason you do all of this is to get this regional k_w value.

Noted, we will revise.

Line 244 why is 45 stations with 10 years of data not enough? are they all clustered together?

Indeed, most of them are in the centre of the basin and do not cover the catchments where CRN derived erosion is measured (shown on Figure 1). We will clarify.

Line 248 this is about 28 km resolution. pretty coarse.

While daily temporal resolution is really fine resolution to drive models that evolve over thousands of years.

That is right, therefore we develop a HR product by downscaling the 0.25° WaterGAP3 data. See also next reply.

Line 252 I don't easily grasp the relevance of this section, especially the second half of the paragraph, starting on line 248. What needs to happen in this paragraph is a more succinct explanation of the data sets used to get a pdf of daily runoff and more importantly, why using these data sets is an improvement on the data from the monitoring networks on the ground.

We will shorten and rephrase this paragraph as:

“To estimate runoff variability for all 30 sub catchments, we use hydrological data derived in the framework of the Earth2Observe Water Resource Reanalysis project (WRR2; Schellekens et al., 2017) available from 1979 to 2014. Specifically, we use the hydrological data calculated with the global water model WaterGAP3 (Water – Global Assessment and Prognosis: Alcamo et al., 2003; Döll et al., 2003) at a spatial resolution of 0.25° and a daily temporal resolution (earth2observe.eu). In the following paragraphs, we explain how we derive (i) a high-resolution runoff map by spatially downscaling this coarse data and (ii) catchment-specific magnitude frequency distributions of discharge (pdf_Q) characterising the temporal variability of runoff.”*

Line 255 nice intro and motivation for methodology here. But, before you get into the detailed explanation of methods, refer readers to figure 6 so they get a visualization of where you're going and why you do this.

Thanks.

We will point the readers to figures 5 and 6:

“The procedure consisted of the following steps and is presented in Figures 5 and 6:”

Line 281 This sentence unnecessarily confusing. Use more words to explain. this section needs an introductory sentence to orient readers.

We will resolve by adding the following text:

“Runoff variability is typically casted in terms of spatial runoff variability (section 2.4.1). However, also the temporal pattern of runoff might influence river incision and is typically represented by discharge magnitude frequency distributions. Constraining the shape of these distributions is important, because the number of large storm events determine the frequency by which thresholds for river incision to occur are exceeded (see section 1.2.2 and references therein).

Line 285 here little k is finally defined. this needs to happen earlier where it is first mentioned.
Noted, we will revise.

Line 294 how important are daily variations in discharge over 9 million years of uplift and erosion?
Good point, we will mention this earlier in the assumption section coming with the river incision models and revisit the issue in the discussion section of the paper.

Line 297 this is all fine and good, thorough work, but the summary/motivation of why you do this needs to be at the beginning of the paragraph. otherwise makes for very heavy reading.
Agreed, see reply above.

Line 300 is this section necessary? Does it really contribute to the main goal of the paper, which I understand to be evaluating the role of rainfall variability on incision rates. this sections feels like overkill. I recommend moving to supplementary materials.

As explained earlier, we do believe this section is critical given the importance of lithological heterogeneity in controlling river incision rates. Therefore, we will keep it in the methodology section.

Or at least the seismicity section can go to supp mat.
Agreed, we kicked it out.

the lithological strength section should actually stay as it's very important later in the paper. Indeed... Should now also be clear to the readers when they arrive at this point, given the enhanced focus on lithology in the abstract/intro

Line 317 where are these data of measured uniaxial compression strength? OK, I have found it now, but this section is confusing. it needs to be more clear and use more words to explain
We will explicitly mention that the uniaxial compressive strength data can be found in Table S4 to enhance clarity.

Line 319 this part definitely seems irrelevant to the main focus of the paper. There are so many other things already going on, this just feels like a distraction. Unless seismic activity is really playing a huge role, in which case maybe the focus of the paper should be on that.

Agreed, we kicked it out.

Line 327 reference figure 12, not table 4.

We will redo the figure numbers in the revised version of the paper and point the reader to both the table and the figure.

Line 331 more explanation and description of figure 12 would be helpful here before launching into another lengthy description of another methodology.

Agreed, we describe all scenarios now in more detail.

Line 336 what about Bayes factors of 1.06 vs 1400 tells us that the data fit a model with variable erodibility better? Needs more explanation.

See comment before.

Line 346 coming back to an earlier comment from near the beginning of the manuscript, it seems the focus of this paper is equally on the effects of spatial variation in both erodibility and runoff. this is not clear/emphasized in the abstract and introduction.

Agreed, we will resolve this by rewriting the abstract, and objectives of the paper. See comments before.

Line 351 spell out model names for section title.

Noted, we will resolve. To clarify, we will also break up this section in two subsections:

4.2. Runoff-based and Stochastic-Threshold Stream Power Models

4.2.1. Runoff-based SPM (R-SPM)

4.2.2. Stochastic-Threshold SPM (ST-SPM)

Line 353 nice explanation of what just happened and what will happen next. manuscript needs more of this in places.

Thanks, and agreed, we will resolve.

Line 360 also good emphasis.

Thanks

Line 362 this under prediction/over prediction trend is not obvious to me. Looks to me like the observational data is scattered somewhat evenly about the modeled data line. If the Nash Sutcliffe number tells us that there is under/over prediction, then explain how that happens. Otherwise, I think such a claim is not supported.

We will rewrite this paragraph

Line 369 these two scenarios evaluate role of little k.

True, we will clarify.

Line 372 little k apparently not so important.

Correct, we will stress this as: *“In scenario 5, k is fixed to the average value for all catchments ($k = 1.01$) whereas in scenario 6, k is set to the catchment specific values as listed in Table 2. Both scenarios (5 and 6) perform well with an NS value equalling 0.71 indicating that temporal runoff variability (k) is not influencing model performance.”*

Line 375 here finally runoff variability is evaluated.

No runoff is evaluated before. This will be clearer in the revised result section.

Line 378 this is misleading, as scenario 7 performs equally well!

We will explicitly mention that both scenarios perform equally well.

Line 379 what's the significance of these lower threshold values?

We will explain and frame it with some data from literature.

Line 380 I agree that the model vs. measured erosion rates look better in 14b compared to 14a. But it's an over-reach to say that ST-SPM "correctly" predicts low erosion rates. There's still a good bit of scatter and error in model vs. measured ero rates. Just modulate the word choice a little here.

Noted, we will revise.

Line 386 some of this context would be helpful earlier in the paper, e.g. near line 142 or section 4.2

Noted, we will revise by pointing the readers to this section

Line 401 how does this relate to the data presented? where do you suspect over/under estimation of ero rates from Be10?

This will be discussed in the next paragraph.

Line 406 these ids are hard to see and find. note that they are in teh northern section of field area and also refer readers to figure 2, can see these areas are steeper.

All good suggestions, we will do so.

Line 409 confusing. is the variability in agreement due to differences in drainage area in each catchment or to over/under estimation of CRN erosion rates? This needs to be more precisely worded, as the following sentences make clear.

We rewrote this paragraph:

“Longitudinal profiles of rivers draining to the knickzone in the Paute catchment show marked knickpoints. This is particularly evident in catchments 9-16 (Figure 1) where k_{sn} values are high (Figure 2) and knickpoints appear in the longitudinal profiles (Figures S3 and S4). Simulated erosion rates for some of these catchments deviate from CRN-derived denudation rates (Figure 8.b, ID’s 13 14 and 16) whereas for others (e.g. ID’s 9 and 11), predictions from the Stochastic-Threshold river incision model show a good agreement with ECRN data. For catchments with a sufficiently large drainage area, modelled incision rates correspond well with ECRN (ID’s 9 and 11 being both ca. 700 km²), most likely because the mechanisms that potentially cause overestimation and underestimation cancel each other out at this scale. For smaller catchments (ID’s 8;13;14 and 16 all being < 12 km²) there is a discrepancy between simulated river incision rates and ECRN.”

Line 427 good point that will have been on the mind of many readers through out the paper. maybe acknowledge this timescale mismatch earlier.

Good suggestion, we will do so by adding a paragraph to the methods section: (3.1)

“The use of CRN-derived denudation rates to calibrate river incision relies on three main assumptions, summarized by Scherler et al. (2017). A first assumption is that the catchment wide denudation rates derived from CRN are representative for long term fluvial incision. Positive correlations between river steepness, k_{sn} and CRN-derived denudation rates support this assumption (Vanacker et al., 2015), except for very small catchments where CRN-derived denudation rates are sensitive to the occurrence of deep-seated landslides. A second assumption is that runoff and rock uplift are uniform within the individual catchments. Given the size of the studied basins, this assumption seems to be reasonable. A third assumption, in particular when using the process-based R-SPM and ST-SPM, is that the runoff data, used to calibrate the incision parameters is representative over the time span which CRN data integrate (1-100 kyr). This is a challenging assumption, given the contemporaneous nature of the available hydrological data. While spatial patterns of runoff, mainly controlled by orographic precipitation, could be assumed broadly similar over the integration time of CRN-derived denudation, this is not necessarily true for the temporal variation in runoff. We will revisit the validity and implications of these three assumptions in the discussion section of this paper. “

Line 437 a bit much detail at this point.

Agreed, we removed part of this paragraph.

Line 444 I must have completely missed this point. Refer readers back to the relevant model runs/figures.

Noted, we will revise.

Line 447 allowed us

Noted, we will revise.

Line 449 given what you just said, now useful are more advanced methods likely to be? where would they be useful?

We will discuss this by adding a sentence.

Line 456 this seems to be the major, clear finding of this work.

We will revise the text to clarify the main findings (and also updated the title of the paper)

Line 467 if this is your conclusion, recommend removing earlier discussion of seismicity.

Agreed, we will revise.

Line 475 this is also a good and significant point that could be highlighted more prominently.

We will do so and mention it in the abstract of the paper.

Line 484 enables us

Noted, we will revise.

Line 485 am i missing something? this scenario does NOT include variation in runoff.

Hmm, we do not exactly know what the reviewer means here. But we will rephrase the sentence and the paragraph in general.

Line 486 above error/confusion makes it hard to evaluate this very important claim.

Agreed, we will rephrase this sentence and the paragraph in general.

Line 494 OK, good point here.

Line 495 yes, but the numbers are only slightly higher for scenario 6 vs scenario 4. How significant is this seemingly small difference?

We will rewrite this paragraph, as well as the paragraph in the results section dealing with these scenarios. In the results section we will add a sentence explicitly mentioning the similarity between these scenarios:

“Note that differences in model performance between R-SPM scenario 2 and ST-SPM scenarios 5-8 are existent but not very pronounced. To evaluate the significance of these differences, our analysis should be repeated on larger datasets capturing a wider variability in denudation rates and hydrology.”

Line 503 i would say that mainly spatial variation in rock erodibility controls river incision patterns. I have to say, I'm not convinced of that rainfall variability matters a huge amount from the data presented here.

We rephrased this paragraph. See also replies above.

“Our finding that spatial patterns in precipitation control river incision patterns corroborate findings in the Himalaya (Scherler et al., 2017) and in the Andes (Sorensen and Yanites, 2019). Sorensen and Yanites (2019) evaluated the role of latitudinal rainfall variability in the Andes on erosional efficiency using a set of numerical landscape evolution model runs. They show that erosion efficiency in tropical climates at low latitudes, where the Paute basin is located, is well captured by the spatial pattern of mean annual precipitation and thus runoff. At higher latitudes (25-50°) where storms are less frequent but still very intense, mean annual precipitation decreases but erosivity is still high due to the intensity of storms (Sorensen and Yanites, 2019). At these latitudes, the spatial variations in storm magnitude are therefore more likely to be reflected in river erosivity and thus catchment mean denudation rates than in the Ecuadorian Andes.”

Line 518 medium? anyway, medium is not a great word choice to describe basin size.

Noted, we will revise.

Line 527 But the simplest version of the model, A-SPM does almost as good of a job! $R^2=0.73$, $NS=0.73$! You must explain this and justify why variable R actually matters!

See comments before. We rephrased this paragraph as:

“In order to account for rock strength variability, which is for the Paute basin mainly ascribed to variations in lithological strength in the study area, we propose the use of an empirical lithological strength index that is based on lithology and age of lithostratigraphic units. Including lithological variability in the models increases the correlation between river steepness and denudation rates and reveals a non-linear relation, which we seek to explain using a stochastic-threshold SPM (ST-SPM). Using a downscaled version of a state-of-the-art hydrological reanalysis dataset, we show that the combination of spatially varying runoff and incision thresholds explains the observed, non-linear relationship. We do not detect, however, an impact of temporal discharge distributions

on river incision. We attribute this lack to the integration time of CRN data and response times of river longitudinal profiles which extend beyond timescales at which discharge distributions can be assumed to be stationary.”

Line 535 I think this conclusion is fair that this study shows potential, but more research is still needed for definitive answers about R variability.

We will keep this message in the revised version of the paper.

Lithology and orographic precipitation control parameterization of river

incision in models requires accounting for environmental heterogeneity: insights from the tropical Andes

Benjamin Campforts^{a,b,c}, Veerle Vanacker^e, Frédéric Herman^d, Matthias Vanmaercke^e, Wolfgang Schwanghart^f, Gustavo E. Tenorio^{g,h}, Patrick Willems^h, Gerard Govers^h

^a Helmholtz Centre Potsdam, GFZ German Research Centre for Geosciences, Potsdam, Germany

^b Institute for Arctic and Alpine Research, University of Colorado at Boulder, Boulder, CO, USA

^c Research Foundation Flanders (FWO), Egmontstraat 5, 1000 Brussels, Belgium

^d Department of Earth and Environmental Sciences, KU Leuven, Celestijnenlaan 200E, 3001 Heverlee, Belgium

^e Earth and Life Institute, Georges Lemaître Centre for Earth and Climate Research, University of Louvain, Place Louis Pasteur 3, 1348 Louvain-la-Neuve, Belgium

^f Institute of Earth Surface Dynamics, University of Lausanne, CH-1015 Lausanne, Switzerland

^g Université de Liège, Département de Géographie, University of Liege, UR SPHERES, Departement of Geography, Clos Mercator 3, 4000 Liège, Belgium

^h Institute of Earth and Environmental Sciences, University of Potsdam, Germany

ⁱ Facultad de Ciencias Agropecuarias, Universidad de Cuenca, Campus Yanuncay, Cuenca, Ecuador

^j Department of Earth and Environmental Sciences, KU Leuven, Celestijnenlaan 200E, 3001 Leuven, Belgium

^k Department of Civil Engineering – Hydraulics Section, KU Leuven, Kasteelpark 40 box 2448, 3001 Leuven, Belgium

Correspondence to: Benjamin Campforts (benjamin.campforts@kuleuven-begz-potsdam.de)

Abstract. Process-based geomorphic transport laws enable Landscape evolution models can be used to assess the impact of rainfall variability on bedrock river incision over geological/millennial timescales. However, isolating the role of rainfall variability on erosion remains difficult in natural environments, in part because the variability of rock strength and its resistance to incision environmental controls on river incision such as lithological heterogeneity are poorly constrained. HereIn this study, we explore spatial differences in the rate of bedrock river incision in the tropical Andes. The Ecuadorian Andes are characterized by strong using three different stream power models. A pronounced rainfall gradients gradient due to orographic precipitation sourced in the Amazon basin. In addition, the tectonic configuration has generated and a profound high lithological heterogeneity. The enable us to explore the relative roles of either these controls in modulating river incision on millennial time scales, however, remains unclear. Using ¹⁰Be catchment wide erosion rates, meteorological and hydrological data, as well as data on bedrock erodibility, we provide quantitative constraints on. First, we use an area-based stream power model to scrutinize the role of lithological heterogeneity on river incision rates. We show that lithological heterogeneity is key to predicting spatial patterns of incision rates. Accounting for lithological heterogeneity reveals a non-linear relationship between river steepness, a proxy for river incision, and cosmogenic radio nuclide (CRN) derived denudation rates. Second, we explore this nonlinearity using runoff-based and stochastic-threshold stream power models, combined with a state-of-the-art hydrological dataset to calculate spatial and temporal runoff variability. Statistical modelling suggests that the importance of rainfall variability and lithological variations. Explicit incorporation of rock erodibility in river incision models predicated on non-linear relationship between river steepness and denudation rates can be attributed to a spatial runoff gradient and incision thresholds. Our findings have two main implications for the stream-power equation enables

Formatted: Font: +Body (Calibri), 12 pt, Font color: Black

Formatted: Left, Line spacing: Multiple 1,08 li

Formatted: Numbering: Restart each section

Formatted: Font: +Body (Calibri), 12 pt, Font color: Black

Formatted: Font: +Body (Calibri), 12 pt, Not Bold, Font color: Custom Color(RGB(33,33,33))

Formatted: Font: 10 pt

Formatted: Font: 10 pt, Superscript

Formatted: Font: 10 pt

Formatted: Font: 10 pt, Italic

Formatted: Left, Space After: 0 pt, Line spacing: Multiple 1,15 li

Formatted: Line spacing: Multiple 1,15 li

Formatted: Line spacing: Multiple 1,15 li

Formatted: English (United Kingdom)

Formatted: English (United Kingdom)

Formatted: Space After: 8 pt, Line spacing: Multiple 1,15 li

Formatted: Superscript

Formatted: Normal, Line spacing: Multiple 1,15 li

Formatted: English (United Kingdom)

40 us to identify a first-order control overall interpretation of CRN-derived denudation rates and the use of river incision models
: (i) applying sophisticated stream power models to explain denudation rates at the landscape scale is only relevant when
accounting for the confounding role of environmental factors such as lithology on river incision rates. Rainfall variability
based on a spatially and temporally explicit hydrological dataset and a stochastic threshold river incision model explain and
45 (ii) spatial patterns in runoff due to orographic precipitation in combination with incision thresholds explain part of the non-
linearity between river steepness and CRN-derived denudation rates. The methodology that we present can be used as a
framework to study the coupling between river incision, lithological heterogeneity and climate at regional differences in river
incision that cannot be attributed to topographical and/or lithological variability.

to continental scales.

50

1. Introduction

1.1. Background

55

Research on how [rainfallclimate](#) variability and tectonic forcing interact to make a landscape evolve over time ~~was, for ahas~~ long ~~time,been~~ limited by the lack of techniques that measure [erosiondenudation](#) rates over sufficiently long timespans (Coulthard and Van de Wiel, 2013). ~~As a consequence~~Consequently, the relative role of [rainfallclimate](#) variability and tectonic processes ~~had tocould only~~ be deduced from sediment archives (e.g. Hay et al., 1988). However, whether sediment archives offer reliable proxies remains ~~an open research question~~contested because sediment sources and transfer times to depositional sites ~~remain largely unknown~~are often shrouded (Bernhardt et al., 2017; Romans et al., 2016). Moreover, ~~estimates from sediment archives have been contested due to potential observation biases (Jerolmack and Paola, 2010; Sadler, 1981)~~(Bernhardt et al., 2017; Jerolmack and Paola, 2010; Romans et al., 2016; Sadler, 1981).

60

65

~~Cosmogenic~~Nowadays, [cosmogenic](#) radionuclides (CRN) contained in quartz minerals of river sediments provide an alternative tool for determining catchment-wide [erosiondenudation](#) rates on a routine basis (Codilean et al., 2018; Harel et al., 2016; Portenga and Bierman, 2011). In sufficiently large catchments ($> 10\text{--}50\text{ km}^2$), ~~a~~ detrital CRN ~~derived~~ [erosiondenudation](#) rates (E_{CRN}) integrate over timescales that average out the episodic nature of sediment supply (Kirchner et al., 2001). Hence, benchmark or natural [erosiondenudation](#) rates can be calculated for ~~human~~, disturbed as well as pristine environments (Reusser et al., 2015; Safran et al., 2005; Schaller et al., 2001; Vanacker et al., 2007).

70

Catchment-wide [erosiondenudation](#) rates have been ~~correlated~~found to [correlate with](#) a range of topographic metrics including basin relief, average basin gradient and elevation (Abbühl et al., 2011; Kober et al., 2007; Riebe et al., 2001; Safran et al., 2005; Schaller et al., 2001). However, in tectonically active regimes, hillslopes tend to evolve towards a critical threshold gradient which is controlled by mechanical rock properties (Anderson, 1994; Roering et al., 1999; Schmidt and Montgomery, 1995). Once slopes approach this critical gradient, mass wasting becomes the dominant processes controlling hillslope response to changing base levels (Burbank et al., 1996). In such ~~a~~ configuration, hillslope steepness is no longer an indication of [erosiondenudation](#) rates and topographic metrics based on hillslope relief become poor predictors of catchment wide [erosiondenudation](#) rates (Binnie et al., 2007; Korup et al., 2007; Montgomery and Brandon, 2002)(Binnie et al., 2007; Korup et al., 2007; Montgomery and Brandon, 2002).

75

80

Contrary to hillslopes, rivers and river longitudinal profiles ~~do capture~~are more sensitive to changes in erosion rates (Whipple et al., 1999). Bedrock rivers in mountainous regions mediate the interplay between uplift and erosion (Whipple and Tucker, 1999; Wobus et al., 2006)(Whipple and Tucker, 1999; Wobus et al., 2006). They incise into bedrock and efficiently convey sediments, thus setting the base level for hillslopes and controlling the evacuation of hillslope derived sediment. Quantifying the spatial patterns of natural [erosiondenudation](#) rates in tectonically active regions [therefore](#) requires detailed knowledge of the processes driving fluvial incision. ~~One of the major outstanding research questions is to understand and~~

Formatted

Formatted

Formatted

Formatted

Formatted

Formatted

85 ~~quantify how fluvial systems respond to external rainfall variability or tectonic forcing~~ (Armitage et al., 2018; Castelltort et al., 2012; Finnegan et al., 2008; Gasparini and Whipple, 2014; Goren, 2016; Scherler et al., 2017; Tucker and Bras, 2000).

90 ~~The use of river~~River morphological ~~proxies~~indices, such as channel steepness (k_{sn}) (~~Wobus et al., 2006~~)(Wobus et al., 2006), ~~have successfully been applied~~ as a predictor for catchment denudation and thus E_{CRN} ~~has successfully been applied~~ by Safran et al. (2005) and ~~since being applied by~~ many others, commonly identifying a monotonically increasing relationship between channel steepness (k_{sn}) (~~Wobus et al., 2006~~)(Wobus et al., 2006) and E_{CRN} (Cyr et al., 2010; DiBiase et al., 2010; Mandal et al., 2015; Ouimet et al., 2009; Safran et al., 2005; Vanacker et al., 2015). Several authors identified a non-linear relationship between k_{sn} and E_{CRN} in both regional (e.g. DiBiase et al., 2010; Ouimet et al., 2009; Scherler et al., 2014; Vanacker et al., 2015) and global compilation studies (Harel et al., 2016). ~~Theoretical models suggest~~Theory suggests that this non-linear relationship ~~reflects~~reflects the dependency of long-term ~~river incision~~denudation on hydrological ~~and, hence,~~ ~~rainfall~~ variability (Deal et al., 2018; Lague et al., 2005; Tucker and Bras, 2000). ~~Hydrological variability affects both temporal and spatial variations in river discharge and the effect of river discharge on denudation and river incision rates can be approximated by theoretical model derivations.~~ However, ~~identifying~~the impact of ~~rainfall~~hydrological variability on incision rates in natural environments has, ~~until now,~~ only been ~~successful for~~successfully identified in a limited number of case studies (DiBiase and Whipple, 2011; Ferrier et al., 2013; Scherler et al., 2017).

100 We identify two ~~outstanding~~limitations hampering ~~wide~~large scale application of river incision models that include ~~rainfall~~hydrological variability. First, ~~the necessary high-resolution~~ hydrological data ~~at high-temporal and spatial resolutions~~ is usually ~~not available, but required because mountain~~unavailable. ~~Mountain~~ regions are typically characterized by large temporal and spatial variation in runoff rates (e.g. Mora et al., 2014). Yet, most of the observational records on river discharge are fragmented and/or have ~~poor~~limited geographic ~~cover~~coverage. Second, large catchments are often underlain by variable lithologies. Studies exploring the role of river hydrology in controlling river incision have ~~hitherto~~mainly focused on regions underlain by rather uniform lithology (DiBiase and Whipple, 2011; Ferrier et al., 2013) or ~~they~~have considered lithological variations to be of minor importance (Scherler et al., 2017). However, tectonically active regions ~~such as the Andes range,~~ ~~have usually~~ experienced tectonic accretion, subduction, active thrusting, volcanism and denudation resulting in a highly variable ~~litho-stratigraphic composition~~lithology over >100 km distances (Horton, 2018). Rock strength is known to control river incision rates, and is a function of its ~~lithological~~ composition and ~~lithology~~stratigraphic age (Brocard and van der Beek, 2006; Lavé and Avouac, 2001; Stock and Montgomery, 1999), ~~as well as~~ its rheology and fracturing ~~due to tectonic activity~~ (Molnar et al., 2007). If we want to use geomorphic models not only to emulate the response of landscapes to ~~climatically regulated rainfall~~climatic and/or tectonic forces but also to predict ~~absolute erosion~~denudation rates, ~~then we need to account for~~ variations in physical rock properties ~~need to be accounted for~~ (Attal and Lavé, 2009; Nibourel et al., 2015; Stock and Montgomery, 1999). ~~Furthermore~~Even more importantly, these variations in rock erodibility can potentially obscure the relation between river incision and ~~rainfall variability and more specifically the relation between long-term erosion and rainfall rates~~discharge (Deal et al., 2018). Therefore, ~~we posit that~~the climatic effects on ~~erosion~~denudation rates can only be correctly assessed if the geomorphic model accounts for physical rock properties and vice versa. ~~Based on current limitations, we formulate two main objectives: we want (i) to assess the impact of lithological heterogeneity on river incision and (ii) to unravel the role of allogenic (spatial and/or temporal runoff variability) versus autogenic (incision thresholds) controls on river incision. We develop and evaluate our approach in the southern Ecuadorian Andes where detailed lithological information is available as well as a database of CRN-derived denudation rates (Vanacker et al., 2007, 2015).~~

Formatted: Font: Not Bold

Field Code Changed

Formatted: Font color: Text 1

125 In this study, we assess the influence of lithological heterogeneity and rainfall variability on erosion rates in an active tectonic setting in the tropical Andes. We apply different, stream power-based models to the Paute River basin in the Ecuadorian Andes, and subsequently evaluate model performance by comparing modelled river incision rates and CRN derived erosion rates. Thereby, we aim to answer two research questions: First, do spatial variations in lithology correlate with rates of river incision? Second, are rates of river incision further modulated by rainfall variability?

130 **2.1.2. River incision models**

130 Bedrock rivers are shaped by several processes including weathering, abrasion-saltation, plucking, cavitation and debris scouring (Whipple et al., 2013). ~~Explicitly accounting for all these processes would render models too complex for simulations over timescales relevant to understand the uplift-climate-lithology-erosion conundrum. Therefore, river incision is typically simulated by assuming a functional dependence of river incision on the shear stress (τ , [Pa]) exerted by the river on its bed. Several models have been proposed to simulate the dependence of long-term river incision on shear stress (Dietrich et al., 2003) where the drainage Area-based Stream Power Model (A-SPM) is the most commonly used (Howard, 1994; Lague, 2014):~~

135
140
145
150
155 However, explicitly accounting for these processes renders models too complex at spatial and temporal scales relevant to understand landscape evolution of entire mountain ranges. Therefore, a broad variety of models have been proposed to simplify the complex nature of river incision dynamics (Armitage et al., 2018; Lague et al., 2005; Shobe et al., 2017; Venditti et al., 2019). Most river incision models assume a functional dependence of river incision on the shear stress (τ , [Pa]) exerted by the river on its bed (Sklar et al., 1998; Whipple and Tucker, 1999). However, within the family of shear stress / stream power models, several approaches exist. Most commonly used is the Area-based Stream Power Model (A-SPM), explicitly representing the universally observed inverse power relation between channel slope and drainage area (Howard, 1994; Whipple and Tucker, 1999). Parametrization of the A-SPM is purely empirical and involves calibration of three incision parameters (an erosion efficiency parameter, an area exponent and a slope exponent). Given the interdependency of these parameters (e.g. Campforts and Govers, 2015; Croissant and Braun, 2013; Roberts and White, 2010), there is an ongoing effort to calibrate river incision models using a process oriented strategy where small scale observations and physical mechanisms are upscaled to the landscape scale (Venditti et al., 2019). In particular and not exclusively, ongoing efforts evaluate how the three incision parameters are affected by (i) the presence incision thresholds (e.g. DiBiase and Whipple, 2011; Lague, 2014), discharge variability (DiBiase and Whipple, 2011; Lague et al., 2005; Snyder et al., 2003; Tucker and Bras, 2000) and the spatial and temporal distribution of runoff (Deal et al., 2018; Ferrier et al., 2013; Lague et al., 2005; Molnar et al., 2006). In this paper, we evaluate how two of such derived models (the Stochastic-Threshold and Runoff-based Stream Power Model, respectively ST-SPM and R-SPM) can be used to explain measured variations in denudation rates at the landscape scale.

155 **1.2.1. Area-based Stream Power Model**

The Area-based Stream Power Model (A-SPM, Howard, 1994) is a first, lumped statistical approach to represent river incision:

$$E = K' A^m S^n \quad (1)$$

in which E is the long term river erosion ($L t^{-1}$), K' ($L^{1-2m} t^{-1}$) quantifies the erosional efficiency as a function of rock erodibility and erosivity, A (L^2) is the upstream drainage area, S [$L L^{-1}$] is the channel slope, and m and n are exponents whose values depend on lithology, rainfall variability and sediment load.

Eq. (1) can be rewritten as a function of the channel steepness, k_s :

$$E = K' k_s^n \quad (2)$$

where k_s can be written as the upstream area-weighted channel gradient:

$$k_s = SA^\theta \quad (3)$$

In which $\theta = m/n$ is the channel concavity (Snyder et al., 2000; Whipple and Tucker, 1999). In order to compare steepness indices from different locations, θ is commonly set to 0.45 and the channel steepness is referred to as the normalized steepness index, k_{sn} (Wobus et al., 2006) (Wobus et al., 2006). Variations in k_{sn} are often used to infer uplift patterns, by assuming a steady state between uplift and erosion (Kirby and Whipple, 2012). In transient settings, where steady state conditions are not necessarily met, the k_{sn} values can be used to infer local river incision rates (Harel et al., 2016; Royden and Taylor Perron, 2013).

Notwithstanding empirical evidence supporting the A-SPM such as the scaling between drainage area and channel slope in steady state river profiles (Lague, 2014) or its capability to simulate transient river incision pulses (Campforts and Govers, 2015), the A-SPM is a semi-empirical geomorphic 'law' with several shortcomings reviewed in Lague (2014). Most notably, the A-SPM does not explicitly simulate the effect of incision thresholds for river incision to occur (Lague, 2014), albeit numerical simulations have shown that the use of a slope exponent n (Eq. (1)) greater than unity can reproduce erosion rates obtained with models explicitly accounting for incision thresholds (Gasparini and Brandon, 2011).

A state-of-the-art river incision model to simulate the impact of hydrological variability on river incision efficiency is the Stochastic Threshold Stream Power Model (ST-SPM) (Crave and Davy, 2001; Deal et al., 2018; Lague et al., 2005; Snyder et al., 2003; Tucker and Bras, 2000). The ST-SPM explicitly acknowledges the existence of a shear stress threshold (τ_c) which must be overcome to entrain sediment and bedrock. By incorporating stochasticity of the river discharge in the equation, the ST-SPM enables to simulate the frequency of erosive events and their impact on long-term river incision. We refer to literature for a full derivation of the ST-SPM (Crave and Davy, 2001; Deal et al., 2018; Lague et al., 2005; Snyder et al., 2003; Tucker and Bras, 2000).

When using the A-SPM, the effect of autogenic (caused by intrinsic river dynamics such as incision thresholds and changes in channel width) and allogenic (originating from the transient response of river dynamics to extrinsic changes such as climate variability) controls is assumed to be accounted for in the model parameters (K' , m and n). For example, it has been shown that incision thresholds translate into a slope exponent n greater than unity when applying the A-SPM (Lague, 2014). Notwithstanding empirical evidence supporting the A-SPM such as the scaling between drainage area and channel slope in steady state river profiles (Lague, 2014) or its capability to simulate transient river incision pulses

(Campforts and Govers, 2015), the lumped modelling approach of the A-SPM cannot be used to evaluate the role of autogenic or allogenic river response.

1.2.2. Stochastic-Threshold Stream Power Model

The Stochastic-Threshold Stream Power Model (ST-SPM, Crave and Davy, 2001; Deal et al., 2018; Lague et al., 2005; Snyder et al., 2003; Tucker and Bras, 2000) does simulate the impact of hydrological variability and incision thresholds on river incision and thus enables us to evaluate the role of autogenic or allogenic river response.

The ST-SPM is calculated in two components. The first component involves the formulation to calculate consecutive steps. First, instantaneous river incision (I , [$L t^{-1}$]) is calculated as:

$$I(Q^*) = KQ^{*\gamma}k_s^n - \psi \quad (4.a)$$

$$K = k_e k_t^\alpha k_w^{-\alpha} \bar{R}^{-m}; \psi = k_e \tau_c^\alpha \quad (4.b)$$

$$\gamma = \alpha\alpha(1 - \omega_s); m = \alpha\alpha(1 - \omega_b); n = \alpha\beta \quad (4.c)$$

in which Q^* represents the dimensionless normalized daily discharge calculated by dividing daily discharge Q [$L^3 t^{-1}$] by mean-annual discharge \bar{Q} [$L^3 t^{-1}$], k_e [$L^{2.5} t^{-2} m^{-1.5}$] is the erosional efficiency constant, \bar{R} [$L t^{-1}$] is the mean annual runoff, α is the shear stress exponent reflecting the nature of the incision process (Whipple et al., 2000), ψ is the threshold term [$L t^{-1}$], and k_t , k_w , α , β , ω_a and ω_b are channel hydraulic parameters described in Table 1.

In a second component, long term river erosion/incision is calculated by multiplying the instantaneous river incision, I , calculated for a discharge of a given magnitude (Q^*) with the probability for that discharge to occur ($pdf(Q^*)$, see section 5.1.2) and subsequently integrating this product over the range of possible discharge events specific to the studied timescale (DiBiase and Whipple, 2011; Lague et al., 2005; Scherler et al., 2017; Tucker and Bras, 2000; Tucker and Hancock, 2010):

$$E = \int_{Q_c^*}^{Q_m^*} I(Q^*) pdf(Q^*) dQ^* \quad (5)$$

in which Q_c^* is the minimum normalized discharge which is required to exceed the critical shear stress (τ_c) and Q_m^* is the maximum possible normalized discharge over the time considered.

1.2.3. Runoff-based Stream Power Model

A third river incision model further discussed in derived from the paper ST-SPM, is the Runoff-based SPM (R-SPM). The R-SPM shares its derivation with similar to the ST-SPM but assumes river that the incision thresholds to be negligible ($\psi = 0$) and that discharge to be constant over time ($Q^* = 1$), simplifying Eq. (5) to:

Formatted Table

Formatted: Font: Italic, Font color: Text 2

Formatted: Font: Italic

Formatted: Font: Italic

Formatted: Indent: First line: 1,27 cm

Formatted: Font color: Auto

$$E = Kk_s^n \quad (6)$$

In the following sections, we first describe the study area, characterize the lithological configuration by developing a lithological erodibility index and compile a database to represent runoff variability. Second, we present the methods and assumptions used for calibrating and simulating river incision. In a third section, the modelling results are presented: we start by evaluating the impact of lithological heterogeneity on river incision rates using an area-based river incision model (A-SPM). We then evaluate to what extent the variability in denudation rates can be explained by spatial and/or temporal runoff variability and the existence of incision thresholds using the R-SPM and ST-SPM. In a final section, we discuss our findings, highlight the implications of our work and discuss further perspectives.

3.1. Methods

3.1.1. Optimization of model parameters

The presented forms of the stream power model all depend on river steepness, k_w , known to correlate well with E_{CRN} (DiBiase et al., 2010; Quimet et al., 2009; Scherler et al., 2017; Vanaecker et al., 2015). Moreover, E_{CRN} integrate over timespans that average out the episodic nature of erosion and over spatial extents large enough to average out the stochastic nature of hillslope processes. Moreover, if we assume that river incision occurs at rates of catchment-wide denudation, E_{CRN} can be used to constrain models of river incision (cfr. DiBiase and Whipple, 2011; Scherler et al., 2017).

To optimize model parameters, we maximize the Nash Sutcliffe model efficiency (NS, Nash and Sutcliffe, 1970) between observed erosion (O) and modelled river incision (M):

$$NS = 1 - \frac{\sum_{i=1}^{i=nb} (O_i - M_i)^2}{(O_i - \bar{O})^2} \quad (7)$$

where nb is the number of E_{CRN} samples. The NS coefficient ranges between $-\infty$ and 1 where 1 indicates optimal model performance explaining 100% of the data variance. When $NS = 0$, the model is as good a predictor as the mean of the observed data. When $NS \leq 0$, model performance is unacceptably low. The NS coefficient has been developed in the framework of hydrological modelling but has been applied in wide range of geomorphologic studies (e.g. Jelinski et al., 2019; Nearing et al., 2011).

3.2. River incision models

In a first set of model runs, we evaluate the performance of the A-SPM in predicting E_{CRN} rates. To account for rock strength variability Eq. (2) is rewritten as:

$$E = k_\alpha \bar{L}_R k_{SR}^{*n} \quad (8)$$

where k_α ($L^{1-2m} t^{-1}$) is the erosional efficiency parameter and \bar{L}_R is a dimensionless catchment mean lithological erodibility value.

In a second set of model runs, we evaluate whether the R-SPM can explain regional differences in river incision that cannot be attributed to topographical and/or lithological variations. To account for rock strength variability Eq. (6) is rewritten as:

Field Code Changed

Formatted: English (United States)

Formatted: English (United States)

$$E = K \bar{L}_R k_{sr}^{-n} \quad (9)$$

An overview of the parameter values required to solve the R-SPM is given in Table 1. Only the value of k_r is based on a regional calibration of the hydraulic geometry scaling (see section 4.4). Other parameters are set to commonly used values (Deal et al., 2018; DiBiase and Whipple, 2011; Scherler et al., 2017). Actively incising bedrock channels are often covered by a layer of sediment. Therefore, we assume that river incision is scaled to the bed shear stress similar to bedload transport (Meyer-Peter and Müller, 1948) and set a to $3/2$ (cfr. DiBiase and Whipple, 2011; Scherler et al., 2017). We use the Darcy-Weisbach resistance relation and coefficients ($\alpha = \beta = 2/3$) to calculate shear stress exerted by the river flow on its bed and assume a friction factor of 0.08 resulting in a flow resistance factor k_r of $1000 \text{ kg m}^{-2/3} \text{ s}^{-4/3}$ (e.g. Tucker, 2004). The use of Darcy-Weisbach friction coefficients in combination with $a = 3/2$ results in a value for the slope exponent equal to unity ($n = 1$, see Eq. (4)). Based on these theoretical derivations, we fix n to unity when constraining the R-SPM. Note that this contrasts to the first set of model runs (application of the A-SPM), where we allow n to vary. By fixing n to unity, we want to verify whether spatial variations in runoff (incorporated in K from Eq. 9) can explain variations in incision rates otherwise ascribed to non-linear river incision. The only parameter not fixed to a constant value is the erosivity coefficient k_e , which is optimized by maximizing the NS coefficient (see section 3.1).

Formatted: Font: Italic

In a final set of model runs, we apply the ST-SPM (Eq. (4)) which is adjusted to account for rock strength variability as:

$$I = K_{st} \bar{L}_R Q^{a+k_{sr}^{-n}} \psi \quad (10)$$

To derive long term erosion rates (E), Eq. (10) is integrated over the probability density function of discharge magnitudes (Eq. (5)) which requires values for the lower (Q_e^*) and the upper (Q_m^*) limit of the integration interval. Constraining Q_m^* is difficult based on observational records alone as they might miss some of the most extreme flooding events. However, when simulating incision rates over long time spans and thus considering long return times of Q_m^* (>1000 y), the solution of Eq. (5) is insensitive to the choice of Q_m^* (Lague et al., 2005). We therefore set Q_m^* to *infinity* in all our model runs. The critical discharge (Q_e^*) for erosion to occur can be derived from Eq. (10) by setting I equal to 0:

$$Q_e^* = \left(\frac{\psi}{K_{st} \bar{L}_R k_{sr}^{-n}} \right)^{\frac{1}{\beta}} \quad (11)$$

The impact of spatial variations in runoff and discharge variability is evaluated by setting \bar{R} and k respectively to the catchments specific values or the mean of these values (listed in Table 2). Parameters left free during optimization are the erosivity coefficient k_e and the critical shear stress τ_e^* . Parameter values of both variables are optimized by maximizing the NS coefficient (see section 3.1).

4.2. Study area

2.1. Geology

4.1.2.1.1. Tectonics and geomorphic setting

Formatted: Heading 3

The Paute River is a 6530 km² transverse drainage basin: (2.9°S, 79°W); it has its source in the eastern flank of the Western Cordillera, traverses the Cuenca intramontane basin and cuts through the Eastern Cordillera before joining the Santiago river, a tributary of the Amazon (Figure 1; Hungerbühler et al., 2002; Steinmann et al., 1999). The Paute basin has a moderate relief with 90% of the slopes having hillslope gradients below 0.30 m m⁻¹ (Vanacker et al., 2007). Where the Paute River cuts through the Eastern Cordillera, the topography is rough with steep hillslopes (90th percentile of slope gradients = 0.40 m m⁻¹) and deeply incised river valleys (Guns and Vanacker, 2013).

Oblique accretion of terranes to the Ecuadorian margin during the Cenozoic, resulted in a diachronous exhumation and cooling history along the Ecuadorian Cordillera system (Spikings et al., 2010). South of 1°30' S, where the Paute basin is situated, three distinct stages of elevated cooling have been reported during the Paleogene at 73-55 Ma, 50-30 Ma and 25-18 Ma, corresponding to a total cooling from ca. 300°C to ca. 60°C (Spikings et al., 2010). In the Western Cordillera, no elevated cooling is observed during the Paleogene and extensional subsidence of the Cuenca basin allowed synsedimentary deposition of marine, lacustrine and terrestrial facies until the Middle to Late Miocene (Hungerbühler et al., 2002; Steinmann et al., 1999). The collision between the Carnegie ridge and Ecuadorian trench at some time between the Middle to Late Miocene (Spikings et al., 2001) resulted in uplift of the Western Cordillera and caused a tectonic inversion of the Cuenca basin (Hungerbühler et al., 2002; Steinmann et al., 1999). Based on a compilation of mineral cooling ages available for the Cuenca basin, Steinman et al. (1999) estimated a mean rock uplift rate of ca. 0.7 mm yr⁻¹ and a corresponding surface uplift of ca. 0.3 mm yr⁻¹ from 9 Ma to present.

The Paute basin is characterized by a tropical mountain climate (Muñoz et al., 2018). Despite the presence of mountain peaks up to ca. 4600 m (Figure 1), the region is free of permanent snow and ice (Celleri et al., 2007). The region's precipitation is regulated by its proximity to the Pacific Ocean (ca. 60 km distance), the seasonally shifting of the Intertropical Convergence Zone (ITCZ), and the advection of continental air masses sourced in the Amazon basin, giving rise to an orographic precipitation gradient along the eastern flank of the Eastern Cordillera (Bendix et al., 2006). Total annual precipitation is highly variable within the Paute basin and ranges from ca. 800 mm in the center of the basin, at the center of the Inter-Andean valley, up to ca. 3000 mm in the eastern parts of the catchment (Celleri et al., 2007; Mora et al., 2014).

2.1.1. Lithological strength

The erodibility map was developed using an empirical, hybrid classification method: it combines information on the lithological composition (Aalto et al., 2006) and the age of non-igneous formations assuming higher degrees of diagenesis and increased lithological strength for older formations (cfr. Kober et al., 2015). Adding age information to evaluate lithological strength has advantages because lithostratigraphic units are typically composed of different lithologies but mapped as a single entity because of their stratigraphic age. The lithological erodibility (L_E) is calculated as:

$$L_E = \frac{2}{7}L'$$
$$L' = \begin{cases} \frac{(L_A + L_L)}{3}, & \text{non-igneous rocks} \\ \frac{L_L}{2}, & \text{igneous rocks} \end{cases} \quad (7)$$

300 With L_A a dimensionless erodibility index based on stratigraphic age (Figure 2.a), and L_L a dimensionless erodibility index based on lithological strength (Table 1), similar to the erodibility indices published by Aalto (2006). Note that L_A varies between 1 (Carboniferous) to 6 (Quaternary) whereas L_L ranges between 2 (e.g. granite) to 12 (e.g. unconsolidated colluvial deposits). The lithological strength thus has a double weight, resulting in L' values ranging between 1 and 6. For igneous rocks, only L_L is considered assuming that the lithological strength of igneous rocks remains constant over time. For river incision parameters to be comparable to other published ranges, L_E is finally scaled around one by multiplying L' with 2/7. L_E therefore ranges between 2/7 and 14/7. A description of the lithological units, the age of the formations and their lithological strength (L_A , L_L and L_E) is provided in Table S3.

305 Using Eq. 7, we developed the erodibility map of Ecuador (Figure S1) and the Paute catchment (Figure 2.c), based on the 1M geological map of Ecuador (Egüez et al., 2017). The lithological erodibility values were compared with field measurements (n = 9) of bedrock rheology by Basabe (1998). An overview of measured lithological strength values is provided in Table S4 (e.g. uniaxial compressive strength). Figure 2.b shows good agreement ($R^2 = 0.77$) between the lithological erodibility index, L_E , and the measured uniaxial compressive strength.

315 **4.2.2.2. CRN-derived erosion-denudation rates**

Catchment-wide denudation rates are derived from in-situ produced ^{10}Be concentrations in river sand. At the outlet of 30 sub-catchments (Figure 1, Table 2), fluvial sediments were collected. We refer to Vanacker et al. (2015) for details on sample processing and derivation of CRN denudation rates taking into account altitude dependent production, atmospheric scaling and topographical shielding (Dunai, 2000; Norton and Vanacker, 2009; Schaller et al., 2002). CRN concentrations are not corrected for snow or ice coverage because there is no evidence of glacial activity during the integration time of CRN-derived denudation rates (Vanacker et al., 2015). Three data points were excluded from model optimization runs: two catchments with basin area smaller than 0.5 km² (MA1 and SA), and one catchment with an exceptionally low ^{10}Be concentration that can be attributed to recent landslide activity (NG-SD; see Vanacker et al., 2015).

320 ~~mean erosion rates are derived from in-situ produced ^{10}Be concentrations in river sand. At the outlet of 30 sub-catchments indicated in Figure 1 and Table 2 (dataset published in Vanacker et al., 2015), fluvial sediments were collected. For the ^{10}Be analysis, pure quartz was extracted from the 0.25–2.5 mm grain size fraction of the alluvial material. The ^{10}Be was extracted from purified sand using standard methods described in von Blanckenburg et al. (1996, 2004) and the $^{10}\text{Be}/^9\text{Be}$ ratios were measured in BeO targets with accelerator mass spectrometry at ETH Zürich. We refer to Vanacker et al. (2015) for details on sample processing and derivation of CRN erosion rates taking into account altitude dependent production, atmospheric scaling and topographical shielding (Dunai, 2000; Norton and Vanacker, 2009; Schaller et al., 2002). CRN concentrations are not corrected for snow or ice coverage because there is no evidence of glacial activity during the integration time of CRN-derived erosion rates (Vanacker et al., 2015). Note that three data points were excluded from model optimization runs: two catchments with basin area smaller than 0.5 km² (MA1 and SA), and one catchment with an exceptionally low ^{10}Be concentration that can be attributed to recent landslide activity (NG-SD; see Vanacker et al., 2015).~~

325 **4.3. River steepness**

335 **2.3. River steepness is calculated morphology**

Formatted: Font: Italic

Based on a gap-filled SRTM v3 DEM with a 1 arc second resolution (Farr et al., 2007; NASA JPL, 2013), we calculate river steepness for all channels having with drainage areas of more than $\geq 0.5 \text{ km}^2$ and is averaged average it over 500 m reaches, based on a gap-filled SRTM v3 DEM with a 1 arc second resolution (Farr et al., 2007; NASA JPL, 2013). Because the The optimized concavity θ for the Paute catchment (0.42; Text S1), is close to the frequently used value of 0.45, we fix concavity to the reference value of 0.45 and report river steepness as normalized river steepness (k_{sn}) in the remainder of this paper. The spatial pattern of k_{sn} values (Figure 3) is a result of the transient geomorphic response to river incision initiated at the Andes Amazon transition zone (Vanacker et al., 2015). To evaluate the extent to which transient river features influence simulated erosion denudation rates, chi-plots (χ) for all studied sub catchments are calculated following Royden and Perron, (2013) and given in the supplementary materials (Text S1; Figure S4; Royden and Taylor Perron, 2013).

To constrain the value of k_w , used in the process-based incision models (Eqs. 4 and 6), we calibrate the relationship between bankfull river width (W_b) and discharge (Leopold and Maddock, 1953):

$$W_b = k_w \bar{Q}^{\omega_b} \quad (8)$$

in which $k_w [L^{1-3\omega_b} t^{\omega_b}]$ and ω_b are scaling parameters regulating the interaction between mean annual discharge \bar{Q} and incision rates (Eq. 4). We constrain k_w by analysing downstream variations in bankfull channel width for a fraction of the river network (cfr. Scherler et al., 2017). River sections are selected based on the availability of high-resolution optical imagery in Google Earth, and river width was derived using the ChanGeom toolset (Fisher et al., 2013a; figure S5).

The power-law fit between Q and W yields a value of 0.43 for the scaling exponent, ω_b , with an R^2 of 0.51 (Figure 4). This value lies within the range of published values 0.23-0.63 (Fisher et al., 2013b; Kirby and Ouimet, 2011). To maintain a dimensionally consistent stream power model, ω_b was fixed to a value of 0.55. When doing so, the fit remains good ($R^2 = 0.5$) and we obtained a k_w value of $3.7 \text{ m}^{-0.65} \text{ s}^{0.55}$ that is used in the remainder of the paper.

4.4. River channel width

Bankfull river width (W_b) varies with discharge as (Leopold and Maddock, 1953):

$$W_b = k_w \bar{Q}^{\omega_b} \quad (12)$$

In which $k_w [L^{1-3\omega_b} t^{\omega_b}]$ and ω_b are scaling parameters regulating the interaction between mean annual discharge \bar{Q} and incision rates (Eq. (4)). We constrain k_w by analysing downstream variations in bankfull channel width for a fraction of the river network (cfr. Scherler et al., 2017). River sections are selected based on the availability of high-resolution optical imagery in Google Earth, and river width was derived using the ChanGeom toolset (Fisher et al., 2013a; figure S5).

The power-law fit between Q and W yields a value of 0.43 for the scaling exponent, ω_b , with an R^2 of 0.51 (Figure 3). This value lies within the range of published values 0.23-0.63 (Fisher et al., 2013b; Kirby and Ouimet, 2011). To maintain a dimensionally consistent stream power model, ω_b was fixed to a value of 0.55. When doing so, the fit remains good ($R^2 = 0.5$) and we obtained a k_w value of $3.7 \text{ m}^{-0.65} \text{ s}^{0.55}$ that is used in the remainder of the paper.

5. Environmental drivers

Formatted: Font: Italic

Formatted: Font: Italic

Formatted: Font: Italic

Formatted: Font: Italic

5.1.1.1.1. Rainfall

2.4. The mean-catchment Runoff variability

Evaluating the role of spatial and temporal runoff variability (Eqs. 5 and 6) requires estimates of catchment specific runoff (\bar{R}) and the probability density function of daily discharge ($pdf(Q^*)$) are required to simulate long-term river incision with the ST-SPM, spatial variability) and discharge (temporal variability). Although measured runoff data and discharge records are available for the Paute basin (Molina et al., 2007; e.g. Mora et al., 2014; Muñoz et al., 2018), the monitoring network of about 20 meteorological and 25 existing hydrological stations having at least 10 years of data does not allow to capture the spatial variability present in the different sub-catchments of the 6530 km² basin (Figure 1). We therefore Paute basin (Figure 1). To estimate runoff variability for all 30 sub-catchments, we use hydrological data derived in the framework of the Earth2Observe Water Resource Reanalysis project (WRR2; Schellekens et al., 2017) available from 1979 to 2014. Specifically, we use the hydrological data calculated with the global water model WaterGAP3 (Water – Global Assessment and Prognosis: Alcamo et al., 2003; Döll et al., 2003) at a spatial resolution of 0.25° and a daily temporal resolution (earth2observe.eu). In the following paragraphs, we explain how we derive (i) a high-resolution runoff map by spatially downscaling this coarse data and (ii) catchment-specific magnitude frequency distributions of discharge ($pdf(Q^*)$) characterising the temporal variability of runoff.

2.4.1. Spatial runoff patterns

More specifically, we use the hydrological data calculated with the global water model WaterGAP3 (Water – Global Assessment and Prognosis: Alcamo et al., 2003; Döll et al., 2003). Through a sequence of storage equations, WaterGAP3 simulates the terrestrial part of the A global hydrological cycle-reanalysis dataset such as WaterGAP has been calibrated against data from 1319 river discharge stations monitored by the Global Runoff Data Centre (GRDC) (Schmied et al., 2014), of which 10 stations are situated in the Ecuadorian Andes. In the framework of WRR2, the WaterGAP3 is forced with ERA-Interim data and the Multi-Source Weighted-Ensemble precipitation (MSWEP) product (Beek et al., 2017).

5.1.1.1.1.1. Spatial runoff patterns

Using a global hydrological reanalysis dataset such as WaterGAP has the advantage of providing provides daily runoff data over several decades and makes our methodology transferable to other regions. However, a spatial resolution of 0.25° is not always sufficient insufficient to represent highly variable regional trends in water cycle dynamics over mountainous regions (Mora et al., 2014) and in small catchments. Therefore, we downscale the Ecuadorian WaterGAP3 data to a resolution of 2.5 km by amalgamating rain gauge data with the reanalysis product. The procedure consisted of the following steps: and is presented in Figures 5 and 6:

- (i) The relationship between precipitation (P) and runoff (R) is constrained from the fit between monthly mean values for P and R available for all Ecuadorian WaterGAP 0.25° pixels (Figure 4)(Figure 5).
- (ii) A high resolution mean annual precipitation map (P_{RIPW}) is calculated by downscaling the WaterGAP precipitation data (P) using a series of rain gauge observations (338 stations, 1990-2013) from the Ecuadorian national meteorological service (INAMHI; available from <http://www.serviciometeorologico.gob.ec/biblioteca/>). A residual

inverse distance weighting (RIDW) method is applied to amalgamate mean annual gauge data with the mean annual WaterGAP3 precipitation map. First, the differences between the gauge and WaterGAP data are interpolated using an IDW method (Figure S6). Second, the resulting residual surface is added back to the original P data. A similar approach is often applied to integrate gauge data with satellite products and we refer to literature for further details on its performance (e.g. Dinku et al., 2014; Manz et al., 2016). A high resolution mean annual precipitation map (P_{RIDW}) is calculated by downscaling the WaterGAP precipitation data (P) using a series of rain gauge observations (338 stations, 1990–2013) collected by the Ecuadorian national meteorological service (INAMHI; available from <http://www.serviciometeorologico.gob.ec/biblioteca/>). A residual inverse distance weighting (RIDW) method is applied to amalgamate mean annual gauge data with the mean annual WaterGAP3 precipitation map. First, the differences between the gauge and WaterGAP data are interpolated using an IDW method (Figure 5). Second, the resulting residual surface is added back to the original P data. A similar approach is often applied to integrate gauge data with satellite products and we refer to literature for further details on its performance (e.g. Dinku et al., 2014; Manz et al., 2016). Figure 6.a shows P for the Paute region, and Figure 6.c its downscaled equivalent (P_{RIDW}).

- (ii) All daily Figure 6.a shows P for the Paute region, and Figure 6.c its downscaled equivalent (P_{RIDW}).
- (iii) Daily precipitation data (12784 daily grids between 1979 and 2014) are downscaled to 2.5 km using the ratio between P_{RIDW} and P , thereby assuming that the mean annual correction for precipitation also holds for daily precipitation patterns.
- (iv) The relationship between P and R (Figure 4)(Figure 5) is used to derive downscaled daily runoff values from the downscaled precipitation data for every day between 1979 and 2014.

The mean annual runoff map for the Paute basin is shown in Figure 6. Figure 6.b and its downscaled equivalent in Figure 6.d. Mean annual values are further used to calculate mean catchment runoff (\bar{R}) and the discharge variability (next paragraph) for every sub-catchment described in Table 2. The mean catchment specific runoff averaged for all catchments equals $0.82 \pm 0.35 \text{ m yr}^{-1}$.

2.4.2. Frequency magnitude distribution of orographic discharges

Figure 6.d. Mean annual values are further used to calculate mean catchment runoff (\bar{R}) and the discharge variability (next paragraph) for every sub-catchment described in Table 2. The mean catchment specific runoff averaged for all catchments equals $0.82 \pm 0.35 \text{ m yr}^{-1}$.

5.1.2.1.1. Frequency magnitude distribution of orographic discharges

Runoff variability is typically casted in terms of spatial runoff variability (section 2.4.1). However, also the temporal pattern of runoff might influence river incision and is typically represented by discharge magnitude frequency distributions. Constraining the shape of these distributions is important, because the number of large storm events determine the frequency by which thresholds for river incision to occur are exceeded (see section 1.2.2 and references therein).

The probability distribution of discharge magnitudes consists of two components: at low discharges, the frequency of events increases exponentially with increasing discharge (Lague et al., 2005) whereas at high discharge, the frequency of

435 events decreases with increasing discharge following a power law distribution (Molnar et al., 2006). An inverse gamma distribution captures this hybrid behaviour and can be written as (Crave and Davy, 2001; Lague et al., 2005):

$$pdf(Q^*) = \frac{k^{k+1}}{\Gamma(k+1)} e^{-\frac{k}{Q^*}} Q^{*-(2+k)} \quad (9)$$

440 in which Γ is the gamma function and k is a discharge variability coefficient, k represents the scale factor of the inverse gamma distribution and $(k+1)$ the shape factor. Previous studies used a single, average k -value to characterize regional discharge: DiBiase and Whipple (2011) use a constant k value for the San Gabriel mountains whereas Scherler et al. (2017) use a constant k value for high and low discharge but distinguish between Eastern Tibet and the Himalaya. However, given the strong variation in temporal precipitation regimes in the Paute basin (Celleri et al., 2007; Mora et al., 2014) ~~and the recently recognized role of spatial hydrological variability on river incision rates (Deal et al., 2018)~~, we explicitly evaluated the role of temporal runoff variability by calculating catchment-specific discharge distributions from the WRR2 WaterGAP dataset.

445 Daily variations in discharge at the sub-catchment outlets (Figure 1) were calculated by weighing flow accumulation with runoff (R_{RDW} , see section 5.1.1). For every catchment, the complementary cumulative distribution function ($ccdf$) of the daily discharge was fitted through the observed discharge distribution as:

$$ccdf(Q^*) = \Gamma(k/Q^*, k+1) \quad (10)$$

450 where Γ is the lower incomplete gamma function. Figure 7 illustrates the fit between the WaterGAP derived discharge distribution and the optimized $ccdf$ for one of the catchments. Site specific discharge variability values (k) are calculated for all catchments and listed in Table 2. Obtained k -values range between 0.8 and 1.2 with a mean of 1.01 ± 0.12 .

3. Methods

5.1. The presented river incision models (A-SPM, R-SPM and ST-SPM in section 1.2) ~~Geology: seismic activity and lithological strength~~

455 We aim to develop a new erodibility map for Ecuador, using an empirical, hybrid classification method. Therefore, we combine all depend on river steepness, k_{gr} , known to correlate well with E_{CRN} (DiBiase et al., 2010; Ouimet et al., 2009; Scherler et al., 2017; Vanacker et al., 2015), ~~information on the lithological composition (Aalto et al., 2006) and the age of non-igneous formations assuming higher degrees of diagenesis and increased lithological strength for older formations (cfr. Kober et al., 2015).~~ Adding age information to evaluate lithological strength has advantages because lithostratigraphic units are typically composed of different lithologies but mapped as a single entity because of their stratigraphic age. The lithological erodibility (L_L) is calculated as:

$$L_L = \frac{2}{7} L^t \quad (15)$$

$$L^t = \begin{cases} \frac{(L_A + L_L)}{3}, & \text{non-igneous rocks} \\ \frac{L_L}{2}, & \text{igneous rocks} \end{cases}$$

Field Code Changed

Formatted: English (United States)

Formatted: English (United States)

465 With L_A a dimensionless erodibility index based on stratigraphic age (Figure 7), and L_L a dimensionless erodibility index based on lithological strength (Table 1), similar to the erodibility indices published by Aalto (2006). Note that L_A varies between 1 (Carboniferous) to 6 (Quaternary) whereas L_L ranges between 2 (e.g. granite) to 12 (e.g. unconsolidated colluvial deposits). The lithological strength thus has a double weight, resulting in L' values ranging between 1 and 6. For igneous rocks, only L_L is considered assuming that the lithological strength of igneous rocks remains constant over time. For river incision parameters to be comparable to other published ranges, L_L is finally scaled around one by multiplying L' with $2/7$. L_E therefore ranges between $2/7$ and $14/7$. A description of the lithological units, the age of the formations and their lithological strength (L_A , L_L and L_B) is provided in Table S3.

470 Using Eq. (15), we developed a detailed erodibility map of Ecuador (Figure S1), based on the 1M geological map of Ecuador (Egüez et al., 2017). The erodibility map was validated by comparing the L_E values. Moreover, E_{CRN} integrate over timespans that average out temporal fluctuations of denudation rates and over spatial extents which are sufficient to average out the erratic nature of hillslope processes. Therefore, E_{CRN} can be used to constrain models of river incision provided a set of assumptions that we first describe below.

3.1. CRN-derived denudation rates to calibrate river incision

475 The use of CRN-derived denudation rates to calibrate river incision relies on three main assumptions, summarized by Scherler et al. (2017). A first assumption is that the catchment wide denudation rates derived from CRN are representative for long term fluvial incision. Positive correlations between river steepness, k_{sp} , and CRN-derived denudation rates support this assumption (Vanacker et al., 2015), except for very small catchments where CRN-derived denudation rates are sensitive to the occurrence of deep-seated landslides. A second assumption is that runoff and rock uplift are uniform within the individual catchments. Given the size of the studied basins, this assumption seems to be reasonable. A third assumption, in particular when using the process-based R-SPM and ST-SPM, is that the runoff data, used to calibrate the incision parameters is representative over the time span which CRN data integrate (1-100 kyr). This is a challenging assumption, given the contemporaneous nature of the available hydrological data. While spatial patterns of runoff, mainly controlled by orographic precipitation, could be assumed broadly similar over the integration time of CRN-derived denudation, this is not necessarily true for the temporal variation in runoff. We will revisit the validity and implications of these three assumptions in the discussion section of this paper.

3.2. River incision models

490 with field measurements ($n = 9$) of bedrock rheology by Dasabe (1998). An overview of measured lithological strength values is provided in Table S4. Figure 9 shows good agreement ($R^2 = 0.77$) between the lithological erodibility index, L_E , and the measured uniaxial compressive strength confirming the validity of the classification method.

495 To evaluate whether seismic activity could explain differences in river incision rates, we calculated catchment mean Peak Ground Acceleration (PGA) with an exceedance probability of 10% in 50 years. PGA values are derived from a recently published hazard assessment for South America (Petersen et al., 2018) combining assembled catalogues of earthquake frequency and size, fault geometries, seismicity rate models and ground motion models all integrated in the Global Earthquake Model (GEM; Pagani et al., 2014). PGA (g) only varies marginally within the study area (Figure 11, Table 2). Therefore, we did not

Formatted: Font: Italic

consider seismic activity in the remainder of this paper although its influence should be evaluated when simulating river incision rates at larger spatial scales characterized by a stronger variability in PGA.

6. Results

6.1. Empirical river incision model (A-SPM)

In a first set of model runs (Table 4), we evaluate the performance of the area-based SPM (A-SPM) in predicting E_{CRN} rates. To account for rock strength variability Eq. 2 is rewritten as:

$$E = k_a \overline{L_E} k_{sn}^n \quad (11)$$

where $k_a (L^{1-2m})$ is the erosional efficiency parameter and $\overline{L_E}$ is a dimensionless catchment mean lithological erodibility value. Given its empirical nature, where the effect of allogenic (e.g. runoff variability) and autogenic (e.g. incision thresholds and river width dynamics) controls of fluvial processes is integrated within the empirical scaling parameters (K , m and n), the A-SPM does not enable to identify the role of spatial or temporal runoff variability and incision thresholds.

In a second set of model runs, we evaluate to what extent more advanced SPMs can be used to understand the role of these allogenic and autogenic processes. We start by evaluating the performance of a runoff-based SPM (R-SPM). To account for rock strength variability Eq. 6 is rewritten as:

$$E = K \overline{L_E} k_{sn}^n \quad (12)$$

An overview of the parameter values required to solve the R-SPM is given in Table 1. Only the value of k_v is based on a regional calibration of the hydraulic geometry scaling (see section 2.3). Other parameters are set to theoretical values (reported by Deal et al., 2018; DiBiase and Whipple, 2011; Scherler et al., 2017). Actively incising bedrock channels are often covered by a layer of sediment (Shobe et al., 2017). Therefore, we assume that river incision is scaled to the bed shear stress as for bedload transport (Meyer-Peter and Müller, 1948) and set a to $3/2$ (cfr. DiBiase and Whipple, 2011; Scherler et al., 2017). We use the Darcy-Weisbach resistance relation and coefficients ($\alpha = \beta = 2/3$) to calculate shear stress exerted by the river flow on its bed and assume a friction factor of 0.08 resulting in a flow resistance factor k_r of $1000 \text{ kg m}^{-7/3} \text{ s}^{-4/3}$ (e.g. Tucker, 2004). The use of Darcy-Weisbach friction coefficients in combination with $a = 3/2$ results in a value for the slope exponent equal to unity ($n = 1$, see Eq. 4). Based on these theoretical derivations, we fix n to unity when constraining the R-SPM. Note that this contrasts to the first set of model runs (application of the A-SPM), where we allow n to vary. By fixing n to unity, we want to verify whether spatial variations in runoff (incorporated in K from Eq. 12) can explain variations in incision rates otherwise ascribed to non-linear river incision. The only parameter not fixed to a constant value is the erosivity coefficient k_e , which is optimized as described in section 3.3.

In a final set of model runs, we apply the Stochastic-Threshold SPM (ST-SPM) to evaluate the role of temporal precipitation variability and thresholds for incision (Eq. 4). Here, we adjust the ST-SPM to account for rock strength variability as:

$$I = K \overline{L_E} Q^{\gamma} k_{sn}^n - \psi \quad (13)$$

Formatted: Font: Italic

525 To derive long-term erosion rates (E), Eq. 13 is integrated over the probability density function of discharge magnitudes (Eq. 5) which requires values for the lower (Q_c^*) and the upper (Q_m^*) limit of the integration interval. Constraining Q_m^* is difficult based on observational records alone as they might miss some of the most extreme flooding events. However, when simulating incision rates over long time spans and thus considering long return times of Q_m^* (>1000 y), the solution of Eq. 5 is insensitive to the choice of Q_m^* (Lague et al., 2005). We therefore set Q_m^* to *infinity* in all our model runs. The critical discharge (Q_c^*) for erosion to occur can be derived from Eq. 13 by setting I equal to 0:

$$Q_c^* = \left(\frac{\psi}{K_{st} \bar{L}_E k_{sn}^n} \right)^{\frac{1}{n}} \quad (14)$$

The impact of spatial variations in runoff and discharge variability is evaluated by setting \bar{R} and k respectively to the catchment specific values or the mean of these values (listed in Table 2, Eq. 4). Parameters left free during optimization are: the erosivity coefficient k_e and the critical shear stress τ_c^* . Parameter values of both variables are optimized as described in section 3.3.

535 3.3. Optimization of model parameters

We propose three metrics to evaluate the performance of the different river incision models. A first one is the commonly used model error (ME):

$$ME = \sum_{i=1}^{i=nb} \sqrt{\left(\frac{O_i - M_i}{\sigma_i} \right)^2} \quad (15)$$

540 where nb is the number of E_{CRN} data points, O_i are the catchment specific measured E_{CRN} denudation rates, M_i represents the catchment specific modelled river incision and σ_i represents the catchment specific standard deviation on E_{CRN} . The advantage of the ME is that it explicitly incorporates the error on the analytical data (E_{CRN}) by weighing the model error with the analytical error. However, errors on CRN data are heteroscedastic: they systematically increase with increasing denudation rates. Although the ME thus provides a good metric to evaluate overall model performance, the metric is not well suited to optimize model parameters in an optimization procedure: too much weight will be given on optimization of the model in the lower regime of the denudation spectrum where measured errors on E_{CRN} are low whereas higher measured E_{CRN} data will not be approximated well because of large associated errors. To compensate for the effect of heteroscedasticity we rescale values O_i , M_i and E_i using a logarithm with base 10 when calculating ME (Herman et al., 2015). In this paper, ME will be used to evaluate model performance, but not to optimize model parameters.

550 A second metric is the coefficient of determination, R^2 . Contrary to ME , R^2 evaluates the explained variance of the model giving all observations the same weight, regardless their analytical error. However, when model parameters result in an offset between simulated and observed data (i.e. the intercept of the fit), this can still result in a high R^2 .

We therefore use the Nash Sutcliff model efficiency to optimize model parameters (NS, Nash and Sutcliffe, 1970):

$$NS = 1 - \frac{\sum_{i=1}^{i=nb} (O_i - M_i)^2}{(O_i - \bar{O})^2} \quad (16)$$

The NS coefficient ranges between $-\infty$ and 1 where 1 indicates optimal model performance explaining 100 % of the data variance. When $NS = 0$, the model is as good a predictor as the mean of the observed data. When $NS <= 0$; model performance is unacceptably low. The NS -coefficient has been developed in the framework of hydrological modelling but has been applied in wide range of geomorphologic studies (e.g. Jelinski et al., 2019; Nearing et al., 2011).

4. ~~derived erosion rates (E_{CRN}).~~ Comparing model results with CRN-derived denudation rates

In the following sections, we compare simulated erosion rates, obtained with the river incision models presented in Eq. 11 – Eq. 13 with measured CRN-derived denudation rates. We start with the use of the A-SPM (Eq. 11) to evaluate the extent to which lithological variability controls denudation rates. Once the impact of lithological heterogeneity on river incision is clarified, we evaluate whether runoff variability and incision thresholds can explain variations in E_{CRN} derived denudation rates. To this end, two process-based river incision models are evaluated (the R-SPM and ST-SPM, presented in Eq. 12 and Eq. 13 respectively). Optimized parameters and model performance of all model scenarios are listed in Table 4. Best fit results of a selected number of model runs are presented in Figure 7 and Figure 8. An overview of model fits for all the scenarios listed in Table 4 is given in Figures S8, S9 and S10.

4.1. Area-based stream power model

In a first set of model runs we evaluate the use of an Area-Based Stream Power Model (A-SPM) to explain observed variations in CRN-derived denudation rates (E_{CRN}). We optimize river incision parameters for four scenarios (Table 4: A-SPM scenario's 1 – 4); in the first two scenarios, the slope exponent, n is left as a free parameter. In the second two scenarios, the slope parameter is fixed to unity ($n = 1$).

In A-SPM scenario 1 (Table 4, Figure 7.a), we assume a spatially uniform, long term river incision (E) is a power function of the normalized river steepness k_{sn} , scaled by an erodibility (\bar{L}_E fixed to 1 in Eq. 11) and leave the erosion efficiency coefficient (K'). By optimizing K' and the slope parameter n as free parameters during model optimization. The optimized fit between simulated erosion (E , Eq. 2) and E_{CRN} , K' and n are constrained is shown in Figure 7.a. The fit is surrounded by a lot of data scatter resulting in a NS model efficiency of 0.5, a R^2 of 0.5, a ME of 3.25 and an optimized value for n of 1.06 (Figure 12.a, Table 4). When including optimized values for K' and n of respectively $0.57 \text{ m}^{0.1} \text{ s}^{-1}$ and 1.12. The fit between simulated and measured denudation rates hints to the existence of a correlation between E_{CRN} and river incision rates. The fit shown in Figure 7.a, shows that modelled erosion rates for catchments with a low mean erodibility index (= high resistance to erosion) are mostly overpredicted (plotting below the 1:1 line) whereas modelled erosion rates of catchments with a high erodibility index are mostly underpredicted (plotting above the 1:1 line).

In A-SPM scenario 2 (Table 4, Figure 7.b), we quantify the impact of varying lithology by using catchment specific mean values for the lithological erodibility values (\bar{L}_E), in Eq. 11) and leaving k_n and n as free optimization parameters. The optimized fit between simulated erosion (E , Eq. 11) and E_{CRN} is shown in Figure 7.b. Optimization results in a NS model efficiency of 0.73, a R^2 of 0.73, a ME of 2.23 and optimized values for k_n and n of respectively $0.07 \text{ m}^{0.1} \text{ s}^{-1}$ and 1.64. Considering lithological erodibility strongly increases ($NS = 0.73$) and the optimized value of n equals 1.63.

To evaluate whether including spatially varying erodibility values also increases the predictive power of the river incision model, we performed a linear Bayesian regression analysis between E_{CRN} and the simulated long term river erosion

Formatted: Font color: Auto

Formatted: Font: Italic

590 *E*. Figure 13 shows that the posterior probability of linear regression coefficients close to one is higher and with less spread when considering spatially varying lithological erodibility values. Moreover, when *E* is only a function of k_{sr} , the Bayes factor equals 1.06, in comparison to a value of ca. 1400 when *E* is a function of both k_{sr} and \overline{L}_E (Table 4). This implies that a river incision model accounting for variable erodibility values is supported by the data (Jeffreys, 1998).

reduces data scatter surrounding the fit. The importance of lithological strength in controlling the A-SPM and the k_{sr} - E_{CRN} relation confirms that strong metamorphic and plutonic rocks erode at significantly slower rates than lithologies which are less resistant to weathering such as sedimentary/volcaniclastic deposits of loose volcanic mixtures. The empirical rock strength classification/erodibility index we developed appears to provide an appropriate scaling of relative rock strength: analysis of residuals did not reveal any significant relation of residuals with lithology.

600 When using spatially variable, catchment specific lithological erodibility values (\overline{L}_E) (Figure 12 (Figure 7.b), the *n* coefficient of the SPM is considerably larger than unity ($n = 1.6364$) and the k_{sr} - E_{CRN} relationship becomes non-linear, corroborating earlier findings documented in e.g. Gasparini and Brandon (2011). While this may be due to the fundamental properties of river incision and erosion processes, the shape of the relation may also be affected by spatial covariates other than lithology. In the following sections, we will investigate whether this nonlinear k_{sr} - E_{CRN} relationship can be explained by the presence of incision thresholds, variations in runoff, or a combination of both. To evaluate the impact of a variable *n* exponent on the performance of the empirical A-SPM, we executed two more model optimizations.

605 6.2. R-SPM and ST-SPM

In A-SPM scenario 3 (Table 4, Figure S8.c), we assume a spatially uniform lithology and erodibility (\overline{L}_E fixed to 1 in Eq. 11), fix *n* to 1 and only leave *K'* to be optimized as a free model parameter. With a NS model efficiency of 0.5, a R^2 of 0.5, a ME of 3.2 and an optimized value for *K'* of $1.00 \text{ m}^{0.1} \text{ s}^{-1}$, the model fit and performance is similar to the values obtained in scenario 1.

610 In A-SPM scenario 4 (shown in Table 4, Figure S8.d), lithological variability is considered (using catchment specific values for \overline{L}_E in Eq. 11), *n* is fixed to 1 *K'* is a free model parameter. With a NS model efficiency of 0.51, a R^2 of 0.56, a ME of 3.05 and an optimized value for *K'* of $1.4 \text{ m}^{0.1} \text{ s}^{-1}$, model performance is much lower than when leaving the slope exponent *n* as a free parameter (A-SPM scenario 2). This result shows that the apparent lack of a non-linear relationship between river steepness (k_{sr} , representing river incision rates) and E_{CRN} (scenario 1 and 2) can be explained by lithological heterogeneity which is masking the existence of such non-linear relationship. Once lithological variability is considered, a linear relationship with $n=1$ between k_{sr} values and E_{CRN} (this scenario, A-SPM 4) is performing less well than a river incision model where this relationship is non-linear (with $n > 1$).

4.2. Runoff-based and Stochastic-Threshold Stream Power Models

620 The previous analysis shows that the explanatory power of the A-SPM model, and therefore the k_{sr} - E_{CRN} relationship, strongly improves when considering spatial variations in lithological erodibility/lithology. Moreover, when considering variations in lithological erodibility, river incision is found to be non-linearly dependent on the channel slope (*S*), with $n = 1.63$. In a next step we evaluate whether this non-linear relation can be explained by spatial and/or temporal rainfall variability and/or the existence of thresholds for river incision (Table 5) (Table 4: R-SPM scenarios 1 - 2 and ST-SPM scenarios 1 - 8, Figure 8).

4.2.1. Runoff-based SPM (R-SPM)

In a first set of model runs, we evaluate the performance of the runoff-based Stream Power Model (R-SPM in combination with Eq. 12) to evaluate the role of spatially variable runoff using catchment specific values for mean runoff (Table 2). When R derived from the WaterGAP data, reported in Table 2 and shown in Figure 6).

In R-SPM scenario 1 (Table 4, Figure S9.a), lithological variability is not considered (\bar{L}_E fixed to 1, R-SPM Scenario 1 in Table 5), the R-SPM does not perform better (Eq. 12). With a NS model efficiency of 0.49 than a ME of 3.57 and an R^2 of 0.51, model performance is comparable to the regular A-SPM under uniform lithology with n fixed to 1 ($NS = 0.50$; Table 4). This illustrates that studying spatial runoff variability is not feasible when ignoring the confounding role of lithological erodibility on erosion/denudation rates. When

In R-SPM scenario 2 (Table 4, Figure 8a), lithological erodibility variability is considered (R-SPM Scenario 2 in Table 5), the use of the R-SPM results in a good fit between modelled river erosion and observed E_{CRN} rates (Figure 14.a). Although including catchment mean runoff improves the model fit ($R^2=0.75$), the R-SPM model overpredicts low erosion rates and underpredicts high erosion rates (Figure 14.a), resulting in a Nash Sutcliffe using catchment specific values for \bar{L}_E in Eq. 12). With a NS model efficiency of 0.70 which is lower than the R^2 , a ME of 2.61 and an R^2 of 0.75, model performance is close to that of the regular A-SPM under uniform lithology with $n \gg 1$ ($NS = 0.72$). This model simulation therefore suggests that spatial variations in runoff can account for the non-linearity in the k_{sp} - E_{CRN} relationship: while slope dependency in the R-SPM is fixed to unity (see derivation in Eq. 4a – 4c), the model is capable of explaining the spatial pattern in denudation rates. This implies that orographic rainfall and thus runoff gradient as shown in Figure 6 influences the efficiency of river incision. The offset between the R^2 (0.75) and NS (0.70) values can be attributed to the way in which these metrics work: whereas R^2 evaluates the goodness of the linear fit between modelled and measured observations, NS evaluates the absolute differences between modelled and observed denudation rates. Hence, for the NS model efficiency to be high, observations must fit on the 1:1 line (Figure 8.a). However, most of the simulated values for low denudation rates are overestimated when using the optimized parameter values of the R-SPM and plot below the 1:1 line (Figure 8a). Therefore, we conclude that the R-SPM performs well in predicting measured denudation rates albeit low denudation rates are overestimated resulting in a NS and ME value which are respectively slightly lower and higher than those of the empirical A-SPM. In the following section we evaluate whether introducing temporally variable runoff coefficients or/and incision thresholds can further improve the performance of a process-based river incision model.

4.2.2. Stochastic-Threshold SPM (ST-SPM)

In a second final series of model runs, we evaluated the performance of the ST-SPM. Table 5 provides use the Stochastic-Threshold Stream Power Model (ST-SPM, Eq. 13) to evaluate the role of spatially variable runoff (catchment specific R , reported in Table 2 and show in Figure 6) in combination with catchment specific runoff variability (k , reported in Table 2) and the presence of incision thresholds (τ_c in ψ in Eqs. 4 and 10). Table 4 reports details on the different model set-ups. In the first three scenarios, where ST-SPM is optimized to the observed E_{CRN} data considering all possible combinations (4) of uniform or spatially variable catchment mean runoff (R) and uniform or spatially variable catchment mean runoff variability (k). For reference, the 4 scenarios include both uniform and spatially variable lithological erodibility, L_E (8 scenarios in total),

Formatted: Font: Italic

Formatted: Font: Italic

665 In ST-SPM scenarios 1-4 (Table 4, Figures S10.a-d), the ST-SPM is optimized assuming a constant erodibility (L_E fixed to 1). Optimized values for τ_c are close to zero in the first three scenarios, suggesting the lack of a critical incision threshold. Similar to what has been found for the R-SPM, model performance is not any better compared to the use of a simple A-SPM when not considering lithological variability. This confirms that optimizing more complex river incision models (such as the ST-SPM) has little added value when the heterogeneity in environmental conditions (lithological heterogeneity) is not considered.

670 In scenario 4 ST-SPM scenarios 5 and 5-6 (Table 4, Figures S10.e-f), catchment mean runoff (\bar{R}) is fixed to the average value of all catchments (0.82 m yr^{-1}), in order to evaluate the role of (i) variations in observed temporal runoff variability (k) and (ii) optimized values for the incision threshold (τ_c). In scenario 45, k is fixed to the average value for all catchments ($k = 1.01$) whereas in scenario 56, k is set to the catchment specific values as listed in Table 2-Table 2. Both scenario 4 and scenarios (5 and 6) perform well with an NS value equalling 0.71 indicating. Optimized values for τ_c are ca. 30 Pa. Scenarios 4 and 5 suggest that considering the spatial-temporal runoff variability of (k does) is not improve nor decrease the influencing model performance of the ST-SPM in the Paute basin. Regardless the lack of spatially variable runoff (R), both scenarios perform as well as R-SPM scenario 2, where runoff variability was considered. The good performance of ST-SPM scenarios 675 5 and 6 can be attributed to the presence of an incision threshold ($\psi > 0$ in Eq. 13), where τ_c is optimized to a value of ca. 30 Pa (Table 4). Given that the use of the ST-SPM with constant runoff values yields a good model fit suggests that part of the non-linear relationship between river incision and steepness, k_{st} as reported in section 6.1 and E_{CRV} can be attributed to the presence of thresholds for river incision to occur (cfr. Gasparini and Brandon, 2011). In Scenario 6 and 7, \bar{R} is set to the catchment specific values derived from the WaterGAP data (Table 2). Similarly to scenario 4 and 5, using catchment specific values for k does not improve model performance. Using an average k value (1.01) in combination with catchment specific values for runoff results in the highest model performance of all tested scenarios (Scenario 6, NS=0.75). Optimized values for τ_c of ca. 14–15 Pa are lower compared to scenarios 4 and 5. Figure 14.b shows the result of Scenario 6. Contrary to the R-SPM where low erosion rates are overestimated, the ST-SPM does allow to correctly predict low erosion rates due to the consideration of an incision threshold which mainly influences simulated river erosion rates at the lower end of the spectrum.

Formatted: Font: Italic

685 ST-SPM scenarios 7 and 8 (Table 4, Figures S10.e-f and Figure 8b) are similar to scenarios 5 and 6, with the difference that spatial runoff variability is considered by using catchment specific values for runoff (\bar{R} , Table 2). Similarly to scenario 5 and 6, using catchment specific values for k does not improve model performance, resulting in a similar model performance for scenario 7 and 8. Overall, ST-SPM scenarios 6 and 7, result in the highest model performance of all tested scenarios, with a NS model efficiency of 0.75, a ME of 2.22 and 2.21 and an R^2 of 0.75. The optimized model fit for ST-SPM scenario 7 is shown in Figure 8b and corresponds well with the 1:1 line between modelled and observed denudation rates. Optimized values for τ_c are ca. 14–15 Pa, being in the range, but at the lower spectrum of earlier documented values for critical shear stress (e.g. Shobe et al., 2018 report τ_c values between 10 – 1000 Pa). Contrary to the R-SPM where low denudation rates are overestimated (Figure 8a), the ST-SPM does predict low denudation rates better due to the consideration of an incision threshold which mainly influences simulated river denudation rates at the lower end of the spectrum.

Formatted: Font: Not Italic

695 ST-SPM scenarios 7 and 8 have a model error (ME is respectively 2.22 and 2.21) similar to the model error of A-SPM scenario 2 (ME = 2.23). Hence, we conclude that a ST-SPM considering spatial variations in runoff and simulating a critical threshold for river incision performs as well as an A-SPM where the effect of allogenic (runoff variability) and autogenic

(incision thresholds) response is casted in the lumped empirical incision parameters. While the R-SPM and ST-SPM do not necessarily predict spatial patterns in observed E_{CRN} rates better than an A-SPM, they do enable to simulate the effect of runoff variability and incision thresholds and therefore provide an operational tool to simulate past and future climate changes. Note that differences in model performance between R-SPM scenario 2 and ST-SPM scenarios 5-8 are existent but not very pronounced. To evaluate the significance of these differences, our analysis should be repeated on larger datasets capturing a wider variability in denudation rates and hydrology.

7.5. Discussion

7.1.5.1. Are CRN-derived erosion/denudation rates representative for long term river incision processes?

7.1.5.1.1. Equilibrium between river incision and hillslope denudation

Assuming an equilibrium betweenIn theory, rates of hillslope denudation equal rates of river incision and hillslope erosion theoretically holds forif landscapes which are either in a steady state or forif transient landscapes are characterized by rapid hillslope response (e.g. threshold hillslopes). Steady state landscapes can only be achieved under stable precipitationclimatic and tectonic settings that prevail over timescales exceeding several millions of years. Such configurationstability is rarely met in tectonically active regions where riverslandscapes continuously transmit newrespond to environmental perturbations to the upper parts of the catchment (Armitage et al., 2018; Bishop et al., 2005; Campforts and Govers, 2015).

The downstream reaches of the Paute catchment are a good example of a transient landscape where a major knickzone is propagating upstream in the catchment resulting in steep threshold topography downstream of the knickzone (Figure S3 and Vanacker et al., 2015). Facing a sudden lowering of their base level after river rejuvenation, soil production and linear hillslope processes such as soil creep (Campforts et al., 2016; Vanacker et al., 2019) are not any longer able to catch up(Campforts et al., 2016) are not any longer in equilibrium with rapidly incising rivers (Fig. 15 in Hurst et al., 2012). In transient regionssteep topography, hillslopes may transiently evolve to their mechanically limited threshold slope where any further perturbation of threshold hillslopes will result in increased sediment delivery through mass wasting processes such as rockfall or landsliding (Bennett et al., 2016; Blöthe et al., 2015; Burbank et al., 1996; Larsen et al., 2010; Schwanghart et al., 2018). Given the stochasticerratic nature of landslides, not all threshold hillslopes will respond simultaneously to base level lowering depending on local variations in rock strength, hydrology and seismic activity (Broeckx et al., 2019). Therefore, catchments in transient regions might experience erosion in a broad range from moderate to high rates with similar probabilities, land use and seismic activity (Broeckx et al., 2020; Guns and Vanacker, 2014). Therefore, catchments in transient landscapes might experience hillslope denudation with highly variable rates.

Thus, We argue that CRN-derived erosion/denudation rates mightin the Paute basin both overestimate and underestimate long term incision rates in these catchments. Overestimation resultsmay result from the occurrence of recent, deep-seated landslide events, that deliver sediments with low CRN concentration to rivers (Tofelde et al., 2018). Underestimation might, in turn, may occur if long-term hillslope lowering is accomplished by rare and large landslides characterized by the occurrence of rare, large events with awhose return period exceedingperiods exceed the integration time of CRN-derived erosion/denudation rates; (Niemi et al., 2005; Yanites and Tucker, 2010).

Longitudinal profiles of rivers draining to the knickzone in the Paute catchment show marked knickpoints (HD's. This is particularly evident in catchments 9-16 on Figure 4; (Figure 1) where k_{av} values are high (Figure 2) and knickpoints appear

Formatted: English (United Kingdom)

Formatted: English (United Kingdom)

735 [in the longitudinal profiles](#) (Figures S3 and S4). [Figure 14.b shows that simulated](#) Simulated erosion rates for some of these catchments deviate from CRN-derived [erosion denudation](#) rates ([Figure 8.b](#), ID's 13 14 and 16) whereas for others (e.g. ID's 9 and 11), predictions from the [stochastic threshold](#) Stochastic-Threshold river incision model show a good agreement with E_{CRN} data. ~~We attribute this variability to differences in drainage area between these catchments.~~ For catchments with a sufficiently large drainage area, modelled incision rates correspond well with E_{CRN} (ID's 9 and 11 being both ca. 700 km²), most likely because the mechanisms that potentially cause overestimation and underestimation cancel each other out at this scale. For smaller catchments (ID's- 8;13;14 and 16 all being < 12 km²) there is a discrepancy between simulated river incision rates and E_{CRN} .

740 Although river incision [rates models](#) can be used to [estimate general erosionsimulate denudation](#) patterns in large transient catchments ($\gg \geq 10$ km²), there is a need to develop alternative approaches [to simulate erosion rates in transient regions over different spatial scales](#). ~~One such approach could be the explicit integration of including e.g.~~ landslide mechanisms in long term landscape evolution models such as TTLEM (Campforts et al., 2017) or Landlab ([Hobley et al., 2017](#)) to capture the stochastic nature of these processes (Niemi et al., 2005; Yanites et al., 2009)([Hobley et al., 2017](#)).

7.1.2.5.1.2. **Integration timescales of E_{CRN} and k_{sn}**

750 CRN concentrations in detrital sediments integrate over timescales dependent on the erosion rate of the catchment. For a rock density of 2.7 g cm⁻³, the integration time corresponds to the time required to erode ca. 60 cm of rock (Kirchner et al., 2001). E_{CRN} in the Paute basin varies between 5 to 399 mm yr⁻¹ implying integration times ranging from ca. 1.5 to 175 ky. Topographical river profiles on the other hand are the outcome of the dynamic interplay between tectonics, lithology, rainfall variability and internal drainage reorganization over timescales well exceeding one million years. Our analysis reveals the potential role of temporal and spatial variations of rainfall in long term landscape evolution. Integration times of CRN-derived denudation rates measured in the Paute basin are in the order of 1.5-175 ky. In contrast, response times of longitudinal river profiles generally range from 0.25-2.5 Ma (Campforts et al., 2017; Goren et al., 2014; Wobus et al., 2006).

755 Thus, successful identification of a rainfall variability signal is only possible if the signal has been present during the integration timescale of both E_{CRN} and k_{sn} . Given the high sensitivity of extreme precipitation events to climate change (Gorman, 2012), rainfall variability over the last 10-100 ky might be well represented in E_{CRN} rates but not in k_{sn} values which potentially integrate over longer timespans which are most likely characterized by important variations in hydrology. Moreover, we use hydrological data integrating over "only" 35 years to constrain the distribution of river discharge: these data are unlikely to fully capture rainfall variability over the integration timespan of E_{CRN} measurements. Different integration timespans of river profile response, E_{CRN} rates and hydrological data can be expected to affect model performance.

760 765 770 While our dataset does not enable us to fully capture rainfall variability, a distinction can be made between temporal and spatial variations. Contrary to temporal variations controlling frequency and magnitude of discharge events, the spatial gradient in orographic precipitation is (Campforts et al., 2017; Goren et al., 2014; Snyder et al., 2003; Whipple, 2001; Wobus et al., 2006). During both of these time scales it is unlikely that the temporal rainfall distribution that we inferred from 35 years of data remained stationary. Thus, there is little reason to believe that our data fully capture rainfall variability over the response times of river profiles and hillslopes. Contrary to temporal variations, spatial patterns in orographic precipitation are characteristic to the formation of a mountain range at geological timescales (Garcia-Castellanos and Jiménez-Munt, 2015). In

775 the case of the Southern Ecuadorian Andes, orographic precipitation results from moist air advection via the South American
Low-Level flow generates pronounced patterns of orographic precipitation (Campetella and Vera, 2002). The air is lifted as
it passes over the eastern flanks of the Andes, resulting in moist convection fuelled by adiabatic decompression. Onset of
Andean uplift in Ecuador has been reported to be asynchronous from south to north with the onset of the most recent uplift
phase dated back to These patterns likely persisted since at least the most recent uplift phase of Andean uplift in the Late
Miocene (Spikings et al., 2010; Spikings and Crowhurst, 2004). Climate changes over the Miocene-Pliocene probably altered
absolute amounts of precipitation in the Ecuadorian Andes (Goddard and Carrapa, 2018) challenging the use of present day
runoff and discharge distribution to predict long term river incision. However, the orographically induced gradients in
780 precipitation must have been present for timescales exceeding those represented by both k_{crn} and E_{CRN} . This partly explains
why accounting for spatial variations in precipitation does improve the performance of a stochastic threshold SPM contrary
to the use of catchment specific discharge distributions representing temporal discharge variability. Present day rainfall and
runoff gradients (Figure 6) are thus deemed to be representative for times exceeding response times of longitudinal river
profiles and integration times of CRN-derived denudation rates, and warrant the use of contemporaneous runoff data to
785 represent spatial patterns of discharge (section 3.1). Ultimately, performance of the different stream power models underscores
this interpretation. While accounting for spatial patterns in runoff improves the performance of a Stochastic-Threshold SPM
(Table 4 and section 4.2.2), incorporating proxies of temporal discharge variability leads to no improvement of model
performance (the role of k in section 4.2.2).

790 Downscaling the WRR2-WaterGAP reanalysis dataset by amalgamating regional rain gauge data, allowed to obtain a
runoff dataset at a resolution suitable for use in our study. However, to further improve the accuracy of hydrological data, the
use of more advanced methods might be considered. A possible approach is the application of regional climate models (e.g.
Thiery et al., 2015) in regions with pronounced topographic and climatological gradients. Regional climate models have been
shown to simulate rainfall variability more realistically than global re-analysis datasets in mountainous areas (Thiery et al.,
2015) and have been successfully used to explain geomorphic response in such areas (Jacobs et al., 2016).

795 **7.2.5.2. Environmental control on long term river incision rates**

7.2.5.2.1. Geology

800 Incorporating rock strength variability when simulating river incision improves model efficiency for all evaluated SPMs
(Table 4 and Table 5). Our results corroborate earlier findings that established functional dependencies between river incision
and rock physical properties to successfully determine river incision rates. In all our simulations, model efficiency improves
when incorporating rock strength variability (Table 4), which is consistent with earlier studies (Lavé and Avouac, 2001; Stock
and Montgomery, 1999). In this study, rock strength is represented by the absence of generally accepted metrics of erodibility,
we employ an empirically derived lithological erodibility index (L_E , Eq. (15)) based on the age and the lithological
composition of stratigraphic units. Because of Owing to its simplicity, our empirical approach holds potential to this or a similar
805 index can potentially be applied at continental to global scales where detailed information on rock physical properties are not
always usually lacking the detail available. However, at smaller spatial scales, studies evaluating the role of rock strength
heterogeneity on specific river incision processes such as fluvial abrasion will benefit from a more mechanistic approach to
quantify rock strength (Attal and Lavé, 2009; Nibourel et al., 2015). Moreover Notwithstanding, river incision efficiency might
also depend depends on other rock properties such as the density of bedrock fractures, joints and other discontinuities (Whipple

et al., 2000). Fracture density has in turn been linked to spatial patterns of seismic activity (Molnar et al., 2007). Given the limited variability of seismic activity within the Paute basin (Petersen et al., 2018), seismicity was not considered in our statistical regional analysis but should be considered when applying our approach to other regions prone to more seismic activity (Petersen et al., 2018 Figure S2), seismicity was not considered in our statistical regional analysis but could be considered when applying our approach to other regions characterized by more spatial seismic variability.

We show that incorporating spatial patterns of rock strength variability not only reduces the scatter surrounding the modelled river incision versus E_{CRN} -derived erosion/ denudation rates, but also controls the degree of the nonlinearity between river steepness (k_{sn}) and erosion/ denudation rates, expressed by the slope exponent n coefficient in the A-SPM (Figure 12). When not considering rock strength variability, the results in a k_{sn} - E_{CRN} relationship relation that is close to being a linear one for in the Paute catchment (with $n = 1.0607$). This opposes to findings from regional studies where lithology was assumed to be uniform and n has been reported to be larger than 1 (e.g. DiBiase et al., 2010; Lague, 2014; Whittaker and Boulton, 2012). In the Paute basin, the confounding role of lithological variability obscures a non-linear relationship between river incision and channel steepness. Applying advanced process-based river incision models (R-SPM and ST-SPM, Table 5) without correction for this confounding role of lithology has proven to be of no added value in comparison to the application of a simple, purely empirical A-SPM (Table 4 and Table 5).

5.2.2. Rainfall

7.2.2. Rainfall

After correction for lithological strength variability, a non-linear relationship between k_{sn} and E_{CRN} emerges (similar to $n > 1$ in the A-SPM, Figure 12.b). With theory predicting river incision to be linearly dependent on k_{sn} (Eq. (4) when using Darcy-Weisbach friction coefficients), we evaluated whether (i) spatial variation in runoff, (ii) the existence of incision thresholds or (iii) a combination of both can explain this nonlinearity.

Application of the R-SPM enables to include regional variations in runoff and results in a good fit and model efficiency ($R^2=0.75$, $NS=0.7$, R-SPM Scenario 2 in Table 5). This suggests that part of the frequently reported, non-linear relationship between k_{sn} and E_{CRN} can be attributed to the spatial variability of mean annual rainfall. In tectonically active regions, steep river reaches often appear at the edge of the mountain range where mean annual rainfall rates are high due to orographic precipitation. Therefore, if variations in runoff are not considered, the confounding role of orographic precipitation will be accommodated for by a non-linear relationship between river steepness and erosion rates. Application of the R-SPM does allow to account for this effect but results in underestimation of low river incision rates (deviation from the 1:1 line on Figure 14.a). This artefact is overcome when applying the ST-SPM where the explicit simulation of a threshold improves model performance, especially for low erosion rates.

Application of the ST-SPM assuming a constant runoff (ST-SPM Scenario 4 in Table 5), results in a slightly better model efficiency in comparison to the R-SPM scenario with variable runoff ($NS=$ The A-SPM performs well in explaining E_{CRN} when lithology is considered and $n >> 1$ (Figure 9, high NS model efficiency, low ME). For $n = 1$, the performance of the A-SPM is low. The result is consistent with earlier studies reporting $n >> 1$ (e.g. DiBiase et al., 2010; Harel et al., 2016; Ouimet et al., 2009; Scherler et al., 2014), which Lague (2014) attributes to discharge variability and incision thresholds. We tested this hypothesis using the R-SPM and ST-SPM. Our results underscore that the non-linear relationship between k_{sn} and

850 E_{CRN} is largely due to the spatial variability of mean annual runoff. Figure 9 shows that the R-SPM (where n is fixed to the theoretically obtained value of 1) performs better than an A-SPM when n is fixed to 1. This suggests that part of the frequently reported, non-linear relationship between k_{gr} and E_{CRN} can be attributed to the spatial variability of mean annual runoff. In tectonically active regions, steep river reaches often spatially coincide with the edge of the mountain range where mean annual rainfall rates are highest. Accordingly, if variations in runoff are not considered, the effects of orographic precipitation will be partly accommodated for by a non-linear relationship between river steepness and denudation rates. The R-SPM accounts for this effect but results in an underestimation of low river incision rates (Figure 8.a). Moreover, the model error (Figure 9.b), shows that the R-SPM does not perform as well as the A-SPM. In a final set of model runs, we apply the ST-SPM where the explicit simulation of a threshold improves model performance, especially for low denudation rates, resulting in an overall model error which is equal to the one obtained with the A-SPM with $n \gg 1$ (Figure 9). This finding points to the potentially important role of thresholds for river incision to occur.

860 Model performance of the ST-SPM equals the performance of an empirical A-SPM with a slope exponent $\gg 1$ (Figure 9). Our interpretation is that (i) spatial variations in runoff and (ii) the incision thresholds are the causes of an observed non-linear relation between k_{gr} and E_{CRN} . With a seemingly equal model performance, one could wonder what the benefit of the more complex ST-SPM model is over a simple, non-linear A-SPM. The aim of using a ST-SPM is however beyond fitting observed denudation rates: we want to identify to what extent the system is forced by internal allogenic dynamics such as the presence of incision thresholds or external autogenic forces such as runoff variability. Use of the ST-SPM illustrated that both processes can be accounted for in a quantitative way so that future studies can explicitly consider their role when reconstructing past landscape response to external perturbations (e.g. climate change).

870 To further explore the interdependency between incision thresholds and spatial runoff variability, our approach can be applied to CRN datasets, covering regions characterized by more pronounced rainfall gradients (e.g. in Chile: Carretier et al., 2018). Accounting for spatial variations in temporal discharge distributions (with k characterizing the stochastic flood occurrence), did not further improve neither deteriorate model performance (ST-SPM Scenario 7 in Table 5, 8 in Table 4). This is likely due to data limitations: the necessary data to characterize temporal variations in discharge within a given catchment over a timescale that is relevant for CRN-derived erosion denudation rates are, at present, not available.

880 Our finding that mainly spatial patterns in precipitation control river incision patterns corroborate findings in the Himalaya (Scherler et al., 2017) and in the Andes (Sorensen and Yanites, 2019). Sorensen and Yanites (2019) evaluated the role of latitudinal rainfall variability in the Andes on erosional efficiency using a set of numerical landscape evolution model runs. They show that erosion efficiency in tropical climates at low latitudes, where the Paute basin is located, is well captured by the spatial pattern of mean annual precipitation and thus runoff. At higher latitudes (25-50°) where storms are less frequent but still very intense, mean annual precipitation decreases but erosivity is still high due to the intensity of storms (Sorensen

and Yanites, 2019). At these latitudes, the spatial variations in storm magnitude are therefore more likely to be reflected in river erosivity and thus catchment mean erosiondenudation rates than in the Ecuadorian Andes.

8.6. Conclusions and Implications for landscape evolution

890 ~~An increasing number of~~Numerous studies ~~and global compilations~~ report a non-linear relationship between channel steepness and CRN-derived erosiondenudation rates. Based on the growing mechanistic understanding of river incision processes, this nonlinear relationship is often attributed to ~~the existence of~~incision thresholds. Rainfall variability, ~~which is stochastic in nature,~~ controls the frequency of river discharges ~~large enough in magnitude to that~~ exceed ~~these~~incision thresholds. Although the dynamic interplay between stochastic runoff and incision thresholds theoretically results in a non-linear relationship between channel steepness and erosiondenudation rates, coupling theory with field data has been proven challenging. We address this issue ~~for a median-sized in the Paute basin in the Southern Ecuadorian Andes~~ where we scrutinize the relationship between CRN-derived erosiondenudation rates and river incision, ~~simulated with using~~ three different Stream Power Models~~stream power models~~. We show that lithological variability obscures the relationship between channel steepness-based river incision and CRN-derived erosion rates. ~~When not accounting for lithological variability, a process based Stochastic Threshold SPM was not performing any better than a simple, empirical, drainage area based stream power model. Neither could the impact of rainfall variability on river incision rates be assessed derived denudation rates.~~

895 In order to account for ~~the confounding role of~~rock strength variability, which is for the Paute basin mainly ascribed to variations in lithological strength in the study area, we propose the use of an empirical lithological strength index, that is based on ~~the~~lithology and age of lithostratigraphic units. ~~When considering~~Including lithological variability, in the models increases the relationship~~correlation~~ between river steepness and erosiondenudation rates ~~becomes and reveals a~~ non-linear. ~~After integrating the empirical lithological erodibility index into the erosion efficiency coefficient of the ST-SPM, the model is capable relation, which we seek to explain differences in subcatchment erosion rates. Considering river incision thresholds improves modelled erosion rates for slowly eroding catchments characterized by low to moderate relief using a stochastic-threshold SPM (ST-SPM).~~ Using a downscaled version of a state-of-the-art hydrological reanalysis dataset, we furthermore show that spatial variations in the combination of spatially varying runoff explain part of the variability of and incision thresholds explains the observed erosion rates. ~~The, non-linear relationship. We do not detect, however, an impact on river incision of temporal variations in discharge, controlling the magnitude and frequency of fluvial discharge, could not be identified within the studied catchments distributions on river incision.~~ We attribute this partly to the limited CRN dataset ~~but mainly to the lack to the integration time of rainfall~~CRN data which integrate over sufficiently long and response times of river longitudinal profiles which extend beyond timescales at which discharge distributions can be assumed to be recorded in the CRN derived erosion rates stationary.

900 Our study shows the potential of a stochastic threshold stream power model as a tool to explainST-SPM to infer regional and, potentially, continental to global differences in rainfall variability. However, ~~the latter will only be successful after elucidating the confounding role of~~we emphasize that its application needs to account for other environmental variables such as rock strength ~~on river incision rates. Simplifications involved with the use of any Stream Power-. Simplified process representation of stream power-based incision model such as the models (e.g., lack of sediment-bedrock interactions or dynamic channel width adjustments) potentially~~ might explain part of the remaining scatter surroundingbetween predicted ~~versus~~and measured erosiondenudation rates. However, residual analysis showed that most of the remaining scatter occurs in small transient catchments (up to 10 km²-10²) where sporadic mass wasting processes on hillslopes likely obscure the relation

925 ~~between our measurements and predictions. Elucidating this relation further our understanding of landscape evolution over~~
~~different spatial scales in such transient regions, we propose the development of process-based~~~~s potentially fostered by~~
~~dynamic numerical~~ landscape evolutions models ~~which~~ explicitly ~~simulating~~~~simulate~~ the coupling between transient river
adjustment and ~~stochastic~~-hillslope response.

930 *Data availability.*

All data used in this paper is freely available from referenced agencies. Hydrological data is available from
earth2observe.eu and <http://www.serviciometeorologico.gob.ec/biblioteca/>. Topographic data is available from NASA
(NASA JPL, 2013). Lithological data is provided in the supplementary information. Calculations were done in MATLAB
using the TopoToolbox Software (Schwanghart and Scherler, 2014).

935 *Author contribution.*

~~In~~BC conceived the project in collaboration with ~~all the authors, BC designed the project, carried out~~VV, MYM and GG.
BC performed the statistical analysis and ~~took the numerical calculations and wrote~~lead in writing the ~~manuscript~~paper. All
940 authors contributed to ~~editing~~shaping the ~~manuscript~~ research and analyses, as well as writing the paper.

Competing interests.

The authors declare that they have no conflict of interest.

945 *Financial support.*

B. Campforts received a postdoctoral grant from the Research Foundation Flanders (FWO). G. Tenorio received a PhD
950 ~~grant from ARES – the Académie de recherche et d'enseignement supérieur de la Belgique - as part of the PRD research~~
~~cooperation project: Strengthening the scientific and technological capacities to implement spatially integrated land and water~~
~~management schemes adapted to local socio-economic, cultural and physical settings, and a grant from the Secretaría de~~
~~Educación Superior de Ciencia, Tecnología e Innovación de la República del Ecuador.~~

Formatted: English (United Kingdom)

Field Code Changed

Formatted: English (United Kingdom)

9.7. References

- Aalto, R., Dunne, T. and Guyot, J. L.: Geomorphic Controls on Andean Denudation Rates, *J. Geol.*, 114(1), 85–99, doi:10.1086/498101, 2006.
- 955 Abbühl, L. M., Norton, K. P., Jansen, J. D., Schlunegger, F., Aldahan, A. and Possner, G.: Erosion rates and mechanisms of knickzone retreat inferred from ¹⁰Be measured across strong climate gradients on the northern and central Andes Western Escarpment, *Earth Surf. Process. Landforms*, 36(11), 1464–1473, doi:10.1002/esp.2164, 2011.
- Alcama, J., Döll, P., Henrichs, T., Kaspar, F., Lehner, B., Rösch, T. and Siebert, S.: Development and testing of the WaterGAP 2 global model of water use and availability, *Hydrol. Sci. J.*, 48(3), 317–337, doi:10.1623/hysj.48.3.317.45290, 2003.
- 960 Anderson, R. S.: Evolution of the Santa Cruz Mountains, California, through tectonic growth and geomorphic decay, *J. Geophys. Res.*, 99(B10), 20161–20179, doi:10.1029/94JB00713, 1994.
- Armitage, J. J., Whittaker, A. C., Zakari, M. and Campforts, B.: Numerical modelling of landscape and sediment flux response to precipitation rate change, *Earth Surf. Dyn.*, 6(1), 77–99, doi:10.5194/esurf-6-77-2018, 2018.
- 965 Attal, M. and Lavé, J.: Pebble abrasion during fluvial transport: Experimental results and implications for the evolution of the sediment load along rivers, *J. Geophys. Res.*, 114(F4), F04023, doi:10.1029/2009JF001328, 2009.
- Basabe R, P.: Geología Y Geotecnia, in Prevencion de Desastres Naturales en la Cuenca del Paute, Informe Final: Proyecto PreCuPa. Swiss Disaster Relief Unit (SDR/CSS), pp. 1–153, Cuenca, Ecuador., 1998.
- 970 Beek, H. E., Van Dijk, A. I. J. M., Levizzani, V., Schellekens, J., Miralles, D. G., Martens, B. and De Roo, A.: MSWEP: 3-hourly 0.25° global gridded precipitation (1979–2015) by merging gauge, satellite, and reanalysis data, *Hydrol. Earth Syst. Sci.*, 21(1), 589–615, doi:10.5194/hess-21-589-2017, 2017.
- Bendix, J., Rollenbeck, R., Göttlicher, D. and Cermak, J.: Cloud occurrence and cloud properties in Ecuador, *Clim. Res.*, 30, 133–147, doi:10.3354/cr030133, 2006.
- 975 Bennett, G. L., Miller, S. R., Roering, J. J. and Schmidt, D. A.: Landslides, threshold slopes, and the survival of relict terrain in the wake of the Mendocino Triple Junction, *Geology*, 44(5), 363–366, doi:10.1130/G37530.1, 2016.
- Bernhardt, A., Schwanghart, W., Hebbeln, D., Stuu, J.-B. W. and Strecker, M. R.: Immediate propagation of deglacial environmental change to deep-marine turbidite systems along the Chile convergent margin, *Earth Planet. Sci. Lett.*, 473, 190–204, doi:10.1016/j.epsl.2017.05.017, 2017.
- 980 Binnie, S. A., Phillips, W. M., Summerfield, M. A. and Fifield, L. K.: Tectonic uplift, threshold hillslopes, and denudation rates in a developing mountain range, *Geology*, doi:10.1130/G23641A.1, 2007.
- Bishop, P., Hoey, T. B., Jansen, J. D. and Artza, I. L.: Knickpoint recession rate and catchment area: the case of uplifted rivers in Eastern Scotland, *Earth Surf. Process. Landforms*, 778(6), 767–778, doi:10.1002/esp.1191, 2005.
- 985 von Blanckenburg, F., Belshaw, N. S. and O’Nions, R. K.: Separation of ⁹Be and cosmogenic ¹⁰Be from environmental materials and SIMS isotope dilution analysis, *Chem. Geol.*, 129(1–2), 93–99, doi:10.1016/0009-2541(95)00157-3, 1996.
- von Blanckenburg, F., Hewawasam, T. and Kubik, P. W.: Cosmogenic nuclide evidence for low weathering and denudation in the wet, tropical highlands of Sri Lanka, *J. Geophys. Res.*, 109(F3), F03008, doi:10.1029/2003JF000049, 2004.
- Blöthe, J. H., Korup, O. and Schwanghart, W.: Large landslides lie low: Excess topography in the Himalaya-Karakoram ranges, *Geology*, 43(6), 523–526, doi:10.1130/G36527.1, 2015.
- 990 Brocard, G. Y. and van der Beek, P. A.: Influence of incision rate, rock strength, and bedload supply on bedrock river gradients and valley-flat widths: Field-based evidence and calibrations from western Alpine rivers (southeast France), in Special Paper 398: Tectonics, Climate, and Landscape Evolution, vol. 2398, pp. 101–126, Geological Society of America., 2006.
- 995 Broeckx, J., Rossi, M., Lijnen, K., Campforts, B. and Poesen, J. and Vanmaercke, M.: Landslide mobilization: mobilization rates: A global patterns analysis and rates, in Geophysical Research Abstracts, vol. 21, p. 8585, EGU General Assembly model, *Earth-Science Rev.*, 201, 102972, doi:10.1016/j.earscirev.2019.102972, 2020.

Formatted: English (United Kingdom)

- Burbank, D. W., Leland, J., Fielding, E., Anderson, R. S., Brozovic, N., Reid, M. R. and Duncan, C.: Bedrock incision, rock uplift and threshold hillslopes in the northwestern Himalayas, *Nature*, 379(6565), 505–510, doi:10.1038/379505a0, 1996.
- Campetella, C. M. and Vera, C. S.: The influence of the Andes mountains on the South American low-level flow, *Geophys. Res. Lett.*, 29(17), 7-1-7-4, doi:10.1029/2002GL015451, 2002.
- 1000 Campforts, B. and Govers, G.: Keeping the edge: A numerical method that avoids knickpoint smearing when solving the stream power law, *J. Geophys. Res. Earth Surf.*, 120(7), 1189–1205, doi:10.1002/2014JF003376, 2015.
- Campforts, B., Vanacker, V., Vanderborght, J., Baken, S., Smolders, E. and Govers, G.: Simulating the mobility of meteoric ¹⁰Be in the landscape through a coupled soil-hillslope model (Be2D), *Earth Planet. Sci. Lett.*, 439, 143–157, doi:10.1016/j.epsl.2016.01.017, 2016.
- 1005 Campforts, B., Schwanghart, W. and Govers, G.: Accurate simulation of transient landscape evolution by eliminating numerical diffusion: the TTLEM 1.0 model, *Earth Surf. Dyn.*, 5(1), 47–66, doi:10.5194/esurf-5-47-2017, 2017.
- Carretier, S., Tolorza, V., Regard, V., Aguilar, G., Bermúdez, M. A., Martinod, J., Guyot, J. L., Hérail, G. and Riquelme, R.: Review of erosion dynamics along the major N-S climatic gradient in Chile and perspectives, *Geomorphology*, 300, 45–68, doi:10.1016/j.geomorph.2017.10.016, 2018.
- 1010 Castellort, S., Goren, L., Willett, S. D., Champagnac, J. D., Herman, F. and Braun, J.: River drainage patterns in the New Zealand Alps primarily controlled by plate tectonic strain, *Nat. Geosci.*, 5(10), 744–748, doi:10.1038/ngeo1582, 2012.
- Celleri, R., Willems, P., Buytaert, W. and Feyen, J.: Space–time rainfall variability in the Paute basin, Ecuadorian Andes, *Hydrol. Process.*, 21(24), 3316–3327, doi:10.1002/hyp.6575, 2007.
- 1015 Codilean, A. T., Munack, H., Cohen, T. J., Saktura, W. M., Gray, A. and Mudd, S. M.: OCTOPUS: An Open Cosmogenic Isotope and Luminescence Database, *Earth Syst. Sci. Data Discuss.*, 2(November), 1–23, doi:10.5194/essd-2018-32, 2018.
- Coulthard, T. J. and Van de Wiel, M. J.: Climate, tectonics or morphology: what signals can we see in drainage basin sediment yields?, *Earth Surf. Dyn.*, 1(1), 13–27, doi:10.5194/esurf-1-13-2013, 2013.
- Crave, A. and Davy, P.: A stochastic “precipiton” model for simulating erosion/sedimentation dynamics, *Comput. Geosci.*, 27(7), 815–827, doi:10.1016/S0098-3004(00)00167-9, 2001.
- 1020 [Croissant, T. and Braun, J.: Constraining the Stream Power Law: a novel approach combining a Landscape Evolution Model and an inversion method, *Earth Surf. Dyn. Discuss.*, 1\(1\), 891–921, doi:10.5194/esurfd-1-891-2013, 2013.](#)
- Cyr, A. J., Granger, D. E., Olivetti, V. and Molin, P.: Quantifying rock uplift rates using channel steepness and cosmogenic nuclide–determined erosion rates: Examples from northern and southern Italy, *Lithosphere*, 2(3), 188–198, doi:10.1130/L96.1, 2010.
- 1025 Deal, E., Braun, J. and Botter, G.: Understanding the Role of Rainfall and Hydrology in Determining Fluvial Erosion Efficiency, *J. Geophys. Res. Earth Surf.*, 123(4), 744–778, doi:10.1002/2017JF004393, 2018.
- DiBiase, R. A. and Whipple, K. X.: The influence of erosion thresholds and runoff variability on the relationships among topography, climate, and erosion rate, *J. Geophys. Res.*, 116(F4), F04036, doi:10.1029/2011JF002095, 2011.
- 1030 DiBiase, R. A., Whipple, K. X., Heimsath, A. M. and Quimet, W. B.: Landscape form and millennial erosion rates in the San Gabriel Mountains, CA, *Earth Planet. Sci. Lett.*, 289(1–2), 134–144, doi:10.1016/j.epsl.2009.10.036, 2010.
- [Dietrich, W. E., Bellugi, D. G., Sklar, L. S., Stoek, J. D., Heimsath, A. M. and Roering, J. J.: Geomorphic transport laws for predicting landscape form and dynamics, *Geophys. Monogr. Ser.*, 135, 103–132, doi:10.1029/135GM09, 2003.](#)
- 1035 [Dinku, T., Hailemariam, K., Maidment, R., Tarnavsky, E. and Connor, S.: Combined use of satellite estimates and rain gauge observations to generate high-quality historical rainfall time series over Ethiopia, *Int. J. Climatol.*, 34\(7\), 2489–2504, doi:10.1002/joc.3855, 2014.](#)
- Döll, P., Kaspar, F. and Lehner, B.: A global hydrological model for deriving water availability indicators: model tuning and validation, *J. Hydrol.*, 270(1–2), 105–134, doi:10.1016/S0022-1694(02)00283-4, 2003.
- Dunai, T. J.: Scaling factors for production rates of in situ produced cosmogenic nuclides: a critical reevaluation, *Earth Planet. Sci. Lett.*, 176(1), 157–169, doi:10.1016/S0012-821X(99)00310-6, 2000.

Formatted: English (United Kingdom)

Formatted: English (United Kingdom)

- 1040 Egüez, A., Gaona, M. and Albán, A.: Mapa geológico de la República del Ecuador, Escala 1: 1.000. 000., Quito., 2017.
- Farr, T. G., Rosen, P. A., Caro, E., Crippen, R., Duren, R., Hensley, S., Kobrick, M., Paller, M., Rodriguez, E., Roth, L., Seal, D., Shaffer, S., Shimada, J., Umland, J., Werner, M., Oskin, M., Burbank, D. and Alsdorf, D.: The Shuttle Radar Topography Mission, *Rev. Geophys.*, 45(2), RG2004, doi:10.1029/2005RG000183, 2007.
- 1045 Ferrier, K. L., Huppert, K. L. and Perron, J. T.: Climatic control of bedrock river incision, *Nature*, 496(7444), 206–209, doi:10.1038/nature11982, 2013.
- Finnegan, N. J., Hallet, B., Montgomery, D. R., Zeitler, P. K., Stone, J. O., Anders, A. M. and Yuping, L.: Coupling of rock uplift and river incision in the Namche Barwa-Gyala Peri massif, Tibet, *Bull. Geol. Soc. Am. Bull.*, 120(1–2), 142–155, doi:10.1130/B26224.1, 2008.
- 1050 Fisher, G. B., Bookhagen, B. and Amos, C. B.: Channel planform geometry and slopes from freely available high-spatial resolution imagery and DEM fusion: Implications for channel width scalings, erosion proxies, and fluvial signatures in tectonically active landscapes, *Geomorphology*, 194, 46–56, doi:10.1016/j.geomorph.2013.04.011, 2013a.
- Fisher, G. B., Amos, C. B., Bookhagen, B., Burbank, D. W. and Godard, V.: Channel widths, landslides, faults, and beyond: The new world order of high-spatial resolution Google Earth imagery in the study of earth surface processes., 2013b.
- 1055 Garcia-Castellanos, D. and Jiménez-Munt, I.: Topographic Evolution and Climate Aridification during Continental Collision: Insights from Computer Simulations, edited by N. Houlié, *PLoS One*, 10(8), e0132252, doi:10.1371/journal.pone.0132252, 2015.
- Gasparini, N. M. and Brandon, M. T.: A generalized power law approximation for fluvial incision of bedrock channels, *J. Geophys. Res. Earth Surf.*, 116(2), 1–16, doi:10.1029/2009JF001655, 2011.
- 1060 Gasparini, N. M. and Whipple, K. X.: Diagnosing climatic and tectonic controls on topography: Eastern flank of the northern Bolivian Andes, *Lithosphere*, (May), 230–250, doi:10.1130/L322.1, 2014.
- [Goddard, A. S. and Carrapa, B.: Effects of Miocene–Pliocene global climate changes on continental sedimentation: A case study from the southern Central Andes, *Geology*, 46\(7\), 647–650, doi:10.1130/G40280.1, 2018.](#)
- [Goren, L.: A theoretical model for fluvial channel response time during time-dependent climatic and tectonic forcing and its inverse applications, *Geophys. Res. Lett.*, 43\(20\), 10,753–10,763, doi:10.1002/2016GL070451, 2016.](#)
- 1065 Goren, L., Fox, M. and Willett, S. D.: Tectonics from fluvial topography using formal linear inversion: Theory and applications to the Inyo Mountains, California, *J. Geophys. Res. F Earth Surf.*, 119(8), 1651–1681, doi:10.1002/2014JF003079, 2014.
- [Gorman, P. A. O.: Sensitivity of tropical precipitation extremes to climate change, *Nat. Geosci.*, 5\(10\), 697–700, doi:10.1038/ngeo1568, 2012.](#)
- 1070 Guns, M. and Vanacker, V.: Forest cover change trajectories and their impact on landslide occurrence in the tropical Andes, *Environ. Earth Sci.*, 70(7), 2941–2952, doi:10.1007/s12665-013-2352-9, 2013.
- [Guns, M. and Vanacker, V.: Shifts in landslide frequency-area distribution after forest conversion in the tropical Andes, *Anthropocene*, 6, 75–85, doi:10.1016/j.ancene.2014.08.001, 2014.](#)
- 1075 Harel, M. M.-A., Mudd, S. M. and Attal, M.: Global analysis of the stream power law parameters based on worldwide 10 Be denudation rates, *Geomorphology*, 268, 184–196, doi:10.1016/j.geomorph.2016.05.035, 2016.
- Hay, W. W., Sloan II, J. L. and Wold, C. N.: Mass/Age Distribution and Composition of Sediments on the Ocean Floor and the Global Rate of Sediment Subduction, *J. Geophys. Res.*, 93940(10), 933–14, doi:10.1029/JB093iB12p14933, 1988.
- [Herman, F., Beyssac, O., Brughelli, M., Lane, S. N., Leprince, S., Adatte, T., Lin, J. Y. Y., Avouac, J.-P. and Cox, S. C.: Erosion by an Alpine glacier, *Science* \(80-. \), 350\(6257\), 193–195, doi:10.1126/science.aab2386, 2015.](#)
- 1080 [Hobley, D. E. J., Adams, J. M., Nudurupati, S. S., Hutton, E. W. H., Gasparini, N. M., Istanbuloglu, E. and Tucker, G. E.: Creative computing with Landlab: an open-source toolkit for building, coupling, and exploring two-dimensional numerical models of Earth-surface dynamics, *Earth Surf. Dyn.*, 5\(1\), 21–46, doi:10.5194/esurf-5-21-2017, 2017.](#)
- Horton, B. K.: Sedimentary record of Andean mountain building, *Earth-Science Rev.*, 178(November 2017), 279–309, doi:10.1016/j.earscirev.2017.11.025, 2018.

Formatted: English (United Kingdom)

- 1085 Howard, A. D.: A detachment limited model of drainage basin evolution, *Water Resour. Res.*, 30(7), 2261–2285, doi:10.1029/94WR00757, 1994.
- Hungerbühler, D., Steinmann, M., Winkler, W., Seward, D., Egüez, A., Peterson, D. E., Helg, U. and Hammer, C.: Neogene stratigraphy and Andean geodynamics of southern Ecuador, *Earth-Science Rev.*, 57(1–2), 75–124, doi:10.1016/S0012-8252(01)00071-X, 2002.
- 1090 Hurst, M. D., Mudd, S. M., Walcott, R., Attal, M. and Yoo, K.: Using hilltop curvature to derive the spatial distribution of erosion rates, *J. Geophys. Res. Earth Surf.*, 117(F2), n/a-n/a, doi:10.1029/2011JF002057, 2012.
- [Jacobs, L., Dewitte, O., Poesen, J., Delvaux, D., Thiery, W. and Kervyn, M.: The Rwenzori Mountains, a landslide-prone region?, *Landslides*, 13\(3\), 519–536, doi:10.1007/s10346-015-0582-5, 2016.](#)
- [Jeffreys, H.: *Theory of probability*, Clarendon Press., 1998.](#)
- 1095 Jelinski, N. A., Campforts, B., Willenbring, J. K., Schumacher, T. E., Li, S., Lobb, D. A., Papiernik, S. K. and Yoo, K.: Meteoric Beryllium-10 as a tracer of erosion due to post-settlement land use in west-central Minnesota, USA, *J. Geophys. Res. Earth Surf.*, 10, doi:10.1029/2018jf004720, 2019.
- Jerolmack, D. J. and Paola, C.: Shredding of environmental signals by sediment transport, *Geophys. Res. Lett.*, 37(19), 1–5, doi:10.1029/2010GL044638, 2010.
- 1100 Kirby, E. and Ouimet, W.: Tectonic geomorphology along the eastern margin of Tibet: insights into the pattern and processes of active deformation adjacent to the Sichuan Basin, *Geol. Soc. London, Spec. Publ.*, doi:10.1144/sp353.9, 2011.
- Kirby, E. and Whipple, K. X.: Expression of active tectonics in erosional landscapes, *J. Struct. Geol.*, 44, 54–75, doi:10.1016/j.jsg.2012.07.009, 2012.
- Kirchner, J. W., Finkel, R. C., Riebe, C. S., Granger, D. E., Clayton, J. L., King, J. G. and Megahan, W. F.: Mountain erosion over 10 yr, 10 k.y., and 10 m.y. time scales, *Geology*, 29(7), 591, doi:10.1130/0091-7613(2001)029<0591:MEOYKY>2.0.CO;2, 2001.
- Kober, F., Ivy-Ochs, S., Schlunegger, F., Baur, H., Kubik, P. W. and Wieler, R.: Denudation rates and a topography-driven rainfall threshold in northern Chile: Multiple cosmogenic nuclide data and sediment yield budgets, *Geomorphology*, 83(1–2), 97–120, doi:10.1016/j.geomorph.2006.06.029, 2007.
- 1110 Kober, F., Zeilinger, G., Hippe, K., Marc, O., Lendzioc, T., Grischott, R., Christl, M., Kubik, P. W. and Zola, R.: Tectonic and lithological controls on denudation rates in the central Bolivian Andes, *Tectonophysics*, 657, 230–244, doi:10.1016/j.tecto.2015.06.037, 2015.
- Korup, O., Clague, J. J., Hermanns, R. L., Hewitt, K., Strom, A. L. and Weidinger, J. T.: Giant landslides, topography, and erosion, *Earth Planet. Sci. Lett.*, 261(3–4), 578–589, doi:10.1016/j.epsl.2007.07.025, 2007.
- 1115 Lague, D.: The stream power river incision model: evidence, theory and beyond, *Earth Surf. Process. Landforms*, 39(1), 38–61, doi:10.1002/esp.3462, 2014.
- Lague, D., Hovius, N. and Davy, P.: Discharge, discharge variability, and the bedrock channel profile, *J. Geophys. Res. Earth Surf.*, 110(F4), n/a-n/a, doi:10.1029/2004JF000259, 2005.
- 1120 Larsen, I. J., Montgomery, D. R. and Korup, O.: Landslide erosion controlled by hillslope material, *Nat. Geosci.*, 3(4), 247–251, doi:10.1038/ngeo776, 2010.
- Lavé, J. and Avouac, J. P.: Fluvial incision and tectonic uplift across the Himalayas of central Nepal, *J. Geophys. Res. Solid Earth*, 106(B11), 26561–26591, doi:10.1029/2001JB000359, 2001.
- [Leopold, L. B. and Maddock, T. J.: *The Hydraulic Geometry of Stream Channels and Some Physiographic Implications*, Tech. Rep. 252, US Geol. Surv. Professional Pap., 57 pp. and Maddock, T.: *The hydraulic geometry of stream channels and some physiographic implications*. \[online\] Available from: \[https://books.google.com/books?hl=en&lr=&id=K496gE_YsJoC&oi=fnd&pg=PP8&dq=Leopold,+L.+B.,+%26+Maddock,+T.,+\\(1953\\).+The+hydraulic+geometry+of+stream+channels+and+some+physiographic+implications+\\(U.S.+Geol.+Surv.+Prof.+Pap.,+252,+57+p.\\).+Washington,+DC:+U.S.+Government+Printing+Office.&ots=FipJCBq5vj&sig=Ot_PztOjXAUDQveL4k7WdwVw30\]\(https://books.google.com/books?hl=en&lr=&id=K496gE_YsJoC&oi=fnd&pg=PP8&dq=Leopold,+L.+B.,+%26+Maddock,+T.,+\(1953\).+The+hydraulic+geometry+of+stream+channels+and+some+physiographic+implications+\(U.S.+Geol.+Surv.+Prof.+Pap.,+252,+57+p.\).+Washington,+DC:+U.S.+Government+Printing+Office.&ots=FipJCBq5vj&sig=Ot_PztOjXAUDQveL4k7WdwVw30\) \(Accessed 26 September 2019\).](#) 1953.
- 1130 Mandal, S. K., Lupker, M., Burg, J.-P., Valla, P. G., Haghpor, N. and Christl, M.: Spatial variability of 10 Be-derived

Formatted: English (United Kingdom)

Formatted: English (United Kingdom)

- erosion rates across the southern Peninsular Indian escarpment: A key to landscape evolution across passive margins, *Earth Planet. Sci. Lett.*, 425, 154–167, doi:10.1016/j.epsl.2015.05.050, 2015.
- 1135 Manz, B., Buytaert, W., Zulkafli, Z., Lavado, W., Willems, B., Robles, L. A. and Rodríguez-Sánchez, J.-P.: High-resolution satellite-gauge merged precipitation climatologies of the Tropical Andes, *J. Geophys. Res. Atmos.*, 121(3), 1190–1207, doi:10.1002/2015JD023788, 2016.
- Meyer-Peter, E. and Müller, R.: Formulas for Bed-Load Transport, *Proc. Int. Assoc. Hydraul. Struct. Research - Second Meet. Stock. Sweden*, 39–65, doi:1948-06-07, 1948.
- 1140 Molina, A., Govers, G., Vanacker, V., Poesen, J., Zeelmaekers, E. and Cisneros, F.: Runoff generation in a degraded Andean ecosystem: Interaction of vegetation cover and land use, *CATENA*, 71(2), 357–370, doi:10.1016/j.catena.2007.04.002, 2007.
- Molnar, P., Anderson, R. S., Kier, G. and Rose, J.: Relationships among probability distributions of stream discharges in floods, climate, bed load transport, and river incision, *J. Geophys. Res.*, 111(F2), F02001, doi:10.1029/2005JF000310, 2006.
- 1145 Molnar, P., Anderson, R. S. and Anderson, S. P.: Tectonics, fracturing of rock, and erosion, *J. Geophys. Res.*, 112(F3), F03014, doi:10.1029/2005JF000433, 2007.
- Montgomery, D. R. and Brandon, M. T.: Topographic controls on erosion rates in tectonically active mountain ranges, *Earth Planet. Sci. Lett.*, 201(3–4), 481–489, doi:10.1016/S0012-821X(02)00725-2, 2002.
- 1150 Mora, D. E., Campozano, L., Cisneros, F., Wyseure, G. and Willems, P.: Climate changes of hydrometeorological and hydrological extremes in the Paute basin, Ecuadorian Andes, *Hydrol. Earth Syst. Sci.*, 18(2), 631–648, doi:10.5194/hess-18-631-2014, 2014.
- Muñoz, P., Orellana-Alvear, J., Willems, P. and Céleri, R.: Flash-Flood Forecasting in an Andean Mountain Catchment—Development of a Step-Wise Methodology Based on the Random Forest Algorithm, *Water*, 10(11), 1519, doi:10.3390/w10111519, 2018.
- NASA JPL: NASA Shuttle Radar Topography Mission Global 1 arc second., 2013.
- 1155 Nash, J. E. and Sutcliffe, J. V.: River Flow Forecasting Through Conceptual Models Part I—a Discussion of Principles*, *J. Hydrol.*, 10, 282–290, doi:10.1016/0022-1694(70)90255-6, 1970.
- Nearing, M. A., Wei, H., Stone, J. J., Pierson, F. B., Spaeth, K. E., Weltz, M. A., Flanagan, D. C. and Hernandez, M.: A Rangeland Hydrology and Erosion Model, *Trans. ASABE*, 54(3), 901–908, doi:10.13031/2013.37115, 2011.
- 1160 Nibourel, L., Herman, F., Cox, S. C., Beyssac, O. and Lavé, J.: Provenance analysis using Raman spectroscopy of carbonaceous material: A case study in the Southern Alps of New Zealand, *J. Geophys. Res. Earth Surf.*, 120(10), 2056–2079, doi:10.1002/2015JF003541, 2015.
- Niemi, N. A., Oskin, M., Burbank, D. W., Heimsath, A. M. and Gabet, E. J.: Effects of bedrock landslides on cosmogenically determined erosion rates, *Earth Planet. Sci. Lett.*, 237(3–4), 480–498, doi:10.1016/j.epsl.2005.07.009, 2005.
- 1165 Norton, K. P. and Vanacker, V.: Effects of terrain smoothing on topographic shielding correction factors for cosmogenic nuclide-derived estimates of basin-averaged denudation rates, *Earth Surf. Process. Landforms*, 34(1), 145–154, doi:10.1002/esp.1700, 2009.
- Ouimet, W. B., Whipple, K. X. and Granger, D. E.: Beyond threshold hillslopes: Channel adjustment to base-level fall in tectonically active mountain ranges, *Geology*, 37(7), 579–582, doi:10.1130/G30013A.1, 2009.
- 1170 [Pagani, M., Monelli, D., Weatherill, G., Danciu, L., Crowley, H., Silva, V., Henshaw, P., Butler, L., Nastasi, M., Panzeri, L., Simionato, M. and Vigano, D.: OpenQuake Engine: An Open Hazard \(and Risk\) Software for the Global Earthquake Model, *Seismol. Res. Lett.*, 85\(3\), 692–702, doi:10.1785/0220130087, 2014.](#)
- [Petersen, M. D., Harmsen, S. C., Jaiswal, K. S., Rukstales, K. S., Luco, N., Haller, K. M., Mueller, C. S. and Shumway, A. M.: Seismic Hazard, Risk, and Design for South America, *Bull. Seismol. Soc. Am.*, 108\(2\), 781–800, doi:10.1785/0120170002, 2018.](#)
- 1175 Portenga, E. W. and Bierman, P. R.: Understanding Earth’s eroding surface with 10Be, *GSA Today*, 21(8), 4–10, doi:10.1130/G111A.1, 2011.

Formatted: English (United Kingdom)

- Reusser, L., Bierman, P. and Rood, D.: Quantifying human impacts on rates of erosion and sediment transport at a landscape scale, *Geology*, 43(2), 171–174, doi:10.1130/G36272.1, 2015.
- 1180 Riebe, C. S., Kirchner, J. W., Granger, D. E. and Finkel, R. C.: Strong tectonic and weak climatic control of long-term chemical weathering rates, *Geology*, 29(6), 511, doi:10.1130/0091-7613(2001)029<0511:STAWCC>2.0.CO;2, 2001.
- [Roberts, G. G. and White, N.: Estimating uplift rate histories from river profiles using African examples, *J. Geophys. Res.*, 115\(B2\), B02406, doi:10.1029/2009JB006692, 2010.](#)
- Roering, J. J., Kirchner, J. W. and Dietrich, W. E.: Evidence for nonlinear, diffusive sediment transport on hillslopes and implications for landscape morphology, *Water Resour. Res.*, 35(3), 853–870, doi:10.1029/1998WR900090, 1999.
- 1185 Romans, B. W., Castellort, S., Covault, J. A., Fildani, A. and Walsh, J. P.: Environmental signal propagation in sedimentary systems across timescales, *Earth-Science Rev.*, 153, 7–29, doi:10.1016/j.earscirev.2015.07.012, 2016.
- Royden, L. and Taylor Perron, J.: Solutions of the stream power equation and application to the evolution of river longitudinal profiles, *J. Geophys. Res. Earth Surf.*, 118(2), 497–518, doi:10.1002/jgrf.20031, 2013.
- 1190 Sadler, P. M.: Sediment Accumulation Rates and the Completeness of Stratigraphic Sections, *J. Geol.*, 89(5), 569–584, doi:10.1086/628623, 1981.
- Safran, E. B., Bierman, P. R., Aalto, R., Dunne, T., Whipple, K. X. and Caffee, M.: Erosion rates driven by channel network incision in the Bolivian Andes, *Earth Surf. Process. Landforms*, 30(8), 1007–1024, doi:10.1002/esp.1259, 2005.
- 1195 Schaller, M., von Blanckenburg, F., Hovius, N. and Kubik, P. W.: Large-scale erosion rates from in situ-produced cosmogenic nuclides in European river sediments, *Earth Planet. Sci. Lett.*, 188(3–4), 441–458, doi:10.1016/S0012-821X(01)00320-X, 2001.
- Schaller, M., von Blanckenburg, F., Veldkamp, A., Tebbens, L. A., Hovius, N. and Kubik, P. W.: A 30 000 yr record of erosion rates from cosmogenic ¹⁰Be in Middle European river terraces, *Earth Planet. Sci. Lett.*, 204(1–2), 307–320, doi:10.1016/S0012-821X(02)00951-2, 2002.
- 1200 Schellekens, J., Dutra, E., Martínez-De La Torre, A., Balsamo, G., Van Dijk, A., Sperna Weiland, F., Minvielle, M., Calvet, J. C., Decharme, B., Eisner, S., Fink, G., Flörke, M., Peßenteiner, S., Van Beek, R., Polcher, J., Beck, H., Orth, R., Calton, B., Burke, S., Dorigo, W. and Weedon, G. P.: A global water resources ensemble of hydrological models: The earth2Observe Tier-1 dataset, *Earth Syst. Sci. Data*, 9(2), 389–413, doi:10.5194/essd-9-389-2017, 2017.
- Scherler, D., Bookhagen, B. and Strecker, M. R.: Tectonic control on ¹⁰Be-derived erosion rates in the Garhwal Himalaya, India, *J. Geophys. Res. Earth Surf.*, 119(2), 83–105, doi:10.1002/2013JF002955, 2014.
- 1205 Scherler, D., DiBiase, R. A., Fisher, G. B. and Avouac, J.-P.: Testing monsoonal controls on bedrock river incision in the Himalaya and Eastern Tibet with a stochastic-threshold stream power model, *J. Geophys. Res. Earth Surf.*, 122(7), 1389–1429, doi:10.1002/2016JF004011, 2017.
- Schmidt, K. M. and Montgomery, D. R.: Limits to Relief, *Science* (80-.), 270(5236), 617–620, doi:10.1126/science.270.5236.617, 1995.
- 1210 [Schmied, H. M., Eisner, S., Franz, D., Wattenbach, M., Portmann, F. T., Flörke, M. and Döll, P.: Sensitivity of simulated global-scale freshwater fluxes and storages to input data, hydrological model structure, human water use and calibration, *Hydrol. Earth Syst. Sci.*, 18\(9\), 3511–3538, doi:10.5194/hess-18-3511-2014, 2014.](#)
- Schwanghart, W. and Scherler, D.: Short Communication: TopoToolbox 2 - MATLAB-based software for topographic analysis and modeling in Earth surface sciences, *Earth Surf. Dyn.*, 2(1), 1–7, doi:10.5194/esurf-2-1-2014, 2014.
- 1215 Schwanghart, W., Ryan, M. and Korup, O.: Topographic and Seismic Constraints on the Vulnerability of Himalayan Hydropower, *Geophys. Res. Lett.*, 45(17), 8985–8992, doi:10.1029/2018GL079173, 2018.
- [Shobe, C. M., Tucker, G. E. and Barnhart, K. R.: The SPACE 1.0 model: a Landlab component for 2-D calculation of sediment transport, bedrock erosion, and landscape evolution, *Geosci. Model Dev.*, 10\(12\), 4577–4604, doi:10.5194/gmd-10-4577-2017, 2017.](#)
- 1220 [Shobe, C. M., Tucker, G. E. and Rossi, M. W.: Variable-Threshold Behavior in Rivers Arising From Hillslope-Derived Blocks, *J. Geophys. Res. Earth Surf.*, 123\(8\), 1931–1957, doi:10.1029/2017JF004575, 2018.](#)

Formatted: English (United Kingdom)

Formatted: English (United Kingdom)

[Sklar, L., Dietrich, E. and Kppfgka, K.: Profiles and Bedrock Incision Models : Stream Power and the Influence of Sediment Supply \$W = KwQw E = KyAr\$ \(••\) S, 1998.](#)

1225 Snyder, N. P., Whipple, K. X., Tucker, G. E. and Merritts, D. J.: Landscape response to tectonic forcing: Digital elevation model analysis of stream profiles in the Mendocino triple junction region, northern California, *Geol. Soc. Am. Bull.*, 112(8), 1250–1263, doi:10.1130/0016-7606(2000)112<1250:LRTTFD>2.3.CO;2, 2000.

Formatted: English (United Kingdom)

Snyder, N. P., Whipple, K. X., Tucker, G. E. and Merritts, D. J.: Importance of a stochastic distribution of floods and erosion thresholds in the bedrock river incision problem, *J. Geophys. Res. Solid Earth*, 108(B2), 2388, doi:10.1029/2001JB001655, 2003.

1230 Sorensen, C. S. and Yanites, B. J.: Latitudinal trends in modern fluvial erosional efficiency along the Andes, *Geomorphology*, 329, 170–183, doi:10.1016/j.geomorph.2018.12.030, 2019.

Spikings, R., Winkler, W., Seward, D. and Handler, R.: Along-strike variations in the thermal and tectonic response of the continental Ecuadorian Andes to the collision with heterogeneous oceanic crust, *Earth Planet. Sci. Lett.*, 186(1), 57–73, doi:10.1016/S0012-821X(01)00225-4, 2001.

1235 Spikings, R. A. and Crowhurst, P. V.: (U–Th)/He thermochronometric constraints on the late Miocene–Pliocene tectonic development of the northern Cordillera Real and the Interandean Depression, Ecuador, *J. South Am. Earth Sci.*, 17(4), 239–251, doi:10.1016/j.jsames.2004.07.001, 2004.

1240 Spikings, R. A., Crowhurst, P. V., Winkler, W. and Villagomez, D.: Syn- and post-accretionary cooling history of the Ecuadorian Andes constrained by their in-situ and detrital thermochronometric record, *J. South Am. Earth Sci.*, 30(3–4), 121–133, doi:10.1016/j.jsames.2010.04.002, 2010.

Steinmann, M., Hungerbühler, D., Seward, D. and Winkler, W.: Neogene tectonic evolution and exhumation of the southern Ecuadorian Andes: a combined stratigraphy and fission-track approach, *Tectonophysics*, 307(3–4), 255–276, doi:10.1016/S0040-1951(99)00100-6, 1999.

1245 Stock, J. D. and Montgomery, D. R.: Geologic constraints on bedrock river incision using the stream power law, *J. Geophys. Res.*, 104(B3), 4983, doi:10.1029/98JB02139, 1999.

[Thiery, W., Davin, E. L., Panitz, H. J., Demuzere, M., Lhermitte, S. and van Lipzig, N.: The Impact of the African Great Lakes on the Regional Climate, *J. Clim.*, 28\(10\), 4061–4085, doi:10.1175/JCLI-D-14-00565.1, 2015.](#)

1250 Tofelde, S., Duesing, W., Schildgen, T. F., Wickert, A. D., Wittmann, H., Alonso, R. N. and Strecker, M.: Effects of deep-seated versus shallow hillslope processes on cosmogenic ¹⁰Be concentrations in fluvial sand and gravel, *Earth Surf. Process. Landforms*, 43(15), 3086–3098, doi:10.1002/esp.4471, 2018.

Formatted: English (United Kingdom)

Tucker, G. E.: Drainage basin sensitivity to tectonic and climatic forcing: Implications of a stochastic model for the role of entrainment and erosion thresholds, *Earth Surf. Process. Landforms*, 29(2), 185–205, doi:10.1002/esp.1020, 2004.

Tucker, G. E. and Bras, R. L.: A stochastic approach to modeling the role of rainfall variability in drainage basin evolution, *Water Resour. Res.*, 36(7), 1953–1964, doi:10.1029/2000WR900065, 2000.

1255 Tucker, G. E. and Hancock, G. R.: Modelling landscape evolution, *Earth Surf. Process. Landforms*, 35(1), 28–50, doi:10.1002/esp.1952, 2010.

Vanacker, V., von Blanckenburg, F., Govers, G., Molina, A., Poesen, J., Deckers, J. and Kubik, P.: Restoring dense vegetation can slow mountain erosion to near natural benchmark levels, *Geology*, 35(4), 303, doi:10.1130/G23109A.1, 2007.

1260 Vanacker, V., von Blanckenburg, F., Govers, G., Campforts, B. and Kubik, P. W.: Transient river response, captured by channel steepness and its concavity, *Geomorphology*, 228, 234–243, doi:10.1016/j.geomorph.2014.09.013, 2015.

1265 [Vanacker, V., Ameijeiras-Mariño, Y., Schoonejans, J., Cornéilis, J.-T., Minella, J. P. G., Lamouline, F., Vermeire, M. L., Campforts, B., Robinet, J., Van de Broek, M., Delmelle, P. and Opfergelt, S.: Land use impacts on soil erosion and rejuvenation in Southern Brazil, *CATENA*, 178, 256–266, doi:10.1016/j.catena.2019.03.024, 2019.](#)

[Venditti, J. G., Li, T., Deal, E., Dingle, E. and Church, M.: Struggles with stream power: Connecting theory across scales, *Geomorphology*, \(xxxx\), 106817, doi:10.1016/j.geomorph.2019.07.004, 2019.](#)

[Whipple, K. X.: Fluvial landscape response time: How plausible is steady-state denudation?. Am. J. Sci., doi:10.2475/ajs.301.4-5.313, 2001.](#)

1270 Whipple, K. X. and Tucker, G. E.: Dynamics of the stream-power river incision model: Implications for height limits of mountain ranges, landscape response timescales, and research needs, *J. Geophys. Res. Solid Earth*, 104(B8), 17661–17674, doi:10.1029/1999JB900120, 1999.

Whipple, K. X., Kirby, E. and Brocklehurst, S. H.: Geomorphic limits to climate-induced increases in topographic relief, *Nature*, 401(6748), 39–43, doi:10.1038/43375, 1999.

1275 Whipple, K. X., Hancock, G. S. and Anderson, R. S.: River incision into bedrock: Mechanics and relative efficacy of plucking, abrasion, and cavitation, *Geol. Soc. Am. Bull.*, 112(3), 490–503, doi:10.1130/0016-7606(2000)112<490:RIIBMA>2.0.CO;2, 2000.

Whipple, K. X., DiBiase, R. A. and Crosby, B. T.: 9.28 Bedrock Rivers, in *Treatise on Geomorphology*, vol. 9, edited by J. F. Shroder, pp. 550–573, Elsevier, San Diego., 2013.

1280 Whittaker, A. C. and Boulton, S. J.: Tectonic and climatic controls on knickpoint retreat rates and landscape response times, *J. Geophys. Res. Earth Surf.*, 117(F2), n/a-n/a, doi:10.1029/2011JF002157, 2012.

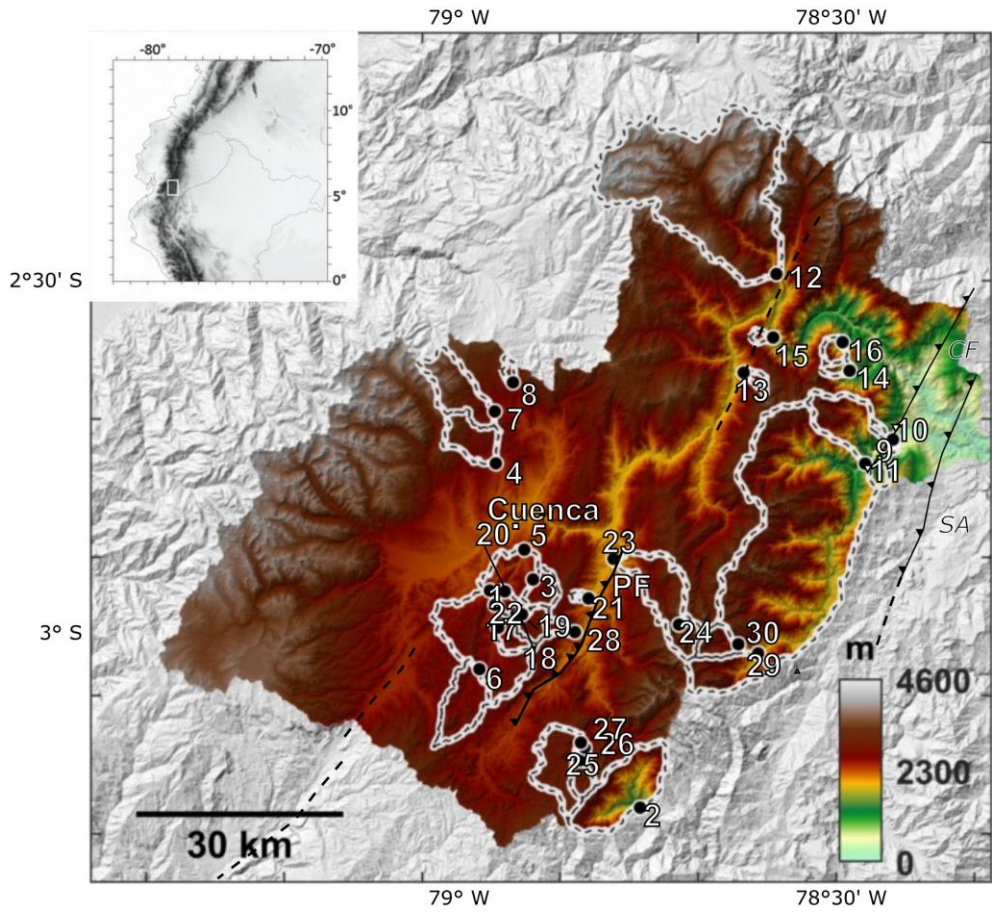
Wobus, C., Whipple, K. X., Kirby, E., Snyder, N., Johnson, J., Spyropolou, K., Crosby, B. and Sheehan, D.: Tectonics from topography: Procedures, promise, and pitfalls, in [Special Paper 398: Tectonics, Climate, and Landscape Evolution](#), vol. 398, pp. 55–74, Geological Society of America., 2006.

1285 Yanites, B. J. and Tucker, G. E.: Controls and limits on bedrock channel geometry, *J. Geophys. Res.*, 115(F4), F04019, doi:10.1029/2009JF001601, 2010.

[Yanites, B. J., Tucker, G. E. and Anderson, R. S.: Numerical and analytical models of cosmogenic radionuclide dynamics in landslide-dominated drainage basins, J. Geophys. Res., 114\(F1\), F01007, doi:10.1029/2008JF001088, 2009.](#)

Formatted: English (United Kingdom)

Formatted: English (United Kingdom)



1290

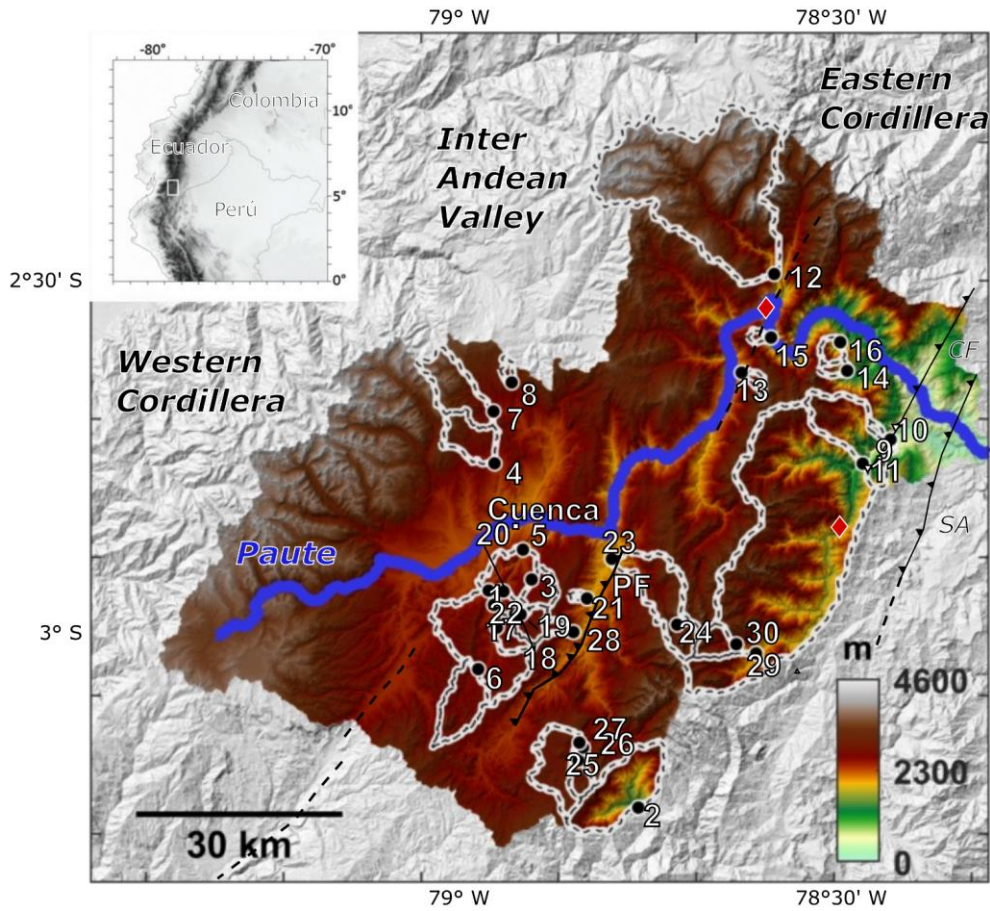


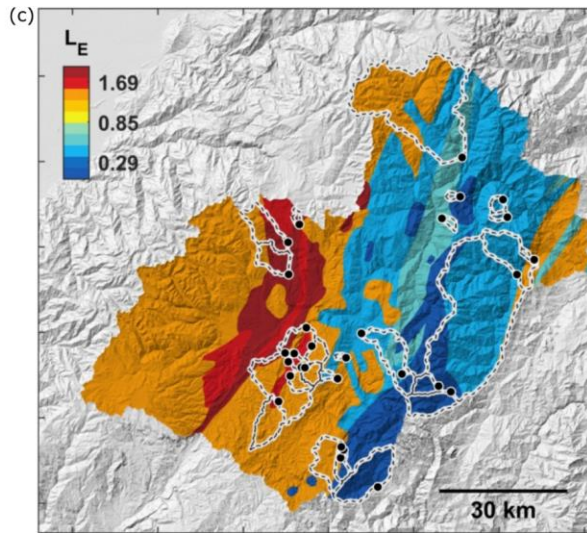
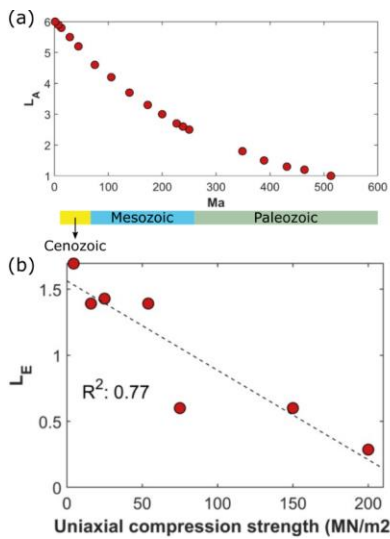
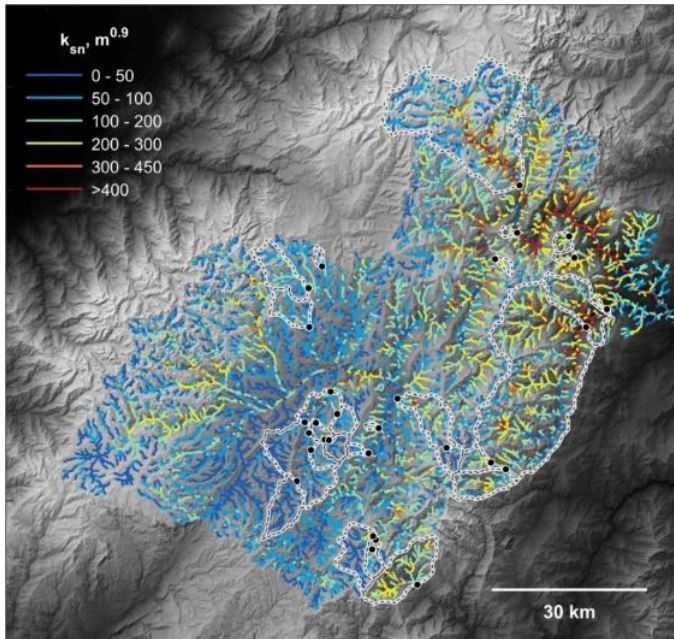
Figure 1. Geomorphic setting of the study area. Numbered Paute catchment. The numbered dots and corresponding watersheds indicate the sampling locations for the CRN-derived erosion rates (Table 2). Major and their corresponding watersheds (Table 2). Full black lines indicate the major faults are drawn with a full black line; PF = the Peltetec Fault, CF = the Cosanga Fault, and SA = the Sub-Andean thrust fault. Concealed faults separating major stratigraphical units are indicated with dashed lines. Elevations are Major knickpoints are indicated as red diamonds. The colour scale indicates elevations, which were derived from the 30 m SRTM v3 DEM (NASA JPL, 2013).

Formatted: Normal

Formatted: Font: Bold

Formatted: Font color: Text 2

1295



1300

Figure 2: The spatial pattern of normalized steepness (k_{sn}) for the Paute basin overlain on hillshade map based on the 30 m SRTM v3 DEM (NASA JPL, 2013). Highest values are observed in two major knick zones in the lower part of the Paute

Field Code Changed

basin where topographic rejuvenation started and a transient incision pulse has propagated from East to West, see also Figure S3.

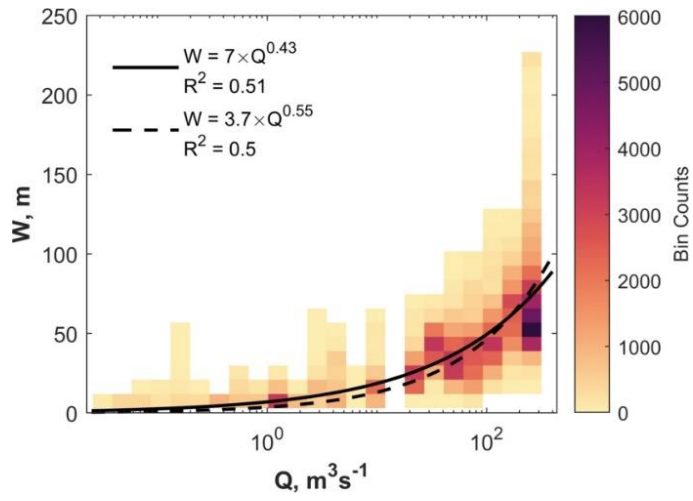
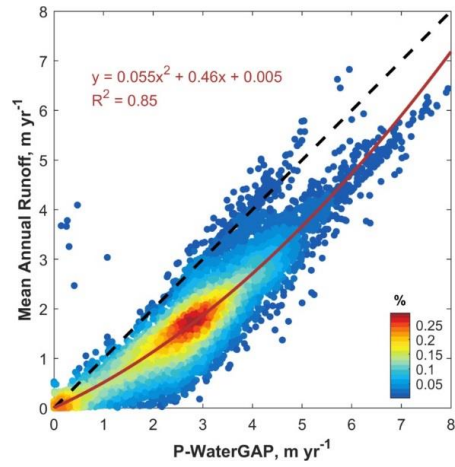
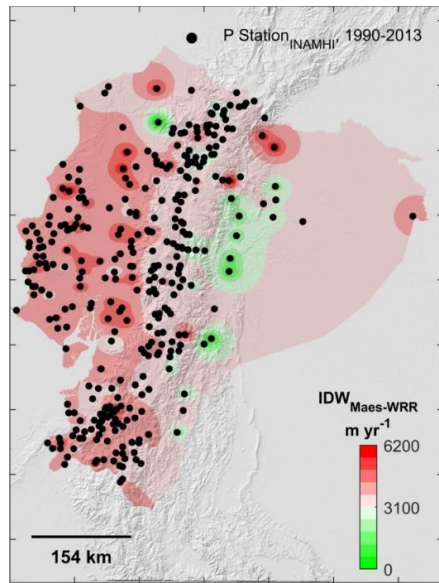


Figure 3. River width (W) as a function of the mean annual discharge (Q), derived from the downscaled R_{RDW} -WRR2 WaterGAP3 data (available from earth2observe.eu).

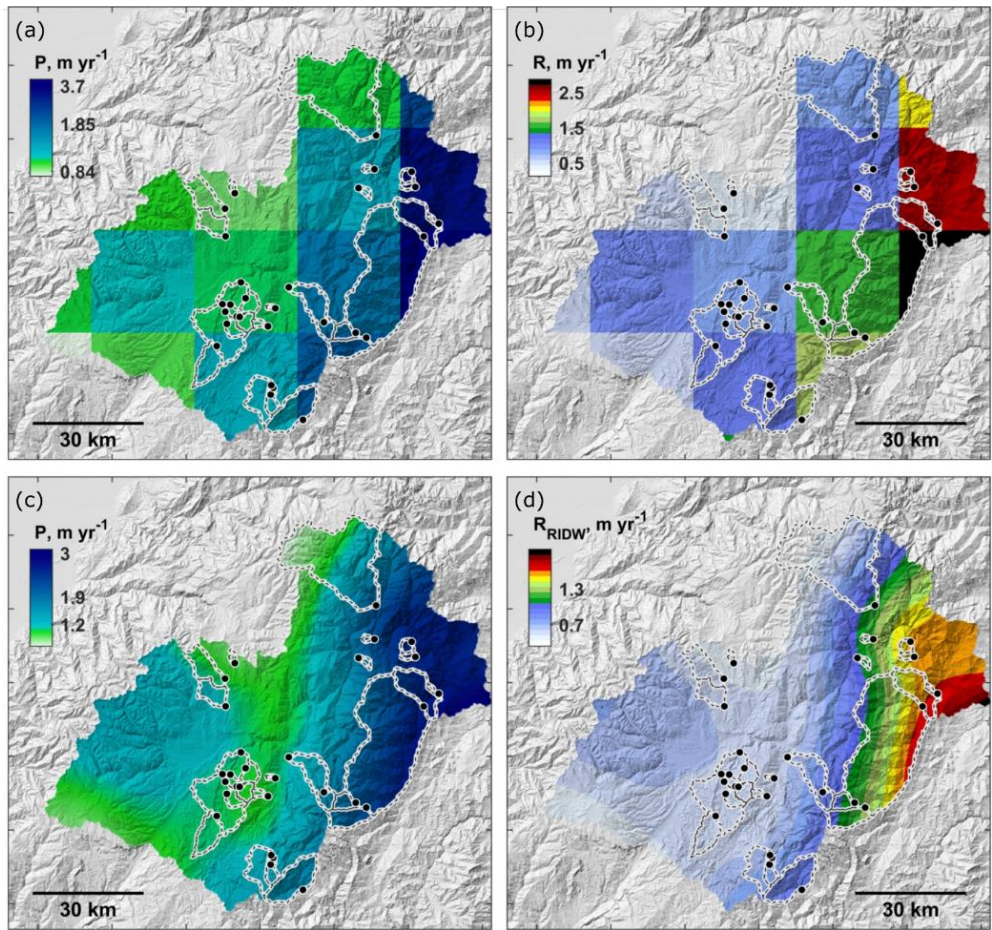
1305



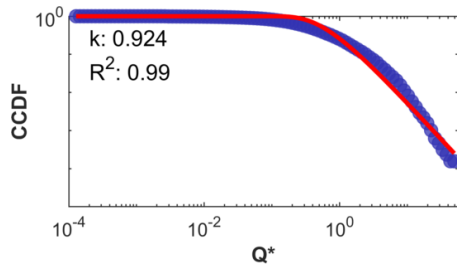
1310 **Figure 4:** Mean monthly runoff versus mean monthly precipitation for all Ecuadorian WaterGAP3 pixels (0.25°; 1979-2014; WaterGAP3 data available from earth2observe.eu).



1315 **Figure 5:** Inverse Distance Weighting (IDW) interpolation between rain gauge data (INAMHI, available from <http://www.serviciometeorologico.gob.ec/biblioteca/>) and WRR2-WaterGAP3 mean annual precipitation overlain on hillshade map based on the 30 m SRTM v3 DEM (NASA JPL, 2013). WaterGAP3 data available from earth2observe.eu.



1320 **Figure 6.** Mean annual rainfall and runoff based on WRR2 WaterGAP3 data overlain on hillshade map based on the 30 m SRTM v3 DEM (NASA JPL, 2013). (a) Precipitation (P , 0.25°), (b) runoff (R , 0.25°), (c) downscaled precipitation (P_{RIDW} ; 2500 m), (d) downscaled runoff (R_{RIDW} ; 2500 m). WaterGAP3 data available from earth2observe.eu.



1325 **Figure 7:** Daily discharge distribution (blue dots) derived at the outlet of one basin (NG-DW) using the downscaled WaterGAP data. The red curve depicts the fitted *cecdf* function (Eq. (14)) and its corresponding discharge variability coefficient (*k*). An overview of *k* values for all sub-catchments is provided in Table 2.

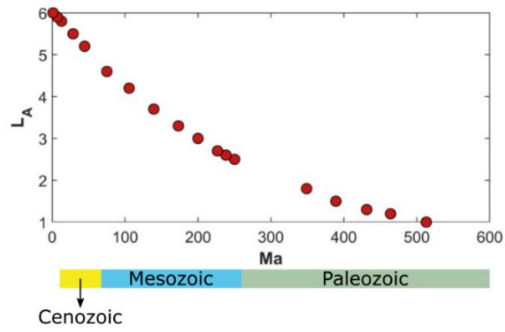


Figure 8: Lithological: Development of empirical lithological erodibility index (L_E) and its application to the Pauté catchment. (a) Proposed lithological erodibility index based on lithological age (L_A). Detailed sub-classifications per lithology can be found in Table S1.

1330

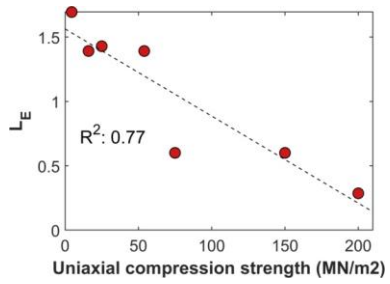


Figure 9(b) Field measurements of uniaxial compressive strength (Basabe R, 1998; Table S4) versus the empirical erodibility index calculated using Eq. (15).7. Note that two out of the nine observations overlap on this plot.

1335

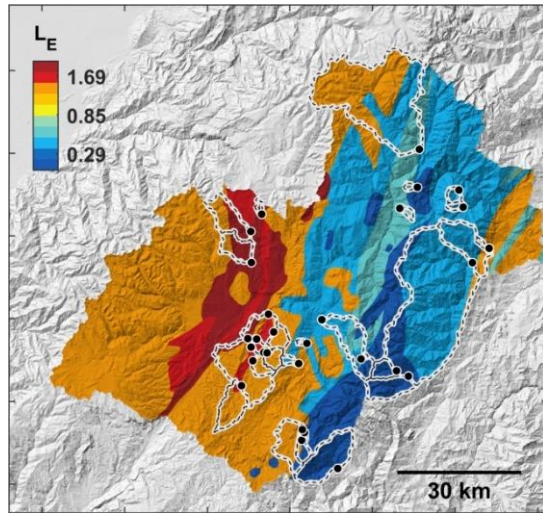
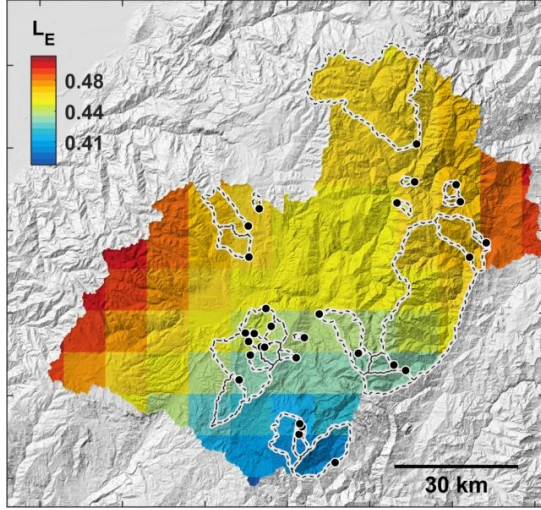


Figure 10: Lithological erodibility index (LE) spatial distribution in the Paute catchment. The underlying topographic map is based on the 30 m SRTM v3 DEM (NASA JPL, 2013). The lithological erodibility map for Ecuador is shown in Figure S1.

1340

Formatted: Font: Italic, Font color: Text 2



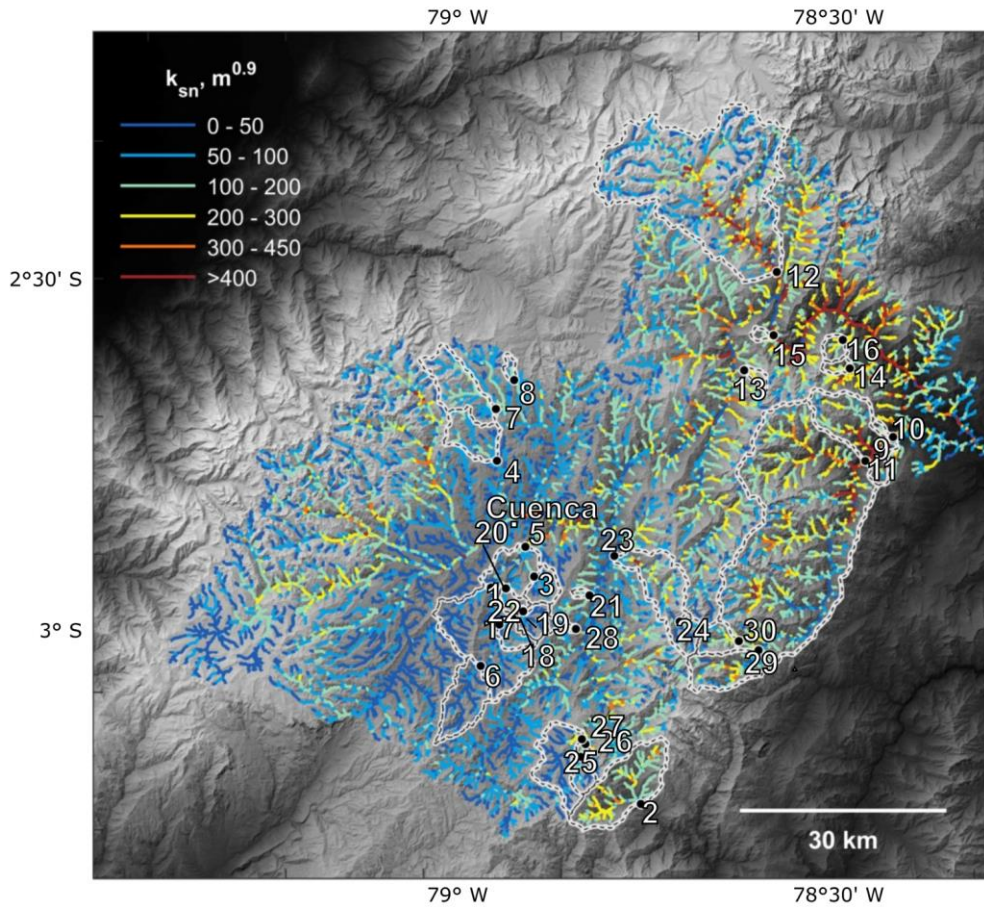


Figure 3: Peak Ground Acceleration (PGA, g) for a 10% probability of exceedance in a 50-year hazard level (Petersen et al., 2018) overlain on hillshade map: **Normalized steepness (k_{sn}) for the Paute basin.** Calculated k_{sn} -values for the Paute basin are overlain with a hillshade map (based on the 30 m SRTM v3 DEM; NASA JPL, 2013). The highest values can be observed in two major knick zones, located in the lower part of the Paute basin. In these zones, topographic rejuvenation started and a transient incision pulse has propagated from East to West (see also Figure S3).

1345

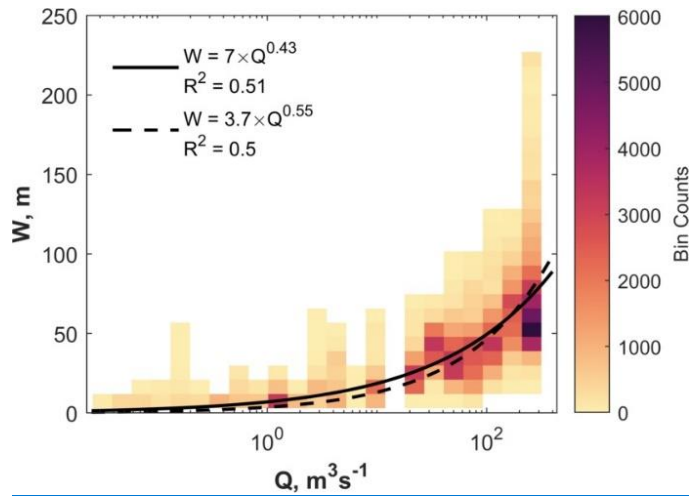


Figure 4. River width (W) as a function of the mean annual discharge (Q). W represents bankfull channel width for a selected number of river sections. These were digitized in Google Earth, using the ChanGeom toolset (Fisher et al., 2013a; figure S5). Mean annual water discharges (Q) were derived from the downscaled R_{RDW} WRR2 WaterGAP3 data (available from earth2observe.eu; see section 2.4).

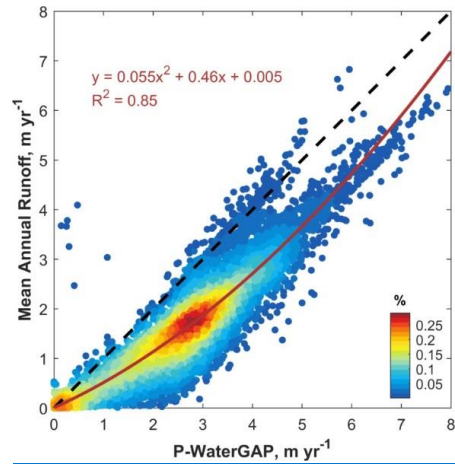


Figure 5: Calibration of the precipitation (P) versus runoff curve (R). Mean annual runoff versus the mean annual precipitation for all WaterGAP3 pixels in Ecuador (0.25°; 1979-2014; WaterGAP3 data available from earth2observe.eu).

1360

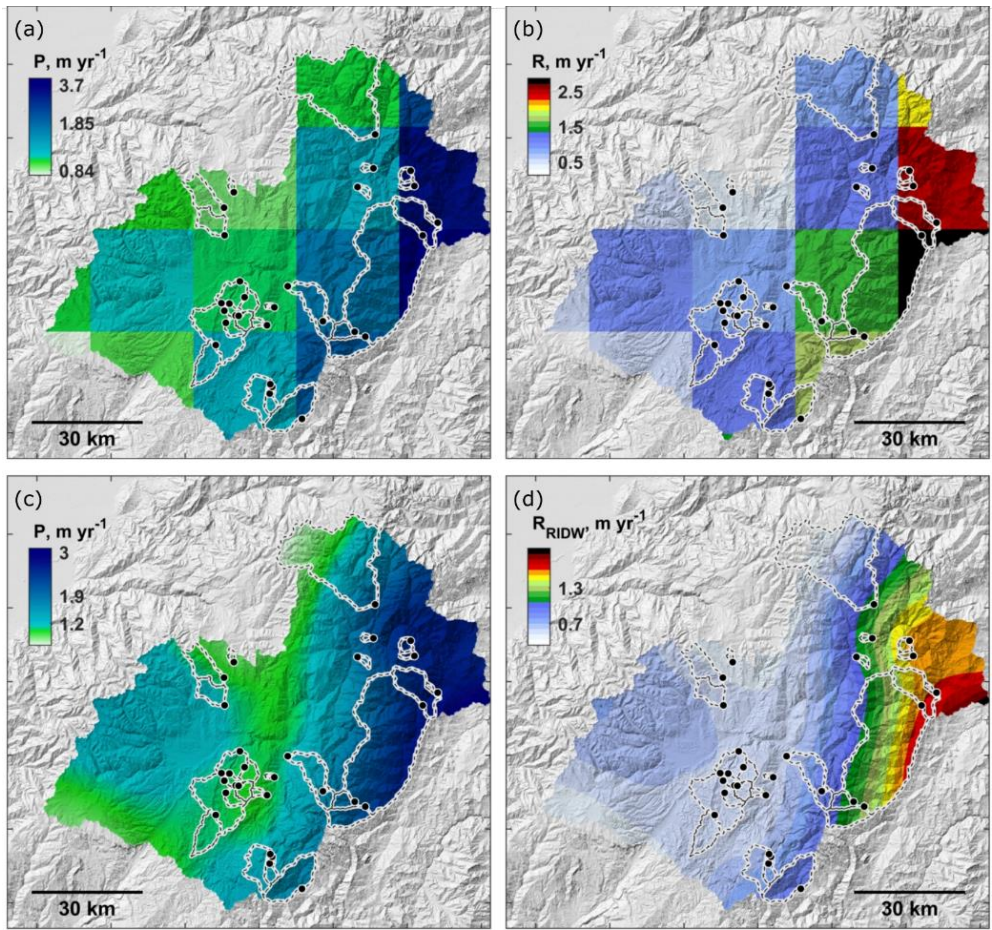
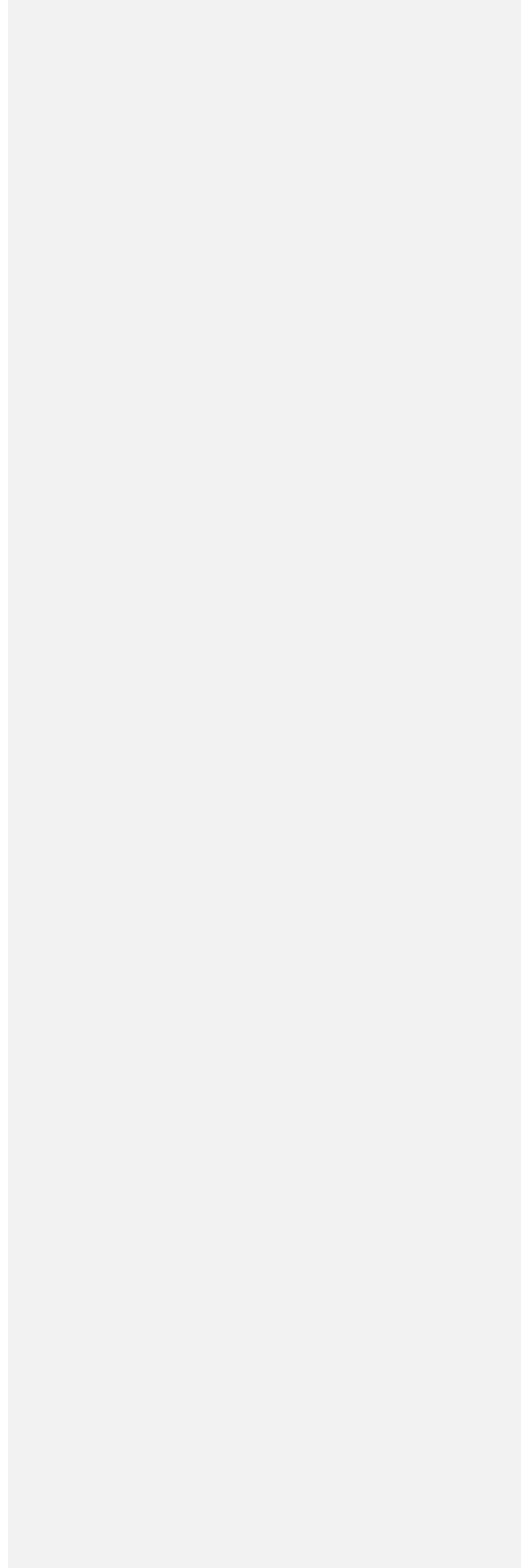


Figure 6. Downscaling of WRR2 WaterGAP3 rainfall and runoff products to high resolution regional maps. (a) WRR2 WaterGAP3 precipitation (P) at the original resolution of 0.25° . (b) Corresponding runoff (R) at the original resolution of 0.25° . (c) Downscaled precipitation (P_{RIDW}) at a resolution of 2500 m. (d) corresponding downscaled runoff (R_{RIDW}) at a resolution of 2500 m. WaterGAP3 data were derived from earth2observe.eu. The underlying hillshade maps are based on the 30 m SRTM v3 DEM (NASA JPL, 2013). The map for Ecuador is shown in Figure S2.

1365

|



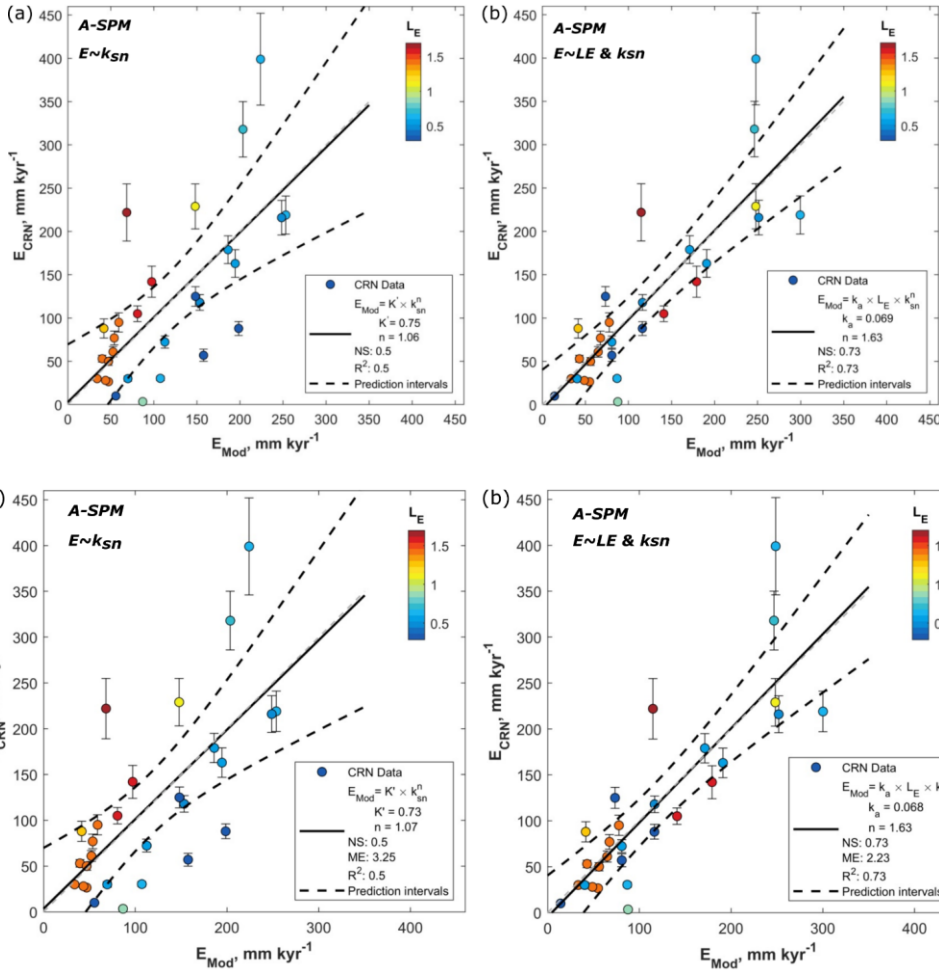
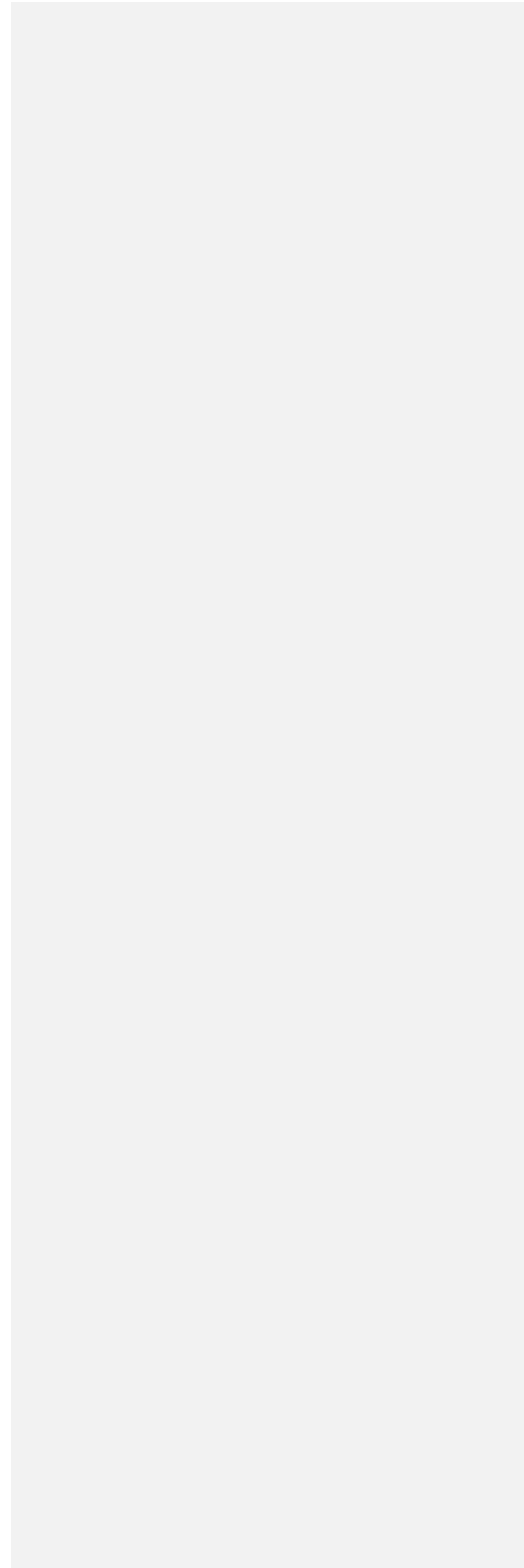


Figure 7 Best fit between **CRN-derived erosion rates (E_{CRN})** and modelled river incision (E_{Mod}) simulated using the drainage Area-area-based Stream Power Model (A-SPM; Eq. (8)). (a) A-SPM, scenario 1 (cf. Table 4) assuming a uniform lithology. Observations are coloured according to the average lithological erodibility of the catchment ($\overline{L_E} = 1$). Low values for $\overline{L_E}$ represent strong rocks, resistant to erosion. High values for $\overline{L_E}$ represent weak rocks, susceptible to erosion. Modelled erosion rates for catchments consisting of strong rocks (blue colours) are mostly over predicted and plot below the 1:1 line. Modelled erosion rates for catchments consisting of weak rocks (red colours) are mostly under predicted and plot above the 1:1 line. (b) A-SPM, scenario 2 (Table 4) where spatially variable lithological erodibility ($\overline{L_E}$ values listed explicitly accounted for in Table 2)-the A-SPM. Catchment specific values for $\overline{L_E}$ are listed in Table 2, while the model parameters are listed in Table 4. A complete overview of all best model fits for A-SPM scenarios 1 - 4 is given in Figure S8.



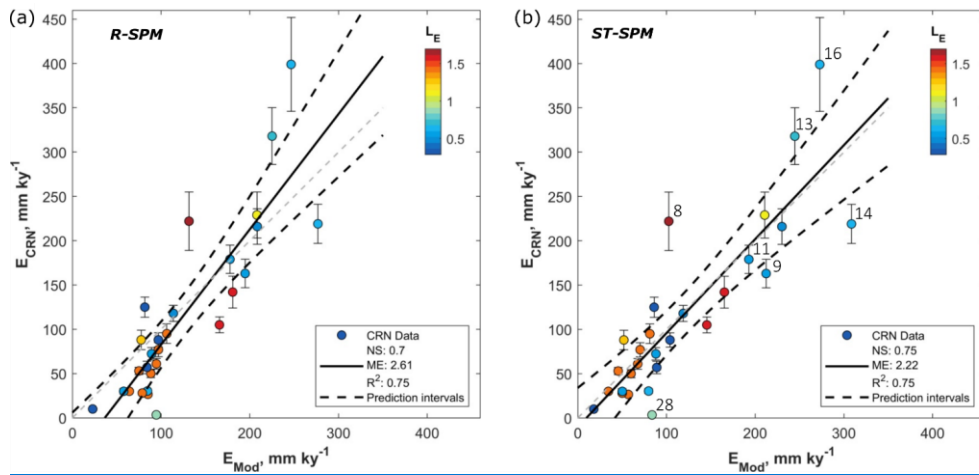
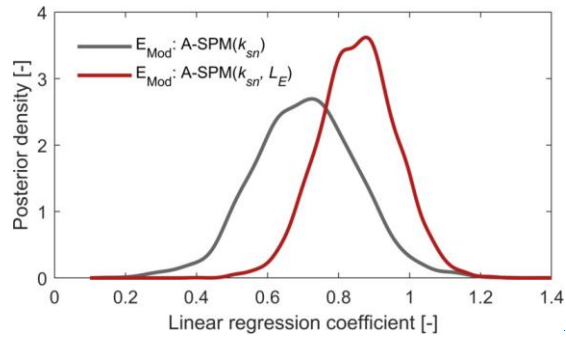


Figure 8 Posterior probability distributions of the coefficients obtained from a linear Bayesian regression between E_{CRN} and E_{Mod} . Bayesian regression was calculated with standardized (z-transformed) variables to enable comparison between the models.

Field Code Changed

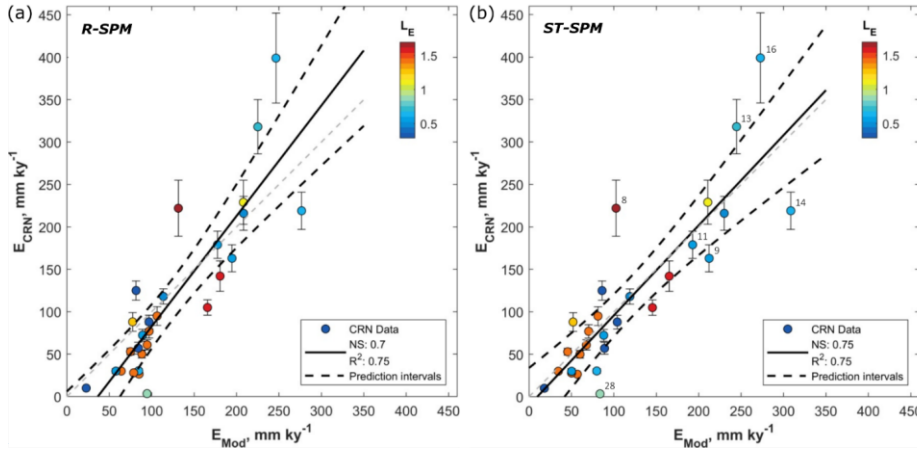


Figure 14 Best fit between **CRN-derived erosion rates (E_{CRN})** and modelled river incision (E_{Mod}) simulated using (a) the **Runoff-based Stream Power Model (R-SPM)** and (b) the **Stochastic-Threshold Stream Power Model (ST-SPM)**. Constant model parameters are listed in Table 1. Free parameters are **Models**. (a) R-SPM, scenario 2 (Table 4) assuming average catchment lithological erodibility (\bar{L}_E) and runoff \bar{R} values (both listed in Table 5; (Table 2). (b) ST-SPM, scenario 7 (Table 4) assuming average catchment lithological erodibility (\bar{L}_E) and runoff (\bar{R}) values, as well as considering a) corresponds to R-SPM Scenario 1 and (b) to ST-SPM Scenario 6; threshold before river incision occurs ($\tau_c = 14\text{Pa}$). Numbered observations in (b) correspond to catchment ID's as listed in Table 2 and discussed in section 7.1. ID's as listed in Table 2 (see also the discussion in section 5). A complete overview of all best model fits for R-SPM scenarios 1 - 2 and ST-SPM scenarios 1 - 8 is given in respectively Figure S9 and Figure S10.

Formatted: Font: Bold

Formatted: Font: Bold

Formatted: Font: Bold

Formatted: Font: Bold

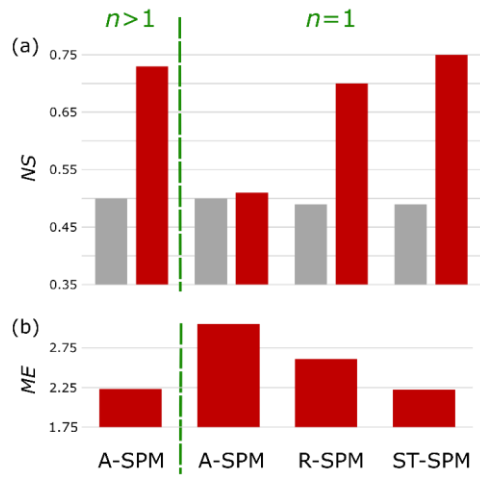


Figure 9: Comparison of model performance of four selected river incision models. (a) Nash Sutcliffe model efficiency (*NS*) for different model scenarios, without (grey bars) or with (red bars) considering lithological heterogeneity. (b) shows the corresponding Model Error (*ME*). The A-SPM model scenario corresponds to the Area-Based Stream Power Model (cf. Figure 7). It performs well when lithological heterogeneity is considered and all parameters are freely calibrated, resulting in a slope-steepness exponent (*n*; cf. Eq. 1) of 1.62 (for a full overview of model parameters, see Table 4). However, for an A-SPM scenario where *n* is fixed to the theoretically derived value of 1, the model performance strongly deteriorates (see main text). R-SPM represents a model scenario that explicitly incorporates runoff variability (cf. Figure 8a). The ST-SPM scenario also includes an incision threshold (cf. Figure 8b). Both scenarios perform well when *n* is fixed to 1 and when considering lithological heterogeneity. Overall, the best model performance (highest *NS* and smallest *ME*) is obtained under the ST-SPM scenario where lithological and runoff variability, as well as river incision thresholds are considered.

1400

1405

1410

Table 1: Constant parameter values used when solving the R-SPM and ST-SPM model parameters

Parameter	Model	Description	Value	Unit
a	R-SPM/ST-SPM	Bed shear stress exponent, with τ^a representing unit stream power if $a=3/2$	3/2	dimensionless
k_r	R-SPM/ST-SPM	Flow resistance factor	1000	$\text{kg} \cdot \text{m}^{-7/3} \cdot \text{s}^{-4/3}$
k_w	R-SPM/ST-SPM	Scaling parameter between bankfull river width and discharge	3.7	$\text{m}^{-0.65} \cdot \text{s}^{-0.55}$
α	R-SPM/ST-SPM	Flow resistance exponent (Darcy-Weisbach)	2/3	dimensionless
β	R-SPM/ST-SPM	Flow resistance exponent (Darcy-Weisbach)	2/3	dimensionless
θ_{ref}	R-SPM/ST-SPM	Reference concavity	0.45	dimensionless
ρ_s	ST-SPM	Sediment particle density	2.7	$\text{g} \cdot \text{cm}^{-3}$
ρ_w	ST-SPM	Fluid density	1	$\text{g} \cdot \text{cm}^{-3}$
τ_c^*	ST-SPM	Shield's number	0.045	dimensionless
ω_b	ST-SPM	downstream channel width variation exponent	0.55	dimensionless
ω_s	ST-SPM	At-a-station channel width variation exponent	0.25	dimensionless

Formatted: Font: 10 pt

1415

Table 2: Properties/Characteristics of the sub-catchments studied in this paper. **ID-s/IDs** correspond to the numbers indicated on [Figure 1-Figure 1](#). The ^{10}Be cosmogenic nuclide derived erosion rates [are/were](#) derived from Vanacker et al. (2015)^a. Coordinates are given in decimal degrees in the WGS84 datum, \bar{L}_E is the [catchment](#)-average lithological index, \overline{PGA} is for the catchment [average](#)-seismicity, k_{sn} is the normalized catchment average steepness, P_{RIDW} and R_{RIDW} are respectively the [catchment](#)-average [downscaled](#) [catchment](#) [average](#) precipitation and runoff and k is the optimized discharge variability coefficient.

ID	Sample	Lat, °	Lon, °	Area, km ²	¹⁰ Be erosion, mm-ka ⁻¹	\bar{L}_E	\overline{PGA} , g	k_{sn} m ^{0.9}	P_{RIDW} , m-yr ⁻¹	R_{RIDW} , m-yr ⁻¹	k
1	BQ	-2.94	-78.93	186.3	53 ± 4	1.44	0.44	41.78	1.06	0.55	1.18
2	CH	-3.22	-78.74	86	88 ± 8	0.34	0.42	187.79	1.59	0.87	0.87
3	CJ	-2.92	-78.88	19.5	95 ± 11	1.43	0.44	60.45	1.02	0.54	1.04
4	DE2	-2.77	-78.93	39.1	105 ± 9	1.61	0.45	80.96	1.14	0.58	1.04
5	JA21	-2.89	-78.89	276	50 ± 4.5	1.45	0.44	48.96	1.05	0.55	1.19
6	MAR	-3.04	-78.95	49.8	30 ± 2	1.43	0.43	35.97	1.07	0.56	1.08
7	NA1	-2.70	-78.92	57.1	142 ± 18	1.54	0.45	96.36	1.04	0.53	1.05
8	NA4	-2.67	-78.90	4.9	222 ± 33	1.69	0.45	69.19	0.87	0.44	1.11
9	NG-DW	-2.73	-78.40	686.8	163 ± 16	0.57	0.45	184.21	2.25	1.33	0.92
10	NG-SD	-2.73	-78.39	3.3	3959 ± 3801	0.89	0.46	231.84	2.62	1.60	0.91
11	NG-UP	-2.78	-78.46	679.1	179 ± 16	0.55	0.44	176.77	2.21	1.31	0.91
12	PA	-2.52	-78.56	424.4	229 ± 26	1.13	0.45	142.61	1.14	0.60	1.16
13	PAL	-2.65	-78.61	6.2	318 ± 32	0.69	0.45	192.24	1.89	1.11	0.88
14	PT-BM	-2.65	-78.46	6.8	219 ± 22	0.60	0.45	236.09	2.50	1.51	0.91
15	PT-QP	-2.61	-78.57	3.4	216 ± 20	0.52	0.45	231.77	2.01	1.16	0.94
16	PT-SD	-2.61	-78.46	11.1	399 ± 53	0.60	0.45	210.28	2.52	1.51	0.93
17	QU	-2.99	-78.92	16.7	77 ± 8	1.43	0.44	55.32	1.02	0.53	1.17
19	RG1-2	-2.96	-78.89	0.9	26.5 ± 2	1.43	0.44	48.87	1.01	0.53	1.13
20	RG2	-2.94	-78.91	29.2	61 ± 6	1.44	0.44	53.96	1.01	0.53	1.12
21	RGD1	-2.94	-78.80	2.2	30 ± 3	0.64	0.44	105.63	1.03	0.55	1.14
18	RGST	-2.97	-78.90	20.2	28 ± 2	1.42	0.44	45.55	1.00	0.52	1.08
22	SA	-2.96	-78.93	0.5	152 ± 19	1.49	0.44	0.04	1.05	0.55	1.16
23	SF1-2	-2.89	-78.77	84	72 ± 7	0.56	0.44	110.46	1.42	0.78	0.83
24	SF2	-2.98	-78.69	1.3	118 ± 9	0.50	0.44	147.45	1.60	0.89	0.80
25	SH	-3.16	-78.81	0.6	10 ± 1	0.29	0.42	57.09	1.34	0.72	0.95
26	SI2	-3.14	-78.81	18.3	30 ± 3	0.58	0.42	70.42	1.38	0.74	0.99
27	SI3	-3.14	-78.81	49.2	88 ± 11	1.30	0.42	43.63	1.28	0.68	1.03
28	SI5	-3.00	-78.81	6	3.4 ± 0.3	0.90	0.43	86.62	0.99	0.53	1.09
29	TH1	-3.01	-78.57	62.1	125 ± 11	0.33	0.43	142.87	1.97	1.13	0.84
30	TH2	-3.01	-78.61	21	57 ± 7	0.33	0.43	151.34	1.86	1.06	0.83

1420

(cf. Eq. 9).

ID	Sample	Latitude °	Longitude °	Area km ²	¹⁰ Be erosion mm ka ⁻¹	\bar{L}_E *	k_{sn} * m ^{0.9}	P_{RIDW} * m yr ⁻¹	R_{RIDW} * m yr ⁻¹	k
1	BQ	-2.94	-78.93	186.3	53 ± 4	1.44	41.78	1.06	0.55	1.18
2	CH	-3.22	-78.74	86	88 ± 8	0.34	187.79	1.59	0.87	0.87
3	CJ	-2.92	-78.88	19.5	95 ± 11	1.43	60.45	1.02	0.54	1.04
4	DE2	-2.77	-78.93	39.1	105 ± 9	1.61	80.96	1.14	0.58	1.04
5	JA21	-2.89	-78.89	276	50 ± 4.5	1.45	48.96	1.05	0.55	1.19
6	MAR	-3.04	-78.95	49.8	30 ± 2	1.43	35.97	1.07	0.56	1.08
7	NA1	-2.70	-78.92	57.1	142 ± 18	1.54	96.36	1.04	0.53	1.05
8	NA4	-2.67	-78.90	4.9	222 ± 33	1.69	69.19	0.87	0.44	1.11
9	NG-DW	-2.73	-78.40	686.8	163 ± 16	0.57	184.21	2.25	1.33	0.92
10	NG-SD ^b	-2.73	-78.39	3.3	3959 ± 3801	0.89	231.84	2.62	1.60	0.91
11	NG-UP	-2.78	-78.46	679.1	179 ± 16	0.55	176.77	2.21	1.31	0.91
12	PA	-2.52	-78.56	424.4	229 ± 26	1.13	142.61	1.14	0.60	1.16
13	PAL	-2.65	-78.61	6.2	318 ± 32	0.69	192.24	1.89	1.11	0.88
14	PT-BM	-2.65	-78.46	6.8	219 ± 22	0.60	236.09	2.50	1.51	0.91

15	PT-QP	-2.61	-78.57	3.4	216 ± 20	0.52	231.77	2.01	1.16	0.94
16	PT-SD	-2.61	-78.46	11.1	399 ± 53	0.60	210.28	2.52	1.51	0.93
17	QU	-2.99	-78.92	16.7	77 ± 8	1.43	55.32	1.02	0.53	1.17
19	RG1_2	-2.96	-78.89	0.9	26.5 ± 2	1.43	48.87	1.01	0.53	1.13
20	RG2	-2.94	-78.91	29.2	61 ± 6	1.44	53.96	1.01	0.53	1.12
21	RGD1	-2.94	-78.80	2.2	30 ± 3	0.64	105.63	1.03	0.55	1.14
18	RGST	-2.97	-78.90	20.2	28 ± 2	1.42	45.55	1.00	0.52	1.08
22	SA ^b	-2.96	-78.93	0.5	152 ± 19	1.49	0.04	1.05	0.55	1.16
23	SF1_2	-2.89	-78.77	84	72 ± 7	0.56	110.46	1.42	0.78	0.83
24	SF2	-2.98	-78.69	1.3	118 ± 9	0.50	147.45	1.60	0.89	0.80
25	SII ^b	-3.16	-78.81	0.6	10 ± 1	0.29	57.09	1.34	0.72	0.95
26	SI2	-3.14	-78.81	18.3	30 ± 3	0.58	70.42	1.38	0.74	0.99
27	SI3	-3.14	-78.81	49.2	88 ± 11	1.30	43.63	1.28	0.68	1.03
28	SI5	-3.00	-78.81	6	3.4 ± 0.3	0.90	86.62	0.99	0.53	1.09
29	TI11	-3.01	-78.57	62.1	125 ± 11	0.33	142.87	1.97	1.13	0.84
30	TI2	-3.01	-78.61	21	57 ± 7	0.33	151.34	1.86	1.06	0.83

^a Catchment MA1 from Vanacker et al. 2015 is not listed because its area (<0.1km²) does not allow to accurately calculate basin the catchment properties listed here.

^b Catchments excluded from model optimization runs (see text)

1425 **Table 3:** Lithological erodibility index [values](#) based on [the](#) lithological strength (L_L). Detailed sub-classifications per lithology can be found in Table S2.

-	L_L
Igneous	2 - 3
Metamorphic (Igneous)	2
Metasedimentary	2 - 4
Strong sedimentary	4
Weak sedimentary	10 - 12
Unconsolidated	12

Table 4: Best-Fit Model Results: A-SPM Overview of the best-fit model results

Model	Nb.	Scenario	Figure	Erosional efficiency	Slope exponent ^d	Erosional efficiency	Slope charge variability	Bayes factor ^c	Runoff	R ²	Mash	Sette	Life ^M	E ₀
				K' $m^{0.1}s^{-1}$	k_a $m^{0.1}s^{-1}$	n -	$\frac{ke}{LS}$ $\frac{-m^{2.5}s^2kg^-}{LS}$	k_s -	τ_{crit} Pa	R m yr ⁻¹				
A-SPM	1	Constant rock erodibility (L _F = 1)	12.a	0.7573	-	1.0607	4.06	-	-	-	0.50	3.25		
	2	Variable rock erodibility	12.b	-	0.06907	1.63	4457	-	-	-	0.73	2.23		
	3			1.00	-	1	-	-	-	-	0.5	3.2		
	4			-	1.4	1	-	-	-	-	0.56	3.05		
	5			-	-	1	8.86×10^{-15}	-	-	-	0.51	3.57		
R-SPM	1		14.a	-	-	1	1.43×10^{-14}	-	-	-	0.75	2.61		
	2			-	-	1	1.13×10^{-14}	1.01	4.08	0.82	0.50	3.22		
ST-SPM	1			-	-	1	1.16×10^{-14}	variable	6.31	0.82	0.50	3.2	0.50	
	2			-	-	1	9.76×10^{-15}	1.01	0.00	variable	0.51	3.75	0.49	
	3			-	-	1	9.88×10^{-15}	variable	0.00	variable	0.52	3.53	0.50	
	4			-	-	1	2.88×10^{-14}	1.01	30.74	0.82	0.72	2.44	0.71	
	5			-	-	1	2.90×10^{-14}	variable	31.06	0.82	0.71	2.48	0.71	
	6			-	-	1	1.86×10^{-14}	1.01	14.21	variable	0.75	2.22	0.75	
	7			-	-	1	1.88×10^{-14}	variable	14.66	variable	0.75	2.21	0.75	
	8			-	-	1								

Inserted Cells

Formatted: Centered

Inserted Cells

Formatted: Font: Bold, Italic

Inserted Cells

Inserted Cells

Formatted: Font: Bold

Formatted: Font: Bold

Formatted: Font: Bold

Formatted: Font: Bold, Italic

Formatted: Font: Bold

Formatted: Font: Italic, Font color: Black

Formatted: Font: Italic

Inserted Cells

Inserted Cells

Formatted: Centered

Inserted Cells

Inserted Cells

Formatted: Centered

Table 5 Best Fit Model Results: R-SPM and ST-SPM

Model	Scenario nb.	Description	Figure	Erosional efficiency ke $m^{2.5}s^{-2}kg^{-1.5}$	Discharge variability k -	Critical Shear stress τ_c Pa	Runoff R $m\text{-yr}^{-1}$	R ²	Nash Sutteliff NS
R-SPM	1	$\overline{L_E}$ fixed ^a	-	8.86×10^{-15}	-	-	-	0.51	0.49
	2	$\overline{L_E}$ variable ^a	14.a	1.43×10^{-14}	-	-	-	0.75	0.70
ST-SPM	1	$\overline{L_E}$ fixed ^a \overline{R} fixed ^b k fixed ^c	-	1.14×10^{-14}	1.01	4.89	0.82	0.50	0.50
	2	$\overline{L_E}$ fixed ^a \overline{R} variable ^b k fixed ^c	-	9.76×10^{-15}	1.01	0.00	variable	0.51	0.49
	3	$\overline{L_E}$ fixed ^a \overline{R} variable ^b k variable ^c	-	9.88×10^{-15}	variable	0.00	variable	0.52	0.50
	4	$\overline{L_E}$ variable ^a \overline{R} fixed ^b k fixed ^c	-	2.86×10^{-14}	1.01	30.74	0.82	0.72	0.71
	5	$\overline{L_E}$ variable ^a \overline{R} fixed ^b k variable ^c	-	2.90×10^{-14}	variable	30.87	0.82	0.71	0.71
	6	$\overline{L_E}$ variable ^a \overline{R} variable ^b k fixed ^c	14.b	1.86×10^{-14}	1.01	14.21	variable	0.75	0.75
	7	$\overline{L_E}$ variable ^a \overline{R} variable ^b k variable ^c	-	1.88×10^{-14}	variable	14.66	variable	0.75	0.75

^a If $\overline{L_E}$ is fixed, a uniform value of 1 is used for all catchments. If $\overline{L_E}$ is variable, catchment specific values for L_E are used (Table 2)(Table 2)

^b If R is fixed, a uniform mean runoff value of 0.8 m yr^{-1} is used for all catchments. If R is variable, catchment specific values are used (Table 2)(Table 2)

^c If k is fixed, a uniform mean discharge variability value of 1.01 is used for all catchments. If k is variable, catchment specific values are used (Table 2)(Table 2)

^d The slope exponent (n) is optimized as a free parameter in A-SPM 1-2. It is fixed to 1 in A-SPM 3-4 (see text)

Formatted: Font: Not Bold

1435